

## Diploma Thesis

# Contribution to the optimised design of combined piled raft foundations (CPRF)

Submitted in satisfaction of the requirements for the degree of  
Diplom-Ingenieur  
of the TU Wien, Faculty of Civil Engineering

---

## Diplomarbeit

# Beitrag zur optimierten Bemessung von Kombinierten Pfahl-Plattengründungen (KPP)

ausgeführt zum Zwecke der Erlangung des akademischen Grades eines  
Diplom-Ingenieurs  
eingereicht an der Technischen Universität Wien, Fakultät für Bauingenieurwesen

von

**Corentin Dufour**

Matr.Nr.: 01623360

unter der Anleitung von

Univ.-Prof. Dipl.-Ing. Dr.techn. **Dietmar Adam**

Univ.-Ass. Dipl.-Ing. **Péter Nagy**, B.Sc

Institut für Geotechnik  
Forschungsbereich für Grundbau, Boden- und Felsmechanik  
Technische Universität Wien,  
Karlsplatz 13/220-02, A-1040 Wien

in Zusammenarbeit mit und Betreuung durch

STRABAG SE, Zentrale Technik  
Donau-City-Str. 9, 1220 Wien

Dipl.-Ing. Dipl.-Ing. Dr.-Ing. **Maximilian Huber**

Wien, im Juni 2018

---



# Preface

The work presented in this master thesis is the result of a cooperation between the Institute of Geotechnical Engineering of the Technical University of Vienna and the company STRABAG SE. It is part of a double degree with the École Centrale de Lyon (France).

I would like to thank all the people that made this work possible sincerely, hence all those who supported me during the writing process of my master thesis and who contributed to its achievement.

Furthermore, I wish to express my profound gratitude to my supervisor at the STRABAG Dr.-Ing Maximilian Huber for his extensive, invaluable and steadfast guidance. Thank you for sharing your knowledge and experience with me, for your interest in my work and for your willingness to answer my questions. Your critical view on the problem addressed in this paper made me think even more critically.

In particular I would like to thank Prof. Dietmar Adam, who gave me the opportunity to do my research project under his supervision, and whose effort and time to review my entire work enabled me to improve the quality of my thesis.

I especially thank Dipl.-Ing. Péter Nagy for his availability and his help regarding various subjects, i.e. both technical and administrative aspects. Thank you for your support and the supply of important documentation as well as for your pertinent remarks on my work.

I would also like to thank Dipl.-Ing Thomas Wieser, who enabled this cooperation thanks to the financial support of the STRABAG and who agreed on the exciting subject of the master thesis.

Likewise, I thank all the colleagues of the Zentrale Technik and in particular Dipl.-Ing Emir Ahmetovic for the positive working environment, which motivated me to accomplish this work.

I am very grateful to Christine Mascha for her answers to my numerous questions throughout my study at the Technical University of Vienna and especially during my master thesis.

I also wish to express my heartfelt thanks to Mag. Barbara Fussi, Alastair Gardner, Mag. René Guggelberger, Mag. Anna Heidlmair, Mag. Michaela Reisner and Mag. Stefanie Trappl for their perceptive and accurate proofreading of my master thesis.

All of this would not have been possible without the unconditional support of my family and friends throughout my whole studies. To them I would like to express my sincere gratitude.



# Abstract

An increasing number of the population lives and works in cities. It is widely expected that these patterns persist as urban areas account for a greater share of activity. This asks for high rise buildings and advanced foundations systems, which are able to transfer high loads from the ground surface into deep layers.

This master thesis focuses on the optimisation of combined piled raft foundations (CPRFs), which are hybrid foundation systems combining the bearing capacity of a foundation raft with the piles. Elements of the foundation exercise a mutual load-bearing effect and present reciprocal interactions as well as interactions with the subsoil. Herein both a semi-analytical approach for the simulation of soil structure interaction and a multi-objective optimisation to minimise the required resources for the deep foundation are used. After outlining the semi-analytical model for the design of pile groups and CPRFs, it is applied in a standard CPRF benchmark from the literature. The obtained design is then optimised using genetic algorithms.

This new design approach enables a rapid and robust semi-analytical approximation of the load-bearing behaviour of the structure, which can facilitate the calculation and cost estimation of projects in the tender phase. It is further implemented in a script capable of an optimised design covering geotechnical as well as structural aspects. By using multi-objective optimisation, better and more cost-effective results have been achieved compared to reference solutions presented in the literature. As far as the overall need for concrete masses for the raft and the piles is concerned, the obtained solutions show significant reduction of required concrete. The findings of these analyses contribute to the cost efficient design of foundation systems combining the need of practical engineering, advanced soil mechanical approaches and optimisation techniques.

It has further been shown that a direct relation between costs and settlement can be established and displayed in the form of a Pareto front. This finding facilitates the evaluation of the possible cost savings with a concrete insight into the increased risks following those savings. The representation of a Pareto front enables a rapid cost-benefit analysis. This optimisation procedure represents a new perspective for constructors and planners, which opens the way for more competitive solutions in foundation design and fosters the optimisation of complex problems in civil engineering.



# Kurzfassung

Ein zunehmender Teil der Bevölkerung lebt und arbeitet in Städten. Es ist zu erwarten, dass diese Tendenz fort dauert, da sich in Ballungsräume ein erheblicher Teil der Wirtschaftstätigkeit konzentriert. Der steigende Wohnraumbedarf in Großstädten bei hohen Grundstückspreisen führt unter anderem zum Bau von Hochhäusern in Ballungsräumen. Diese Hochhäuser fordern hochentwickelte Gründungen, die die hohen Lasten von der Gründungsoberfläche in tiefliegende Bodenschichten übertragen können.

Im Rahmen der vorliegenden Diplomarbeit wurden Kombinierte Pfahl-Plattengründungen (KPP) diskutiert. KPP sind geotechnische Verbundkonstruktionen mit gemeinsamer Tragwirkung von Fundamentplatte und Pfählen, die komplexe Wechselwirkungen aufweisen, sowohl zwischen den einzelnen Strukturelementen als auch mit dem Boden. Ein semi-analytisches Berechnungsverfahren wurde für die Abschätzung der Boden-Bauwerk Interaktion durchgeführt. Darüber hinaus wurde eine multikriterielle Optimierung für die Reduzierung der erforderlichen Ressourcen der Gründung entwickelt. Nachdem das semi-analytische Berechnungsverfahren für Pfahlgruppen und KPP hervorgehoben wird, wird es mit erprobten Beispielen aus der Literatur verglichen. Der daraus resultierende Entwurf wird schlussendlich mittels genetischer Algorithmen optimiert.

Dieses neue Verfahren ermöglicht eine schnelle und robuste Näherung des Tragverhaltens der Gründung, das die Kostenermittlung und die Berechnung in der Ausschreibungsphase unterstützen kann. Zudem wird das Verfahren in einem Skript abgeleitet, welches sowohl die geotechnische als auch die konstruktive Bemessung abdeckt. Anhand multikriterieller Optimierung wurden kosteneffektivere Lösungen im Vergleich zu jenen aus der Literatur erarbeitet. Die Menge an erforderlichem Baumaterial konnte reduziert werden, ohne die Fähigkeiten des Trageverhaltens zu verringern.

Darüber hinaus wurde gezeigt, dass mit Hilfe eines evolutionären Algorithmus eine direkte Verbindung zwischen optimaler Setzung und minimalen Kosten abgeleitet und mittels einer Paretofront dargestellt werden kann. Auf die Gefahr hin, dass die Setzungen zunehmen, kann so festgestellt werden, welche Kosteneinsparungen möglich ist. Die Darstellung der Paretofront ermöglicht außerdem eine schnelle Kosten-Nutzen-Analyse. Dies eröffnet eine neue Sichtweise für Bauunternehmen beziehungsweise Planungsbüros und unterstützt damit sowohl die Planung kompetitiver Lösungen als auch die Optimierung von komplexen Problemstellungen im Bauwesen.





# Résumé

Une part croissante de la population vit et travaille dans les villes et il est très probable que cette tendance persiste étant donné que les aires urbaines concentrent une grande part de l'activité économique. Ce phénomène conduit à un développement des gratte-ciels et des superstructures, édifices nécessitant des fondations capables de transférer de fortes charges de la surface de la fondation jusqu'à des couches de sol plus profondes.

Le présent mémoire se penche sur l'optimisation de fondations mixtes radier-pieux, fondations hybrides combinant la capacité portante d'un radier avec celle d'un groupe de pieux. Les éléments de cette fondation exercent un effet mutuel de portance et présentent des interactions complexes radier-pieux-sol. Une approche semi-analytique pour la simulation de l'interaction sol-structure ainsi qu'une optimisation multi objectifs pour minimiser la quantité de ressources nécessaire sont effectués. Après avoir mis en avant le modèle semi-analytique développé pour modéliser les groupes de pieux et les fondations mixtes, celui-ci est appliqué à des cas concrets pour pouvoir comparer les résultats à ceux obtenus numériquement par diverses études scientifiques. Le design est ensuite optimisé par l'intermédiaire d'algorithmes génétiques.

Cette nouvelle approche de conception permet une approximation rapide et robuste de la capacité portante de la structure, ce qui aide au dimensionnement de la fondation et à l'estimation des coûts lors des procédures d'appel d'offre ou pour concevoir un design préliminaire. Le modèle est implémenté dans un script couvrant aussi bien les aspects géotechniques que structurels. A l'aide d'une optimisation multi-objectif, des résultats plus économiques que ceux obtenus numériquement ont pu être obtenus. Les résultats montrent en effet une réduction significative de la quantité de béton nécessaire pour des performances similaires.

Une relation directe entre le coût de la structure et le tassement, représentée au moyen d'un optimum de Pareto, a par ailleurs été obtenue. Il est ainsi plus facile d'évaluer quelles économies peuvent être effectuées sans pour autant affecter la sécurité de la fondation. Cette représentation sous forme de frontière d'efficacité de Pareto permet une analyse coûts-avantages rapide. La procédure d'optimisation développée représente une nouvelle perspective pour les constructeurs et les bureaux d'études, qui ouvre la voie à des solutions plus compétitives concernant la conception des fondations et l'optimisation de problèmes complexes du génie civil.



# Table of contents

<b>1</b>	<b>Introduction</b>	<b>15</b>
1.1	Scope of the thesis and research objective .....	15
1.2	Methodology .....	16
1.2.1	Literature study .....	17
1.2.2	Pile group and CPRF design.....	17
1.2.3	Optimisation .....	18
1.2.4	Calculation programs.....	18
<b>2</b>	<b>Pile Foundation Systems</b>	<b>19</b>
2.1	Single pile.....	19
2.2	Pile grillage.....	20
2.3	Pile group .....	20
2.4	Combined piled raft foundation.....	23
<b>3</b>	<b>Pile group design</b>	<b>27</b>
3.1	Literature review on pile group design.....	27
3.1.1	Empirical methods.....	28
3.1.2	Analytical methods.....	29
3.1.3	Numerical methods.....	30
3.2	Design approach according to <i>Rudolph</i> (2005) .....	31
3.2.1	Assumptions .....	31
3.2.2	Flexibility coefficients.....	31
3.2.3	Equilibrium of the pile group .....	32
3.2.4	Influence radius .....	33
3.2.5	Failure criterion .....	34
3.2.6	Workflow.....	35
3.3	Modifications and improvements .....	38
3.3.1	Accuracy of the influence radius.....	38
3.3.2	Comparison of flexibility coefficients.....	39
3.3.3	Soil stiffness .....	41
3.3.4	Loading cases .....	42
3.3.5	Geometrical parameters.....	43
3.3.6	Differential settlement.....	43

3.3.7	Object oriented programming.....	45
3.3.8	Workflow.....	45
3.4	Limitations and drawbacks.....	46
<b>4</b>	<b>Design of combined piled raft foundation</b>	<b>49</b>
4.1	Literature review on piled raft foundations .....	49
4.1.1	Equivalent models .....	49
4.1.2	Empirical methods.....	49
4.1.3	Analytical methods.....	50
4.1.4	Numerical methods.....	52
4.2	Design procedure for PRF .....	53
4.2.1	Area of application .....	53
4.2.2	Calculation method requirements for PR design.....	53
4.2.3	Ultimate Limit State - ULS .....	54
4.2.4	Serviceability Limit State - SLS.....	56
4.2.5	Piled raft monitoring.....	57
4.3	Adopted design approach .....	58
4.3.1	Modelling of the raft-soil interaction.....	58
4.3.2	System rigidity .....	59
4.3.3	Workflow.....	61
4.4	Limitations and drawbacks.....	62
<b>5</b>	<b>Case studies on pile groups and piled raft foundations</b>	<b>63</b>
5.1	Pile groups .....	64
5.1.1	Guideline 1.2 .....	64
5.1.2	End bearing pile and skin friction pile.....	68
5.2	Combined piled raft foundation.....	70
<b>6</b>	<b>Optimisation of pile groups and piled raft foundations</b>	<b>77</b>
6.1	Optimisation method .....	77
6.1.1	Problem .....	77
6.1.2	Population.....	78
6.1.3	Algorithm .....	78
6.2	Optimisation of pile groups .....	81
6.2.1	Design parameters .....	82
6.2.2	Objective functions.....	82
6.2.3	Constraints and box boundaries.....	82
6.2.4	Results .....	82

---

6.3	Optimisation of CPRFs .....	84
6.3.1	Rigidity .....	84
6.3.2	Box boundaries .....	85
6.3.3	Results .....	86
6.4	Limitations and drawbacks .....	89
<b>7</b>	<b>Summary and conclusions</b>	<b>91</b>
	<b>References</b>	<b>93</b>
	<b>Table of figures</b>	<b>97</b>
	<b>Table of charts</b>	<b>99</b>
	<b>Appendix A Python Codes</b>	<b>101</b>
A.1	Analytical calculation of a pile group .....	101
A.2	Multi-optimisation of a pile group .....	112
	<b>Appendix B Global and partial safety concept</b>	<b>115</b>
B.1	Global safety concept .....	115
B.2	Partial safety factor concept .....	115
B.3	Comparison of the two concepts .....	117
	<b>Appendix C Optimisation</b>	<b>119</b>
C.1	Academic benchmark .....	119
C.2	Choice of the algorithm .....	121



# 1 Introduction

## 1.1 Scope of the thesis and research objective

Cities are often seen as centres of economic growth, providing opportunities for study, innovation and employment. The growing housing space demand in cities combined with a steep rise in real estate leads to the development of more and more high-rise buildings in city centres. Amongst others, this is the case in Frankfurt am Main, Germany, where numerous skyscrapers were constructed in the last decades (see Figure 1.1).

Design, construction and performance of these superstructures largely rely on the stability of their foundations. Deep foundations are often necessary to transfer loads of such major structures in the subsoil. A possible alternative to these foundations is a combination of elements of shallow foundations on the one hand with elements of deep foundations, on the other hand, forming the so-called Combined Piled-Raft Foundations (CPRF). A CPRF is thus a geotechnical composite construction coupling the bearing effect of both foundation elements raft and piles.

Major advantages of combined piled raft foundations are lower settlements of the whole structure as well as a reduction of the volume of material used in comparison with deep foundations, leading to optimised cost and better economic viability. Thus, such foundations are often chosen for highly loaded buildings or bridge foundations.

This master thesis aims at developing an algorithm capable of a quick, robust and optimised design of CPRFs covering the basic geotechnical as well as structural aspects. This algorithm should be a smart and efficient tool, which allows a rapid and simple adaptation of the local boundary conditions. The calculation time should not exceed some seconds. It should include elaborated approaches such as a non-homogeneous soil model with a linearly increasing modulus or the introduction of a failure criterion. Consequently, the developed algorithm would offer an evolved design but would remain quick and easy to handle.

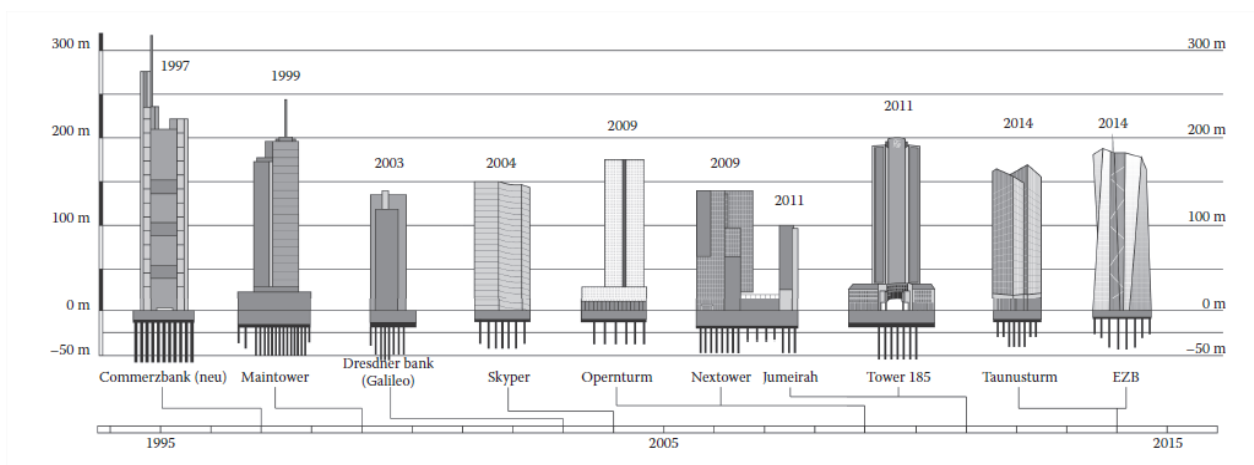


**Figure 1.1:** Development of recent high-rise buildings in Frankfurt am Main, after [31].

This algorithm would be suitable for the preliminary and tender design of a project. Depending on the legal details of the tender documents, one should be able to change the construction concept, the construction material and the static system of a high-rise building in order to meet the required design specifications. The most important purpose of the tender phase is the development of a safe structure with the smallest possible price. However, for detailed analyses and final design, it is recommended to have recourse to numerical methods [24], which are the only ones capable of a realist and trustworthy enough design.

The simplified design of CPRF should be automatized in the developed algorithm so that the calculation can be applied easily and quickly to various projects. This new design approach enables a rapid semi-analytical approximation of the load-bearing behaviour of the structure. In combination with standard structural analysis software such as RFEM, it allows the design of CPRFs after the state of the art. Developing the algorithm with the programming language Python (see Section 1.2.4) allowed to achieve this simplified design process.

Moreover, this semi-analytical calculation method is optimised using mathematical algorithms to minimise the volume of construction material as well as the settlement of the foundation, leading to a set of optimal solutions. This new design strategy is validated through a benchmark comparing the results with tested calculations coming from the CPRF guidelines.

This master thesis is divided into five main parts. Chapter 2 gives an overall view of several pile foundation systems, their way of load transfer to the subsoil and the particularities of the different systems. Chapter 3 covers the design method of pile groups. The thesis is based on a literature study in order to compare different design and calculation methods. In particular, it outlines how the algorithm is developed and describes the improvements realised compared to *Rudolf* (2005) [47]. Chapter 4 deals with the design of combined piled raft foundations. Different design and calculation methods are compared and the developed calculation method is described. Chapter 5 contains case studies on pile groups and CPRFs to test the efficiency and the reliability of the developed solution. A comparison with tested examples coming from the literature is carried out. Chapter 6 treats the optimisation of pile groups and combined piled raft foundations to minimise a multi-objective problem using genetic algorithms. Finally, Chapter 7 summarises the main findings of the thesis and draw conclusions from them.

## 1.2 Methodology

The predefined methodology used to achieve the design of CPRFs is summarised in Figure 1.2.

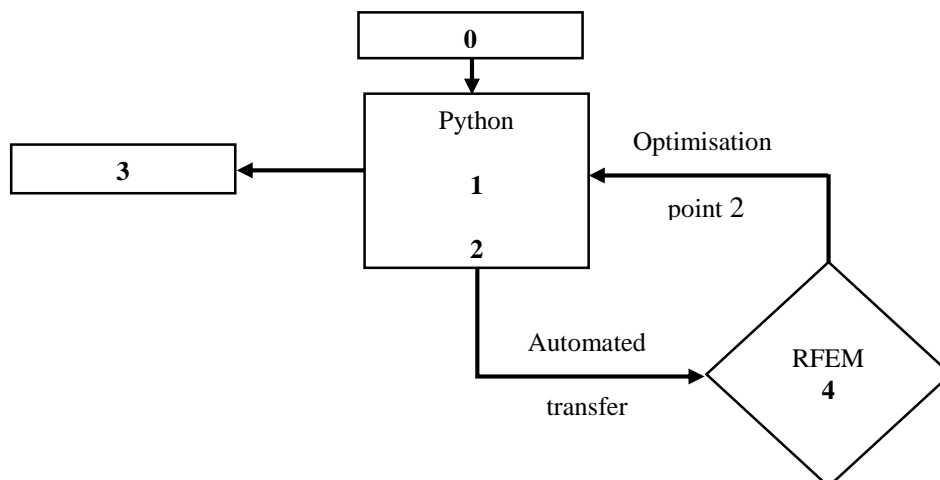


**Figure 1.2:** Workflow representing the methodology followed during the master thesis.



In Figure 1.2 the following abbreviations are used:

- 0 Literature study,
- 1 Analytical description of the load-settlement behaviour of a CPR foundation and development of an adequate Python code,
- 2 Optimisation of the piles (number, spacing, diameter, length...) using multi- objective optimisation,
- 3 Benchmark and comparison with the state of the art and
- 4 Python interface with RFEM.

### 1.2.1 Literature study

A literature study is performed covering, in particular, the concepts of pile group and CPRF design. Different design approaches are summarised and compared with a special focus on global and partial safety factor concepts.

The emphasis is put on analytical approximation procedures, and in particular on a comparison regarding assumptions, expected precision and limits of these procedures. As numerical methods are concerned, the principal point of interest is the constitutive equations used to model the subsoil.

The study regarding multi-criteria optimisation contains fundamentals on mathematical optimisation, pros and cons of different algorithms, possibilities of the programming language Python to achieve the requested optimisation as well as advantages of a Pareto front in the cost calculation.

### 1.2.2 Pile group and CPRF design

An easy way to design CPRF can be achieved following two different possible approaches. One possibility is to begin the calculation studying exclusively a shallow foundation and to incorporate elements of deep foundations as well as the resulting interactions afterwards. The other method is to initiate the calculation with the deep foundation and add the elements of the shallow foundations (such as the slab) subsequently. The latter solution is chosen for this thesis.

The design process is divided into two major steps: analytical design of a pile group (deep foundation) followed by a numerical calculation of the slab using the output parameters of the analytical calculation (i.e. the spring stiffness of each pile). The combination of these two steps provides the desired calculation of a CPRF. Geotechnical as well as constructive aspects are covered in the algorithm, whose input parameters are easily modifiable by the user. The analytical design is based on *Rudolf* (2005) [47], modified and extended to describe the pile group more realistically and to meet the needs of the current codes.

As a first step, the analytical calculation of a pile group is coded into a Python framework based on *Rudolf* (2005) [47]. Adaptations are made to meet the needs of a fast and simultaneously accurate design covering the following points:

- group effect of a pile group,
- stress dependent stiffness,
- settlement differences between distinct piles of a group and
- non-linear load-bearing behaviour.

The analytical calculation procedure of this algorithm is summarised in a workflow that enables an easier comprehension of the method (see Figure 3.3). After this, the load-settlement behaviour of the pile group (and in particular the spring stiffness) is transmitted to the program RFEM to complete the calculation of the CPRF. The stress resultants of the slab are also evaluated with the help of this structure analysis

software. The transfer of the results must be facilitated between Python and RFEM to enable the dimensioning of the foundation slab, which cannot occur with the analytical calculation in Python.

### 1.2.3 Optimisation

The use of the language Python to describe the analytical process enables an easy coupling with an optimisation library also implemented in Python. The modification and the simulation of a multitude of variables are also made possible with the algorithm.

CPRF optimisation must be based on a robust analytical calculation strategy to offer reliable results. In fact, no divergence of the calculation should occur during the numerous iteration steps of the optimisation. That is why a benchmark is necessary, conjointly with a precise study of the relevant input parameters for each defined CPR to optimise. The multi-criteria optimisation aims at finding optimum input parameters such as pile length, pile radius, distribution of the position of piles and thickness of the foundation slab. Those parameters influence the global cubature and in this way the total cost of the structure. In the end, a Pareto front is to be produced to visualise the set of optimal solutions.

### 1.2.4 Calculation programs

Different tools are used in this thesis: the structural analysis software RFEM, the programming language Python and its specific library pygmo.

Python is a universally used high-level, interpreted and dynamic programming language. The design of its code provides code readability and clear structures. The required syntax is said to be more straightforward than the one used in other programming languages. Besides, maintenance is handled easily and the language is accessible. The version used in the study is Python 3.6.2.

The finite element method program RFEM enables a quick and easy modelling of various structures. Both static and dynamic calculations are possible with RFEM. Due to its modular software concept, the basic program can be extended with dedicated modules to meet the needs of each user. The additional module RF-SOILIN permits, for example, the design of shallow foundations using the subgrade reaction modulus method. The version used for this work is RFEM 5.11.

Pagmo (implemented in C++) or pygmo (in Python, for PYthon Global Multi-objective Optimizer) is a scientific library for optimisation problems. It was coded by *Izzo and Biscani* (2017) [27]. It is built around the idea of providing a unified interface and enables the use of a multitude of already implemented algorithms. Its coding style is easy to understand and uses classes to define among others problems, algorithms and populations. It is strongly recommended to use Anaconda [2] to fulfil the installation of the pygmo library, making it easy and straightforward. However, *Izzo and Biscani* (2017) [27] indicate that pygmo is relatively new and that the syntax of the code may change in the next few years. Adapting the algorithm in significant proportions may be necessary. The version of pygmo used in the study is pagmo2-v2.6.

## 2 Pile Foundation Systems

### 2.1 Single pile

Single piles are piles that do not interact with other piles (or to a negligible degree), neither through the ground nor the superstructure [33].

When designing piles, one distinguishes between “internal” and “external” pile capacities. The internal capacity refers to the safety against pile material’s failure (concrete, reinforced concrete, steel, timber, etc.). As for the external capacity, it refers to the analysis of the safety against failure of the ground surrounding the pile. According to EC7 [20], both the ultimate limit state (ULS) and the serviceability limit state (SLS) have to be analysed concerning the internal and the external safety analysis.

Piles can be subject to all types of loading: both vertical and horizontal forces as well as bending moments. Moreover, the actions may interact with each other to a certain degree. For example, the application of horizontal forces leads to the apparition of bending moments but also increases the vertical forces [33]. In most of the cases, however, the non-axial actions are neglected: foundation piles are predominantly axially loaded.

The axial resistance of a single pile can be divided in two components: the base resistance  $R_{b,k}(s)$  and the shaft resistance  $R_{s,k}(s)$ . The pile resistance is then obtained by summing these two components (see Equation (2.1)). Note that  $k$  is the index for the characteristic value.

$$R_{pile,k}(s) = R_{b,k}(s) + R_{s,k}(s) \quad (2.1)$$

The pile shaft resistance  $R_{s,k}(s)$  is calculated as the integral of the skin friction  $q_{s,k}$  over the pile skin surface. The pile base resistance  $R_{b,k}(s)$  as the integral of the end bearing  $q_{b,k}$  over the contact area of the pile base, see Equations (2.2) and (2.3).

$$R_{b,k}(s) = q_{b,k} \frac{D^2 \pi}{4} \quad (2.2)$$

$$R_{s,k}(s) = \int q_{s,k}(s, z) \pi D dz \quad (2.3)$$

Both resistances are generally related to the vertical displacements (described by the settlement  $s$  at the pile head). They are represented in Figure 2.1 until the settlement limit  $s_g$  after Katzenbach *et al.* (2016) [31].

The settlement limit  $s_g$  to mobilise the full base resistance  $R_{b,k}(s_g)$  is defined in Equation (2.4) with  $D_s$  the diameter of the pile shaft.

$$s_g = 0.10 D_s \quad (2.4)$$

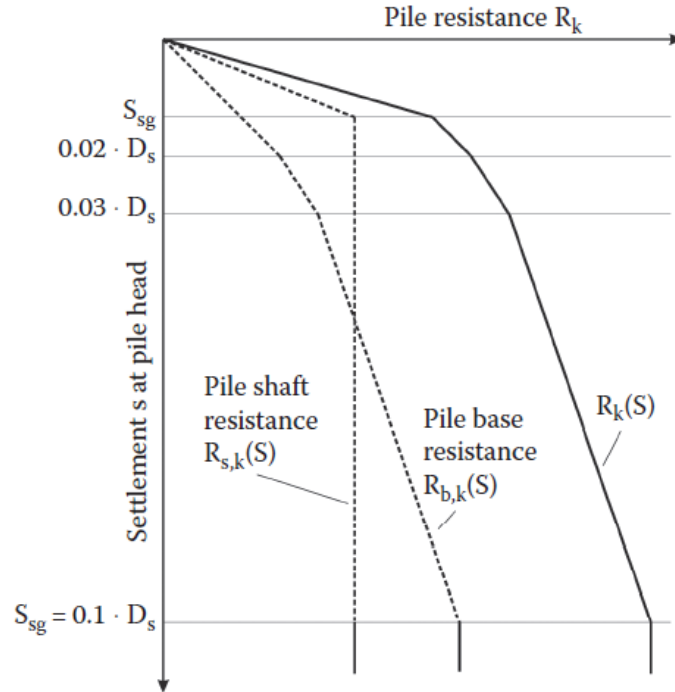


**Figure 2.1:** Characteristic resistance-settlement curve (RSC) of a single pile [31].

The settlement limit  $s_{sg}$  (cm) to mobilise the pile shaft resistance  $R_{s,k}(s_{sg})$  (MN) is defined as

$$s_{sg} = 0.50 R_{s,k} + 0.50 \leq 3.0 \text{ cm} \quad (2.5)$$

Resistance-settlement curves present shapes specific to the resistance predominantly used by a pile to transfer loads to the ground. Two major types of piles can thus be recognised: piles making predominantly use of the shaft resistance (called “skin friction piles”) and piles mostly using the base resistance (“end-bearing piles”) to transfer loads. For a pile subject to shaft resistance, one observes a pronounced curvature of the load-displacement curve. This is because the limit value of the skin friction  $q_s$  is normally reached at relatively small pile displacements. Once  $q_s$  is exceeded, only the base resistance increases notably (that is to say for larger displacements) [34]. As for end-bearing piles, they present a less pronounced curvature for the same reason as explained above (the base resistance increases up to large settlements).

## 2.2 Pile grillage

A pile grillage consists of single piles bound together with the help of a superstructure and positioned far enough to each other so that the interaction between them in terms of pile load-bearing behaviour can be neglected.

## 2.3 Pile group

Several piles form a group if they have an influence on each other regarding their load-bearing behaviour and are united using a common pile cap. The mutual influence of the piles is called group effect or pile-pile interaction. The group effect of axially loaded piles can refer to both the settlement and the resistance.

The settlement-related group effect  $G_s$  is expressed as

$$G_s = \frac{s_G}{s_E} \quad (2.6)$$

The resistance-related group effect  $G_R$  is defined by the factor

$$G_R = \frac{R_G}{n_G R_E} \quad (2.7)$$

- $s_G$  mean settlement in a pile group,
- $s_E$  settlement of an equivalent single pile under the mean pile load of the group,
- $R_G$  overall resistance of the pile group,
- $R_E$  resistance of the single pile at the mean settlement of the pile group and
- $n_G$  number of piles in the group.

The limit distance after which the group effect between two neighbouring piles can be neglected is often taken as  $6D$  or  $8D$ , with  $D$  the pile diameter. However, the limit distance can also take into account other parameters such as the pile length, the Poisson's ratio or the thickness of the compressible layer. The limit distance increases for example with increasing embedment depth  $d$ . For small settlements the equivalent pile group normally displays smaller resistances than single piles. That is, however, the contrary at larger settlements [33].

The load-bearing behaviour of a group of piles differs for every pile depending on its respective position (see Figure 2.2). In low-settlement pile groups, corner piles normally exhibit the highest pile resistances, the central piles the smallest. On the contrary, at larger settlements the distribution among piles can be inverted because of interlocking effects [33].

*Kempfert et al.* (2012) [33] propose an approximation method to calculate the group effect in terms of the settlement (see Equation (2.6)) of compression pile groups. This method is based on nomograms, which are derived from extensive FEM parameter studies made on bored pile groups. The method should be adopted preferentially to determine the settlement behaviour in the serviceability limit state. It is also suited to obtain characteristic pile spring stiffness, which depends on the position within the pile group.

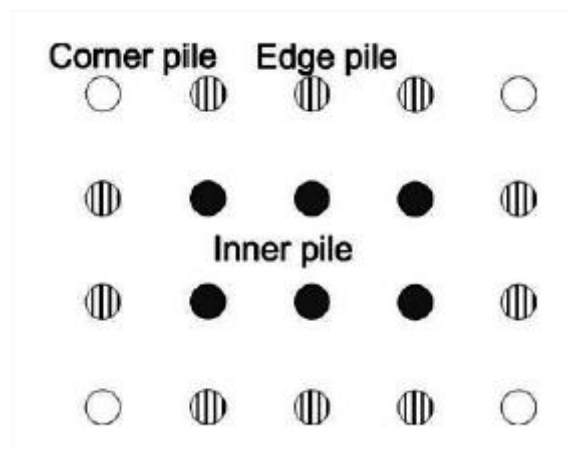


**Figure 2.2:** Pile denomination within a group (adapted from [33]).

The settlement-related group factor  $G_s$ , which enables to determine the mean settlement of a pile group subject to a central, vertical action, is given in Equation (2.8) after *Kempfert et al.* (2012) [33].

$$G_s = S_1 S_2 S_3 \quad (2.8)$$

- $S_1$  factor depending on the influence of the soil parameters and the group geometry (pile length  $L$ , pile embedment depth in load-bearing ground  $d$ , pile centre distances  $a$  as shown in Figure 2.3),
- $S_2$  factor depending on the size of the group as shown in Figure 2.4 and
- $S_3$  pile type influence factor.

Even if the original parameter studies were carried out on bored piles, those results can be extended to other types of piles using the factor  $S_3$ . The factors presented in Equation (2.8) are obtained by reading the established nomograms. These nomograms are differentiated for cohesive and non-cohesive soils regarding their stiffness moduli. In a first approximation, the moduli are set as displayed in Table 2.1 and constitute the application limits.

An example is presented for a cohesive soil of type (II). The factor concerning the influence of the soil type and the group geometry can be read in Figure 2.3, the value of the group size influence factor in Figure 2.4 (depending on the ratio  $a/d$  where  $a$  is the pile spacing and  $d$  the pile embedment depth). A multitude of other nomograms is available in *Kempfert et al.* (2012) [33] to cover a broader range of the ratio  $a/d$  as well as different types of soil. In Figure 2.3 and Figure 2.4,  $F_G$  represents the vertical action on the whole pile group and  $R_{E,s=0.1D}$  the pile resistance of a single pile for a settlement  $s = 0.1 D$  with  $D$  pile diameter.

Finally, it should be mentioned that the pile cap slab is assumed as almost rigid, meaning that the differential settlements within the pile group are neglected.

**Table 2.1:** Characterisation of the soil depending on the stiffness modulus. Adapted from [33].

Type of soil	Stiffness modulus $E_s$ [MN/m <sup>2</sup> ]
cohesive I	5-15
cohesive II	15-30
non-cohesive	$\geq 25$
not load-bearing	$< 5$

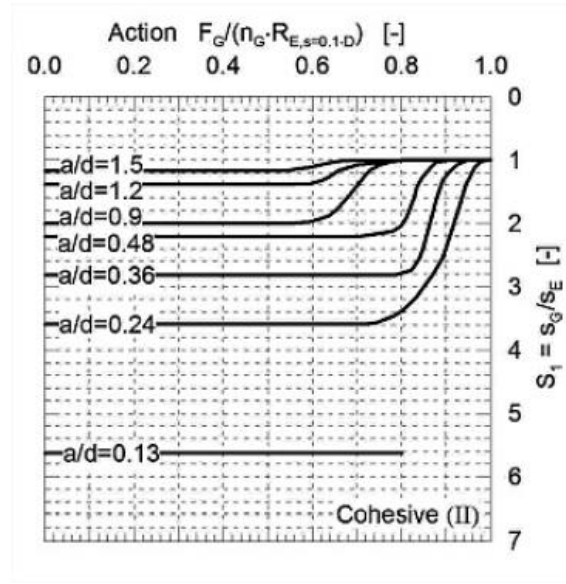


**Figure 2.3:** Nomogram showing the influence of the soil type and the group geometry of a bored pile group for a cohesive soil (group of soil “cohesive II” according to Table 2.1) [33].

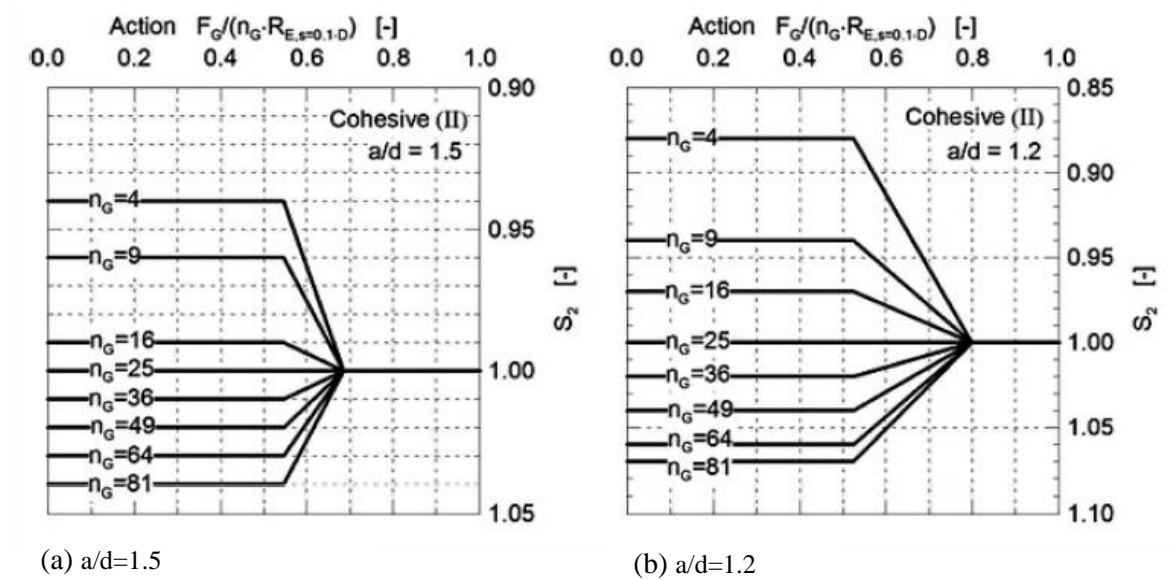


**Figure 2.4:** Nomograms showing the influence of the group size for the determination of the mean settlement of a pile group in a cohesive soil (group of soil “cohesive II” according to Table 2.1) [33].

## 2.4 Combined piled raft foundation

Piled-raft foundations are structures able to transfer loads to the ground with foundation slabs and piles exercising a mutual load-bearing effect [33]. The interactions shown in Figure 2.5 must all be considered simultaneously.

The characteristic value of the total resistance of a piled raft (as a function of the settlement)  $R_{tot,k}(s)$  is therefore composed of the sum of the characteristic values of the resistances of all  $n$  piles of a pile group and of the characteristic value of the resistance of a raft mobilized by contact pressure  $R_{raft,k}(s)$ . The latter is calculated as the integral of the contact pressure  $\sigma(x,y)$  over the area of the pile slab (see Figure 2.6 and Equation (2.9)).

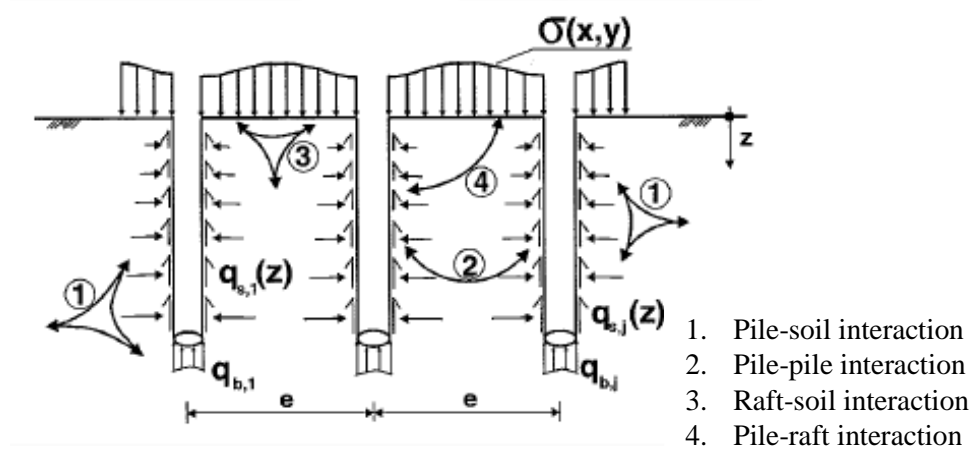


**Figure 2.5:** Soil-structure interaction after [24].

$$R_{tot,k}(s) = \sum_{i=1}^n R_{pile,k,i}(s) + R_{raft,k}(s) \quad (2.9)$$

Where  $R_{pile,k,i}(s)$  is defined in Section 2.1.

The load-bearing effect of a piled raft is defined by the piled raft coefficient  $\alpha_{PR}$  (see Equation (2.10)). This coefficient indicates the part of the total action transferred by the piles. The remaining part of the action is transmitted to the ground using the contact pressure of the foundation slab. A piled raft coefficient of 1 corresponds to a pure pile foundation (calculated after DIN 1054:1976 [13] Section 5) and a coefficient of 0 represents a pure shallow foundation (calculated after DIN 1054:1976 [13] Section 4), see Figure 2.7. This figure shows a qualitative example of the piled raft coefficient depending on the settlement of the piled raft  $s_{PR} \equiv s_{KPP}$  over the settlement of a shallow foundation  $s_{sh} \equiv s_{FI}$  presenting the same foundation area and the same actions as the piled raft.

$$\alpha_{PR}(s) = \frac{\sum_{i=1}^n R_{pile,k,i}(s)}{R_{tot,k,s}(s)} \quad (2.10)$$

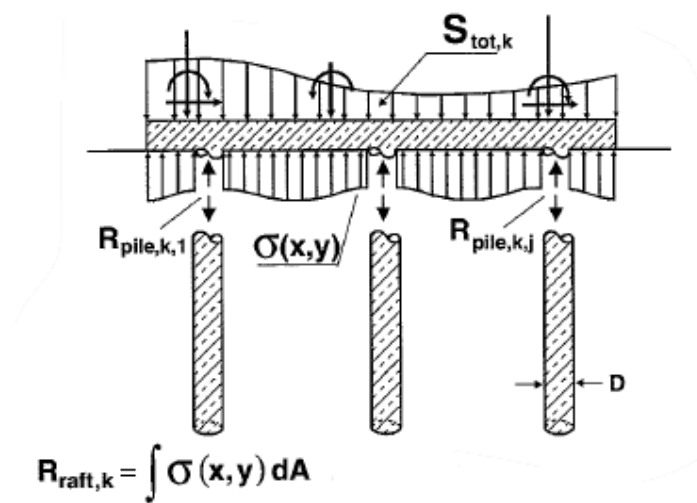


**Figure 2.6:** Combined piled-raft foundation as a geotechnical structure, pile and raft resistances [24].



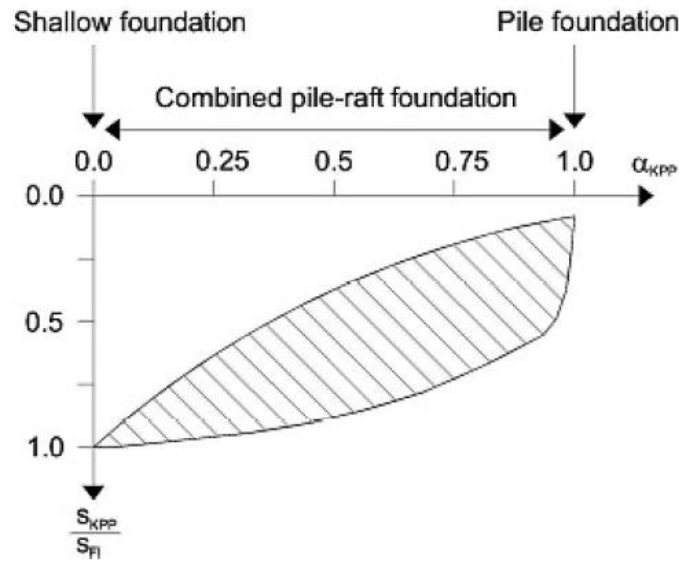


**Figure 2.7:** Settlement of a CPRF depending on the piled raft coefficient  $\alpha_{PR}$ , adapted from [24].

One can mention that the piled raft coefficient depends on the load level and thereby on the settlement of the piled raft. The design of piled raft foundation will be developed more precisely in Chapter 4 of this thesis. Analysis of piled raft foundations follows the German “guidelines for the design, dimensioning and construction of piled raft foundations“ („Richtlinie für den Entwurf, die Bemessung und den Bau von Kombinierten Pfahl-Plattengründungen“ (KPP-Richtlinie *Hanisch et al. (2002)* [24])). Additional advice is to be found in the EC 7-1 Handbook [23]. Exhaustive information regarding pile foundation systems can be found in the Recommendations on piling (EA-Pfähle) of the “Deutschen Gesellschaft für Geotechnik” [33]. The design of pile groups will be discussed in more detail in the following chapter of this thesis.



## 3 Pile group design

### 3.1 Literature review on pile group design

Different methods have been developed to study the settlement behaviour of a pile group. They all differ with regards to their calculation method, the needed input parameters, the precision of the results, the area of application or the computational costs. They can be grouped under three main categories: numerical, analytical and empirical methods.


The most powerful methods are the numerical methods and among them probably the Finite Element Method (FEM). Numerical methods can be applied in almost all cases (non-linear constitutive soil models, stratified soils, etc.), which makes their utilisation attractive. However, these methods require an intensive computational cost and present a high complexity. Boundary Element Methods (BEM) are more tractable as they only proceed in a discretization of the boundaries and not of the entire structure [7], but are nowadays less attractive since the obstacle of the computational cost tends to disappear. In any case, numerical methods require a sufficient experience from the user. Moreover, adequate input parameters have to be chosen correctly.

There are the reasons why analytical methods are still used and developed as they offer an easier solution to a problem or enable a simple preliminary design. The modelling requires less investment but still offers satisfactory results in comparison with a numerical model – the latter one is thought to be more precise. However, these models also contain some input parameters, which have to be estimated (for example the influence radius, see Section 3.2.4).

Empirical models only allow for a rather rough approximation. Their application is suitable for pilot studies or plausibility checks during the design of complex pile groups with other methods. An overview of the above-mentioned design methods is presented Table 3.1. Application fields of the methods (that is to say for which phase of the project the design methods are suitable) are displayed in relation to their complexity (time and cost investment).

The literature review on pile group design is summarised in Table 3.2 after *Rudolf* (2005) [47]. Superposition refers to the displacement fields of individual piles within the group. Some of the mentioned methods are detailed in the following subchapters.

**Table 3.1:** Overview of different calculation methods, design of pile groups, adapted from [37].

Application	Method	Complexity
Preliminary design	Utilisation of approximate methods (analytical, empirical), which offer satisfying results in a limited amount of time.	
Dimensioning	Boundary Element Method (BEM)	
Special investigation and analysis	Finite Difference Method (FDM) Finite Element Method (FEM)	

**Table 3.2:** Calculation methods for a pile group (adapted from [47]).

Method	Approach	Remark
<b>Numerical</b>		
<i>Banerjee and Discroll (1976)</i>	BEM, whole pile group	Linear load-bearing behaviour
<i>Poulos and Davis (1980)</i>	BEM, superposition, influence coefficients	Non-linear load-bearing behaviour
<i>Banerjee and Butterfield (1981)</i>	BEM, whole pile group	Non-linear load-bearing
<i>Randolph and Wroth (1979)</i>	FEM	Elastic load-bearing behaviour, only in SLS
<b>Analytical</b>		
<i>Randolph and Wroth (1979)</i>	Superposition, influence coefficients	Elastic load-bearing behaviour, only in SLS
<i>Chow (1986)</i>	Superposition, influence coefficients	Non-linear load-bearing behaviour
<i>Guo and Randolph (1997)</i>	Superposition, influence coefficients	Elastic pile load-bearing behaviour
<i>Rudolf (2005)</i>	Superposition, influence coefficients	Non-linear behaviour, failure criterion
<b>Empirical</b>		
<i>Skempton (1953)</i>		Displacement pile
<i>Poulos and David (1980)</i>		Rigid pile cap
<i>Hettler (1986)</i>		Cohesive soils

### 3.1.1 Empirical methods

Empirical methods are based on results of laboratory and field tests of equivalent single piles embedded in the same subsoil. The settlement of the group  $s_G$  is obtained by multiplication of the settlement of the equivalent single pile  $s_E$  with the settlement-related group effect  $G_s$  as presented Equation (2.6). The group effect of *Skempton (1953)* [48] is applicable to displacement piles and presented Equation (3.1), where  $B_G$  represents the equivalent width of the pile group ( $B_G$  given in feet).

$$s_G = s_E \left( \frac{4B_G + 9}{B_G + 12} \right)^2 \quad (3.1)$$

Other empirical values of the group effect have been determined, for instance by *Hettler (1986)* [25] for cohesive soils (Equation (3.2)) or by *Poulos and Davis (1980)* [44] Equation (3.3) for pile groups with a rigid pile cap.

$$s_G = s_E \frac{\lambda_G}{\lambda_E} \left( \frac{B_G}{a_s} \right)^{0.35} \quad (3.2)$$

In (3.2),  $\lambda_G$  and  $\lambda_E$  are influence coefficients depending on the embedment depth of the piles (for the group respectively for the single pile), and  $a_s$  represents the pile spacing.

$$s_j = s_E \sum_{i=1}^n R_i \alpha_{ji} + s_{E,j} R_j \quad (3.3)$$

In Equation (3.3),  $\alpha_{ji}$  is an interaction factor defined in *Poulos and Davis* (1980) [44].

### 3.1.2 Analytical methods

Analytical methods developed to design pile groups are mostly based on the theory of elasticity. *Randolph and Wroth* (1979) [46] and *Guo and Randolph* (1997) [22] have adopted an elastic load-bearing behaviour. Non-linear elastic, ideal plastic behaviours can also be modelled, for example, in *Chow* (1986) [7] or in *Rudolf* (2005) [47], the latter one taking a failure criterion into account. Those approaches may combine pure analytical models with empirical values to obtain results as close as possible to those of numerical simulations. The different methods can be distinguished as to whether the subsoil is considered homogenous or not. The widely employed method of *Randolph and Wroth* (1979) [46] following the theory of elasticity is detailed below, while the methods of *Chow* (1986) [7] and *Rudolf* (2005) [47] are presented in the next section.

*Randolph and Wroth* (1979) [46] divide subsoil into two layers, the upper one stretching from the pile head to the pile base and the lower layer representing the stratum under the pile base. It is admitted that the skin friction induces settlements in the upper layer whereas settlements in the lower layer are caused by the base pressure of the pile. It is also assumed that the skin friction is constant over the whole pile.

Considering the vertical equilibrium of an infinitesimal volume of a pile as shown in Figure 3.1 (a), the Equation (3.4) is obtained.

$$\frac{\partial(r\tau)}{\partial r} + r \frac{\partial\sigma_z}{\partial z} = 0 \quad (3.4)$$

The first term of the equation represents the shear stress variation depending on the axial distance to the pile and the second term the increase in vertical stress state with the depth. Following the hypothesis that the increase of the vertical stress is negligible with respect to the modification of the shear stress, the equation of equilibrium can be simplified (the second term is neglected). It ensues the expression of the shear stress in radial direction Equation (3.5) (see Figure 3.1 (b)):

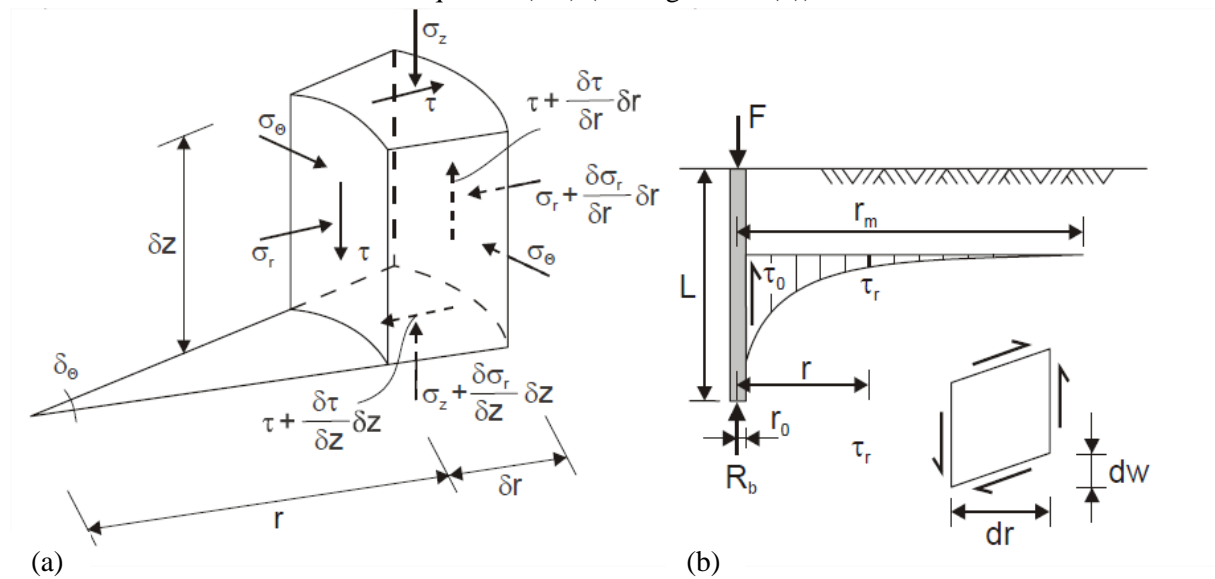


**Figure 3.1:** (a) Stress state of an infinitesimal volume [52] (b) Shear stress distribution on the pile shaft in radial direction [9].

$$\tau_r = \tau_0 \frac{r_p}{r} \quad (3.5)$$

Combining the Equation (3.5) with the equations of the theory of elasticity for a homogeneous and isotropic material, one obtains the expression of the vertical settlement of the pile shaft  $s_s$ :

$$s_s = \frac{2(1+\nu)\tau_0 r_p}{E} \ln \left( \frac{r_m}{r_p} \right) \quad (3.6)$$

- $\tau_0$  skin friction,
- $\nu$  Poisson's ratio,
- $E$  stiffness modulus,
- $r_m$  influence radius (discussed in Section 3.2.4) and
- $r_p$  pile radius.

The resistance of the pile shaft is obtained combining the Equation (3.6) with the expression of the skin friction  $\tau_0 = R_s/A_s$ , where  $A_s$  represents the section of the pile shaft. The result is a relation between the vertical settlement of the pile shaft and its resistance shown Equation (3.7).

$$s_s = \frac{(1+\nu)R_s}{E L \pi} \ln \left( \frac{r_m}{r_p} \right) \quad (3.7)$$

As for the settlement at the pile base, the solution of *Boussinesq* (1885) [5] for a rigid circular fundament in an elastic half-space is adopted, see Equation (3.8).

$$s_b = R_b \frac{1-\nu^2}{E D} \quad (3.8)$$

The relations of the settlements of the pile base and the pile shaft as a function of the resistances (Equations (3.7) and (3.8)) are the basis for the modelling of the pile-pile interaction of various analytical methods.

### 3.1.3 Numerical methods

The first numerical methods developed were based on the theory of elasticity. The early computer programs for pile group analysis are largely inspired by the research of *Banerjee and Discroll* (1976) [4], *Poulos and Davis* (1980) [44] and *Randolph and Wroth* (1979) [46]. Numerical methods have not ceased to be improved until now, leading to very elaborated and realistic models.

*Banerjee and Discroll* (1976) [4] present a BEM where the soil is modelled as a homogeneous, linear elastic material. The computer program developed from his work has since been improved to include a linearly increasing stiffness modulus of the soil. The program developed by *Poulos and Davis* (1980) [44] is based on a simplified BEM for the single pile analysis and the calculation of the interaction factors for two equally loaded identical piles *Chow* (1987) [8]. Soil non-linearity is modelled by limiting the stresses at the pile-soil interface. The program of *Randolph and Wroth* (1979) [46] is based on analytical solutions, either derived theoretically or adapted from finite element results for single piles. The pile-soil interaction is based on interaction factors determined by expressions fitted to the results of finite element analyses [8].

## 3.2 Design approach according to Rudolph (2005)

The analytical calculation method presented in this section is mostly inspired by *Randolph and Wroth* (1979) [46] and extended by *Rudolf* (2005) [47] to take a failure criterion into account, both for the pile shaft and the pile base. The method based on the theory of elasticity after *Randolph and Wroth* (1979) [46] was developed Section 3.1.2. This calculation method enables to study the load-settlement behaviour for higher settlements and until the Ultimate Limit State. The modified and improved calculation method is then coded in a Python script and included in Appendix A.1.

### 3.2.1 Assumptions

Some assumptions have been made to simplify the analytical method. The pile slab is rigid and no deflection occurs (“biegestarre Pfahlkopfplatte” in German). This allows for simplifying the problem to a unique settlement for the whole pile group. This assumption is questionable as Eurocode 7 recommends precisely stating the design of a pile group through the settlement differences (see Section 3.3). No elongation of the piles takes place (“dehnstarre Pfähle”), pile shaft and pile base can therefore be studied separately. The pile group is subject to a predominantly central vertical load (horizontal load and bending moment are neglected).

### 3.2.2 Flexibility coefficients

The solution proposed is based on a linear-elastic soil behaviour using empirical parameters. Flexibility coefficients (or influence coefficients)  $f_{i,j}$  denoting the settlement of the pile  $i$  due to a unit load at the pile  $j$  are introduced. Following the hypothesis that piles are not subject to lengthening, different coefficients for the pile shaft and the pile base can be defined separately:

$$f_s = \frac{s_s}{R_s} \quad (3.9)$$

$$f_b = \frac{s_b}{R_b} \quad (3.10)$$

- $s_s$  settlement of the pile shaft,
- $s_b$  settlement of the pile base,
- $R_s$  resistance of the pile shaft and
- $R_b$  resistance of the pile shaft.

From the expressions of the settlement of a single pile derived from *Randolph and Wroth* (1979) [46] and presented Equations (3.7) and (3.8), both flexibility coefficients for the pile shaft and the pile based are expressed. It has to be mentioned that each pile is divided into several pile layers to better reproduce the pile behaviour up to the failure. This also allows for reproducing a stratified foundation ground if needed.

The coefficient for the pile shaft is defined as follows:

$$f_{s,i,j,k} = \frac{1+\nu}{E L_k \pi} \ln \left( \frac{r_m}{r_{i,j}} \right) \quad (3.11)$$

Where  $L_k$  represents the length of pile segment associated with the considered pile layer and  $r_{i,j}$  the distance between the pile  $i$  and the pile  $j$ . If piles are spaced so far apart that  $r_{i,j} > r_m$  with  $r_m$  the influence radius, the corresponding flexibility coefficient (see Section 3.2.2) is set to zero. Note that for the

influence coefficient  $f_{s,i,i,k}$  of one pile over itself, the value of  $r_{i,i} = r_p$  is used with  $r_p$  the radius of the pile. The coefficient for the pile base is:

$$f_{b,i,j} = \frac{1-\nu^2}{2r_p E} \text{ for } i = j \quad (3.12)$$

$$f_{b,i,j} = \frac{1-\nu^2}{\pi E r_{i,j}} \text{ for } i \neq j \quad (3.13)$$

Other equivalent expressions are commonly seen (for example in *Grabe and Pucker* (2011) [21] or *Chow* (1986) [7]) involving the shear stress modulus  $G$  instead of the stiffness modulus  $E$  using the well-known formula of Equation (3.14), valid for a homogeneous and isotropic material.

$$G = \frac{E}{2(1+\nu)} \quad (3.14)$$

Those expressions of the flexibility coefficients are well appropriate to model the pile-pile interaction in the form of matrices. The gathering of the different flexibility coefficient in matrices simplifies the implementation of the approach into a Python script.

### 3.2.3 Equilibrium of the pile group

The settlement of a pile is expressed as the sum of the products between pile resistance and influence coefficients as expressed Equation (3.15), with  $n_{piles}$  the number of piles in the group and  $n_{layer}$  the number of layers within a pile.

$$\begin{aligned} s_{s,i} &= \sum_{i=1}^{n_{piles}} \left( R_{s,i} \sum_{j=1}^{n_{piles}} \sum_{k=1}^{n_{layer}} f_{s,i,j,k} \right) \\ s_{b,i} &= \sum_{i=1}^{n_{piles}} \left( R_{b,i} \sum_{j=1}^{n_{piles}} f_{b,i,j} \right) \end{aligned} \quad (3.15)$$

Following the hypothesis of a rigid pile cap, the settlement is set to be the same for every pile and allows to deal with the global settlement  $s$ . Thus, one can calculate the settlement of the pile group as well as the resistance load for a given load using the condition of equilibrium. The equation system is expressed as follows:

$$A \mathbf{b} = \mathbf{c} \quad (3.16)$$

That is to say

$$\begin{pmatrix} F_{s,1} & 0 & 0 & 0 & -1 \\ 0 & \dots & 0 & 0 & -1 \\ 0 & 0 & F_{s,n_{layer}} & 0 & -1 \\ 0 & 0 & 0 & F_b & -1 \\ 1 & 1 & 1 & 1 & 0 \end{pmatrix} \begin{pmatrix} R_{s,i,1}^I \\ \dots \\ R_{s,i,n_{layer}}^I \\ R_{b,i}^I \\ s^1 \end{pmatrix} = \begin{pmatrix} 0 \\ \dots \\ 0 \\ 0 \\ 1 \end{pmatrix} \quad (3.17)$$



Where the submatrix  $(f_{s,i,j,k})$  containing the flexibility coefficients of the section  $k$  for every pile is noted  $F_{s,k}$ . Solving this equation in  $\mathbf{b}$ , one has access to the values  $s^I$ ,  $R_{s,i}^I$  and  $R_{b,i}^I$  representing the settlement and the pile resistances subject to a unit load.

$$\mathbf{b} = \mathbf{A}^{-I} \mathbf{c} \quad (3.18)$$

The multiplication with the total load  $F$  finally provides the numerical values of the settlement and of the resistances of the pile group.

$$\begin{aligned} s &= s^1 F \\ R_{b,i} &= R_{b,i}^1 F \\ R_{s,i} &= R_{s,i}^1 F \end{aligned} \quad (3.19)$$

### 3.2.4 Influence radius

As mentioned Section 3.2.2, an influence radius  $r_m$  is introduced to pilot the influence of the group effect between piles. This parameter depicts to what extent the mutual interaction between piles occurs following an empirical law. If piles are spaced so far apart that  $r_{i,j} > r_m$ , the corresponding flexibility coefficient is set to zero (see Figure 3.2).

Different propositions from several authors are regrouped by *Rudolf* (2005) [47] and adapted in Table 3.3. In Table 3.3, the thickness of the compressible layer  $H$  is defined as the thickness of the layer comprised between two incompressible layers, the earth's surface being seen as an incompressible soil layer. According to the definition of *Cooke* (1974) [9], the influence radius depends only on the pile diameter. The influence radius calculated with this simple formula is in almost every case underestimated. Formulas that include not only geometrical but also soil parameters have been developed afterwards to improve the proposition of *Cooke* (1974) [9].

The definition of *Randolph and Wroth* (1979) [46] is initially conceived for single piles and is extended to pile groups using the additional parameter  $r_g$ . This influence radius leads to overestimated values if the pile spacing is too large. Indeed, the additional term  $r_g$  has, in this case, an overstated impact on the influence radius.

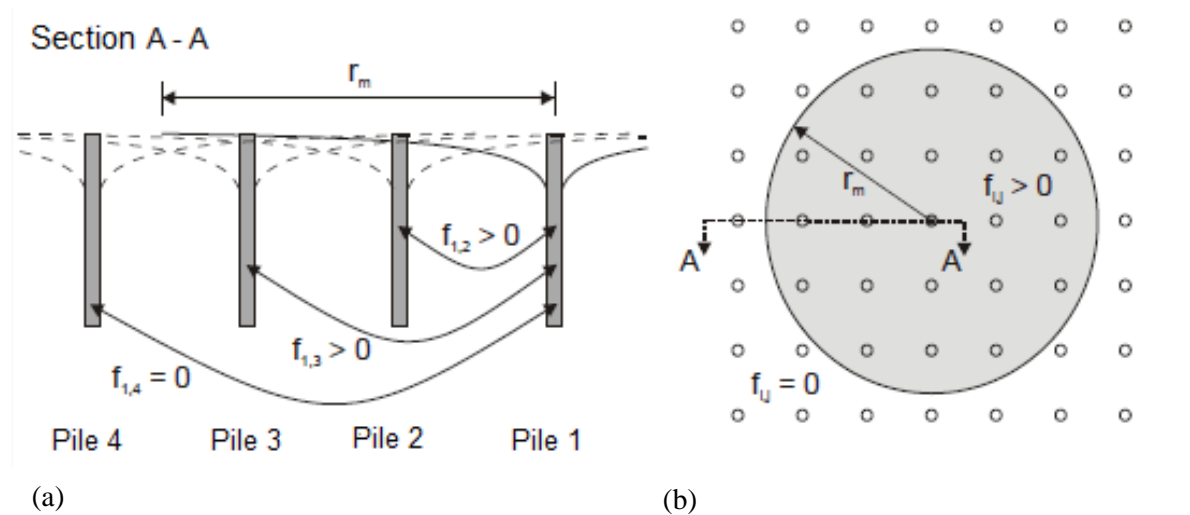


**Figure 3.2:** Dependency on the influence radius with influence coefficients (a) Cross-section through the pile group (b) Plan view of a pile group. Adapted from [47].

**Table 3.3:** Empirical models for the influence radius  $r_m$  (adapted from [47]).

Influence radius $r_m$ (m)	Source
$10 D$	<i>Cooke (1974)</i>
$2.5 L(1 - \nu) + r_g$	<i>Randolph and Wroth (1979)</i>
$1.1 D(1 - 3.5 \nu^{2.5}) \left(\frac{H}{L}\right)^{0.68} \left(\frac{L}{D}\right)^{0.85}$	<i>Liu (1996)</i>
$\alpha L(1 - \nu)$	<i>Lutz (2002)</i>
$\frac{1}{0.18182 + 0.43636 \frac{L}{H}} (1 - \nu) L$	<i>Lutz (2002)</i>
$L$	<i>Rudolf (2005)</i>

$r_g$  radius of the circle having the same area as the pile group

$D$  pile diameter,

$\nu$  Poisson's ratio,

$H$  thickness of the compressible layer,

$\alpha$  factor depending on  $H$  with  $2.5 \leq \alpha \leq 5.5$  and

$L$  pile length.

Both formulas of *Randolph and Wroth (1979)* and *Cooke (1974)* have been criticized – for instance by *Lutz (2002)* [37] – because the influence of the thickness of the compressible layer is not taken into consideration. *Lutz (2002)* [37] suggests that pile-raft and pile-pile interaction factors depend on the thickness of the compressible layer; that is why this depth should also appear in the calculation of the influence radius.

The parameter  $\alpha$  introduced by *Lutz (2002)* [37] to correct and extend the approach of *Randolph and Wroth (1979)* [46] varies between two extreme values, the smallest ( $\alpha = 2.5$ ) is obtained for a relation  $H = 2 L$  and the highest ( $\alpha = 5.5$ ) corresponds to an infinite extensive half-space. To determine the influence of the thickness of the compressible layer, a second empirical model was developed by *Lutz (2002)* [37] consisting of a hyperbolic relation between the coefficient  $\alpha$  and the ratio  $H/L$ .

Studies carried out by *Liu (1996)* [36] show that the influence radius mostly depends on both pile length and pile diameter. An interdependency is also determined between the influence radius and the thickness of the compressible layer, whose impact on the influence radius has a similar order of magnitude as the pile parameters. This formula must be handled carefully because for a substantial thickness of compressible layer, the radius of influence reaches infinite values.

*Rudolf (2005)* [47] mentions that the above presented propositions have been developed based on the linear initial area of the load-bearing behaviour of the pile group and are therefore not adapted to describe the real pile resistance distribution within the group. Based on the results of FEM calculations, *Rudolf (2005)* [47] finally recommends a simple relation between the radius of influence and the pile length.

### 3.2.5 Failure criterion

The failure criterion is evaluated for every pile layer of each pile following the yield criterion of Mohr-Coulomb as shown Equation (3.20).

$$F = \frac{1}{2} \sigma_1 (1 - \sin \varphi) - \frac{1}{2} \sigma_3 (1 - \sin \varphi) - c \cos \varphi \quad (3.20)$$

- $\sigma_1$  principal stress in direction 1,
- $\sigma_3$  principal stress in direction 3,
- $\varphi$  friction angle and
- $c$  cohesion.

The subdivision of the piles in different layers allows for an evaluation of the failure criterion in every section; the resistance-settlement curve thus presents a more realistic shape up to the failure.

A full failure by sliding (slippage) of a pile section is preceded by a non-linear soil behaviour in the surrounding area of the pile layer, which leads to a discontinuity in the soils parameters [7]. If full slippage occurs in a given pile layer, there is no further interaction between that pile section and the other sections of the group.

If the failure criterion is not fulfilled, the matrix  $\mathbf{A}$  gathering the influence coefficients (see Equation (3.17)) has to be adapted. If, for example, the failure occurs on the first layer ( $k = 1$ ) of the pile number 1 of a 2x2 pile group, the corresponding flexibility coefficients of the submatrix  $\mathbf{F}_{s,I}$  whose either index  $i$  or  $j$  with  $i \neq j$  takes the value 1, are set to zero (see Equation (3.21)). This means physically that for next load iterations, no more pile shaft force is added for this pile layer.

$$\mathbf{F}_{s,I} = \begin{pmatrix} f_{s,1,1} & 0 & 0 & 0 \\ 0 & f_{s,2,2} & f_{s,3,2} & f_{s,4,2} \\ 0 & f_{s,2,3} & f_{s,3,3} & f_{s,4,3} \\ 0 & f_{s,2,4} & f_{s,3,4} & f_{s,4,4} \end{pmatrix} \quad (3.21)$$

The last element of the corresponding line (in this example the last element of the first line of the matrix  $\mathbf{A}$  defined Equations (3.16) and (3.17) , i.e. the coefficient -1 that is multiplied with the settlement) is also set to 0. Indeed, when a layer breaks down, no more settlement occurs. Since  $f_{s,1,1}$  is different from 0, the corresponding resistance  $R_{I,I}^I$  of the matrix  $\mathbf{b}$  takes the value 0 to maintain the equilibrium.

It has been shown that usually the failure never happens in the base for usual cases [47] or at least appears for higher settlements (i.e. higher actions) than for the shaft. This is because the base resistance increases up to very large settlements whereas the limit value of skin friction  $q_s$  is usually reached at relatively small pile displacements [34], see Section 2.1. If in any case, a failure occurs in the pile base, the same adaptation of the matrix  $\mathbf{A}$  as for the pile shaft is needed.

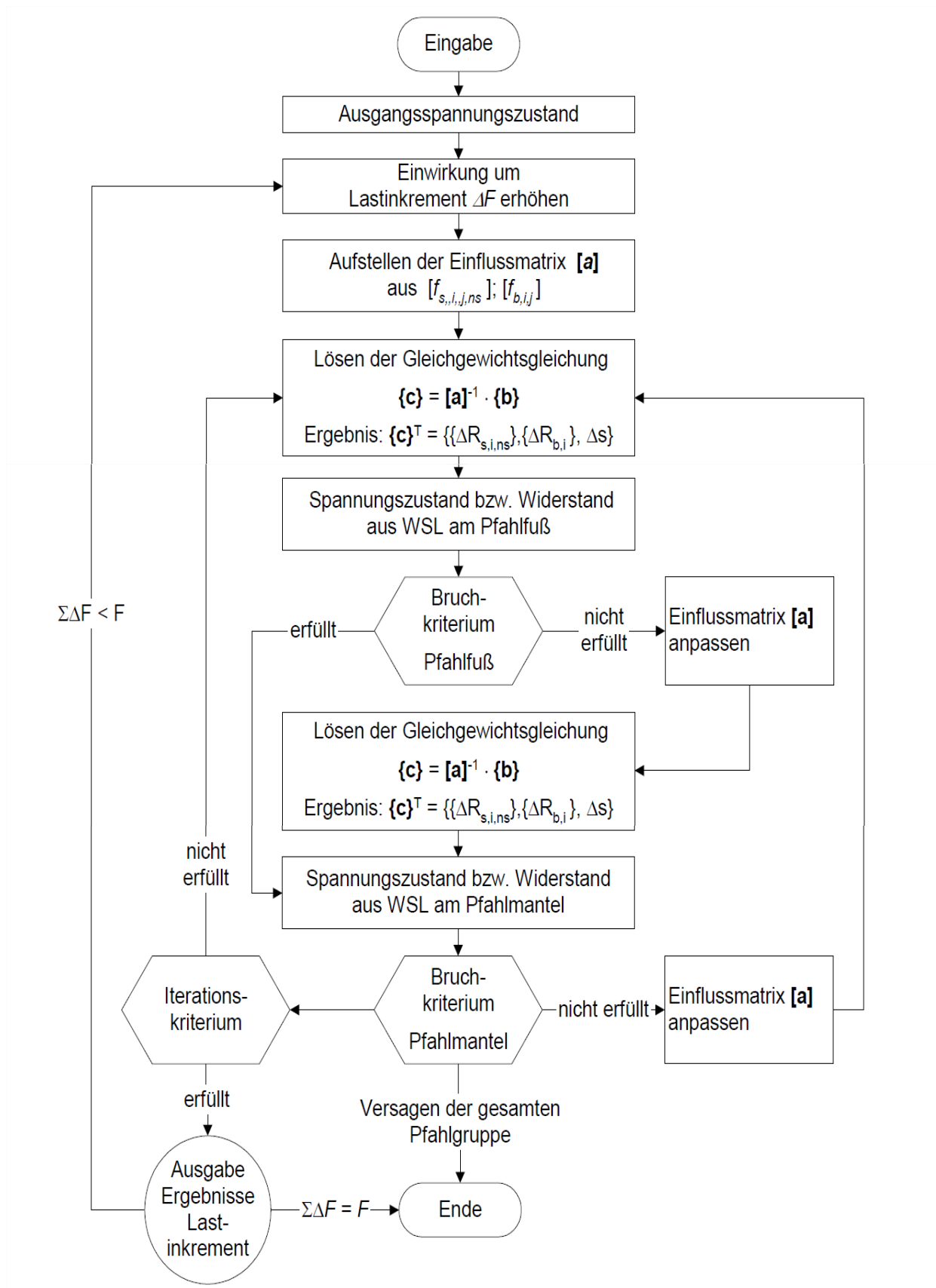
### 3.2.6 Workflow

The implemented calculation method, whose properties and major theories are presented within this section, can be summarised in a workflow (see Figure 3.3). The calculation method proposed by *Rudolf* (2005) [47] is an iterative procedure. By applying the last step by step the non-linear load-settlement behaviour of the soil can be better predicted.

The input parameters are the geometry of the piles and the parameters of the soil. The flexibility coefficients calculated following Equations (3.11) and (3.12) are gathered in the matrix  $\mathbf{A}$  as presented in the Equation (3.18). The equation of equilibrium is calculated for a unit load, the stress and settlement state are set up afterwards using Equation (3.19).

The failure criterion (3.20) is then applied to this state. If the failure criterion of the base is not fulfilled, the matrix  $\mathbf{A}$  is adapted and the equation of equilibrium is solved again, leading to new stress and settlement state (state (1)). Otherwise, the next failure criterion (this time for the shaft) is verified immediately (and the state (1) is simply equal to the initial state (0)). The same pattern is then repeated for the pile shaft, leading (or not) to a new stress and settlement state (state (2)).

The calculation procedure presents two distinct loops: the first one, or major loop, runs until the total load is applied (the incremental load is calculated as the total load divided by the number of increments). The second one, encapsulated within the major loop, is running while the two different stress and settlement states (1) and (2), which are calculated after each failure criterion, do not differ of more than 1% (called iteration criterion).



### 3.3 Modifications and improvements

To describe the pile group more realistically and to render the design applicable to generic structures, modifications and improvements were made to the analytical procedure presented in Section 3.2. Those modifications are in any case required by the current codes (EC7 [20] and DIN 1054:2005 [14]). Indeed, Eurocode 7 introduces new requirements regarding the calculation of pile groups, in particular, a more realistic and precise approach of:

- the group effect of a pile group,
- the settlement differences between piles of a group called differential settlement and
- the non-linear load-bearing behaviour.

The modifications and improvements had a positive effect on the precision in the above-listed features.

#### 3.3.1 Accuracy of the influence radius

To compare the different influence radii obtained with the empirical models in Table 3.3, a 4×4 pile group with a constant pile spacing of six meters and a Poisson's ratio of the soil of 0,4 has been studied. The results are presented in Figure 3.4, which shows the influence radius for the group effect. The radii of influence have to be understood as it is illustrated in Figure 3.2: piles positioned outside each circle see their influence coefficient set to zero whereas piles positioned inside each circle see their influence coefficient calculated following the Equation (3.11). Note that the circles, defined by their corresponding radius of influence, are here represented with their centres in the middle of the pile group to give an overview. Normally, they have to coincide with every pile alternatively, as shown Figure 3.5 using the first pile of the pile group as an example. It can be observed Figure 3.5 that a corner pile interacts with fewer other piles than a centre pile.

As it can be noticed, there are tremendous differences between the obtained radii. The influence radius of *Cooke* (1974)  $r_{m,Cooke} = 6.0$  m is indeed four times smaller than the one of *Lutz* (2002) using the maximal admissible value of  $\alpha$ ,  $r_{m,Lutz, \alpha=5.5} = 26.4$  m. Extreme values are not appropriate to depict the group effect as they lead to either include all the piles within the radius of influence or exclude too many of them.

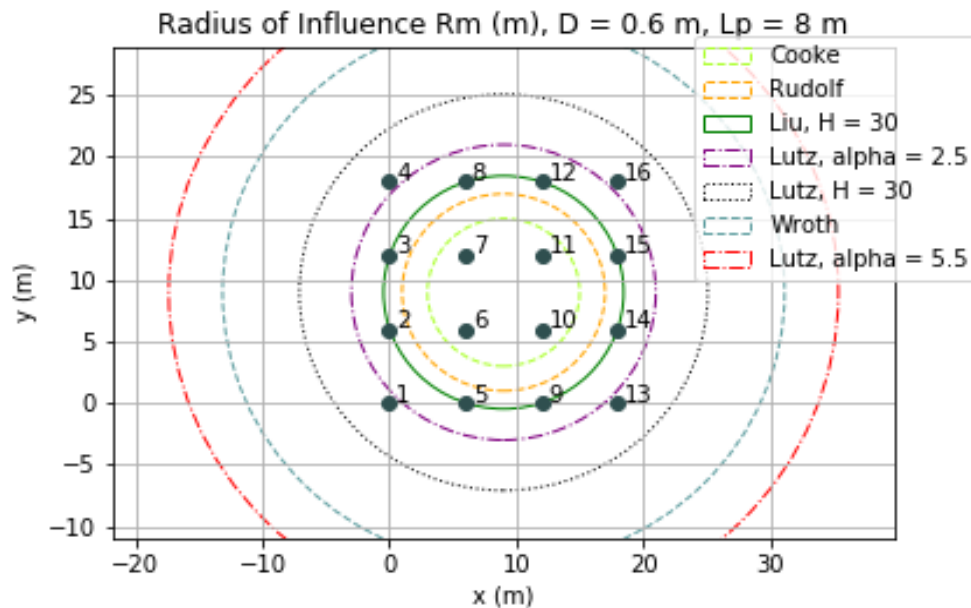


**Figure 3.4:** Representation of the influence radius using different empirical models.

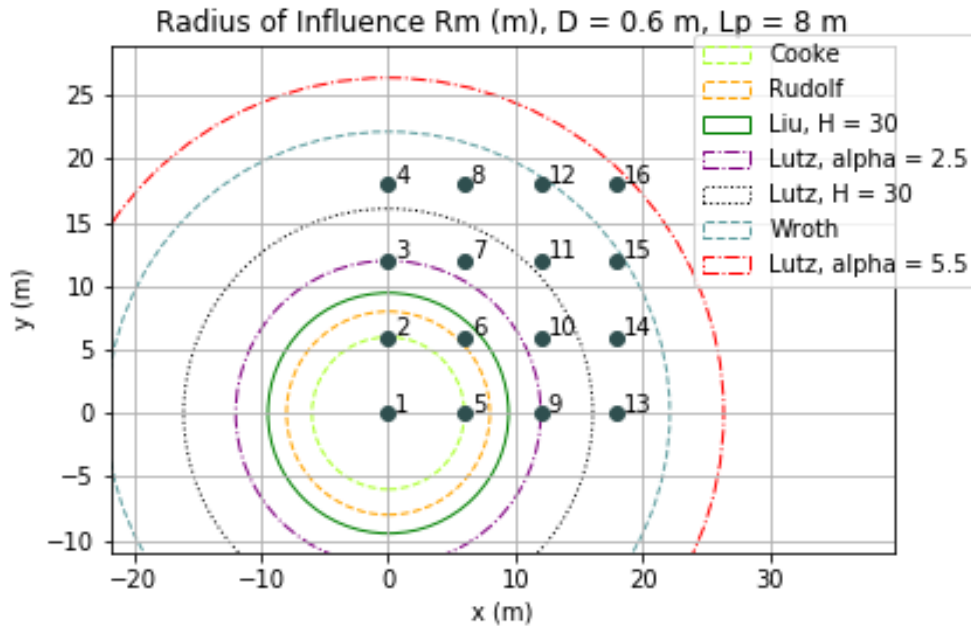


**Figure 3.5:** Radiuses of influence represented with their origin at the pile 1.

The current calculations are based on Lutz's formula with a value of  $\alpha = 2,5$  as it seems to offer the most appropriate trade-off. However, *Rudolf* (2005) [47] mentions that there is no perfect formula for calculating the influence radius. Radiuses are generally overrated, leading to an underestimation of the resistance of the inner piles. Indeed, the flexibility coefficients  $f_{i,j}$  grow as the influence radius increases, that is to say the pile resistance decreases to observe the equilibrium of Equation (3.15).

All empirical models in Table 3.3 were implemented into a Python file. The user can thus easily choose which model to apply. After that, the algorithm asks for the input parameters defined in Table 3.3.

### 3.3.2 Comparison of flexibility coefficients

Two different models of the pile group effect were studied, one by *Rudolf* (2005) [47] presented in Section 3.2 and the other by *Chow* (1986) [7] shown below.

The solution proposed by *Chow* (1986) [7] includes a subdivision of every pile into several nodes as illustrated in the example Figure 3.7. Interaction effects between nodes within the same pile are ignored. That is to say,  $f_{i,j}$  is set to 0 if  $i$  takes values in the nodes of the pile  $j$  (where the load is applied), except if  $i = j$ ; in that case, the same coefficient is applied as in *Rudolf* (2005) [47].

The calculation is based on the continuum mechanic theory of *Mindlin* (1936) [38], which is valid for a vertical point load in a homogeneous, isotropic elastic half-space:

$$f_{i,j} = \frac{1}{16 \pi G(1-\nu)} \left[ \frac{3-4\nu}{R_1} + \frac{8(1-\nu)^2 - (3+4\nu)}{R_2} + \dots \right. \\ \left. \dots + \frac{(z-c)^2}{R_1^3} + \frac{(3-4\nu)(z+c)^2 - 2cz}{R_2^3} + \frac{6cz(z+c)^2}{R_2^5} \right] \quad (3.22)$$

- $z$  depth of the node where the displacement is evaluated (node  $i$ ),  
 $c$  depth of the node where the load is applied (node  $j$ ),  
 $R_1$  equals  $\sqrt{r^2 + (z - c)^2}$   
 $R_2$  equals  $\sqrt{r^2 + (z + c)^2}$   
 $r$  distance between node  $i$  and node  $j$ ,  
 $\nu$  Poisson's ratio and  
 $G$  shear stress modulus.

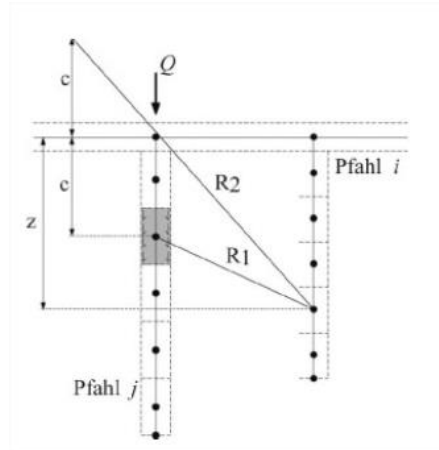


**Figure 3.6:** Calculation of the flexibility coefficients after Mindlin (1936) [38] in [21].

The different parameters are well represented by *Grabe and Pucker* (2011) [21] (see Figure 3.6). If the soil is non-homogeneous, the mean value of the soil shear modulus at node  $i$  and node  $j$  replaces the constant shear modulus of the homogeneous soil.

Both calculation methods are compared by using a simplified two-dimensional pile group composed of three piles and subdivided into twelve nodes (see Figure 3.7). The calculated coefficients are gathered into “Flexibility matrices”, with each element of the matrix containing the corresponding flexibility coefficient, as illustrated in Figure 3.8. The flexibility matrix after *Rudolf* (2005) [47] (Figure 3.8 (a)) appears easy to follow: each pile is represented by a square of the same colour, and there is no subdivision into nodes within a pile. The reciprocal influence of the two border piles – represented by the two squares on the bottom left and the top right of the matrix in white – is smaller than the influence of two neighbouring ones because of the larger distance separating them. The group effect is also more significant for the pile base as for the shaft.

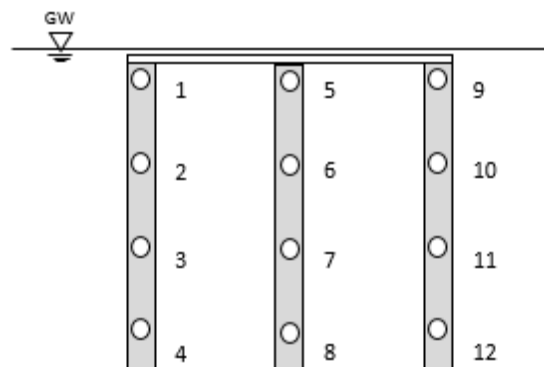


**Figure 3.7:** Position of the nodes for a two dimensional pile group study.



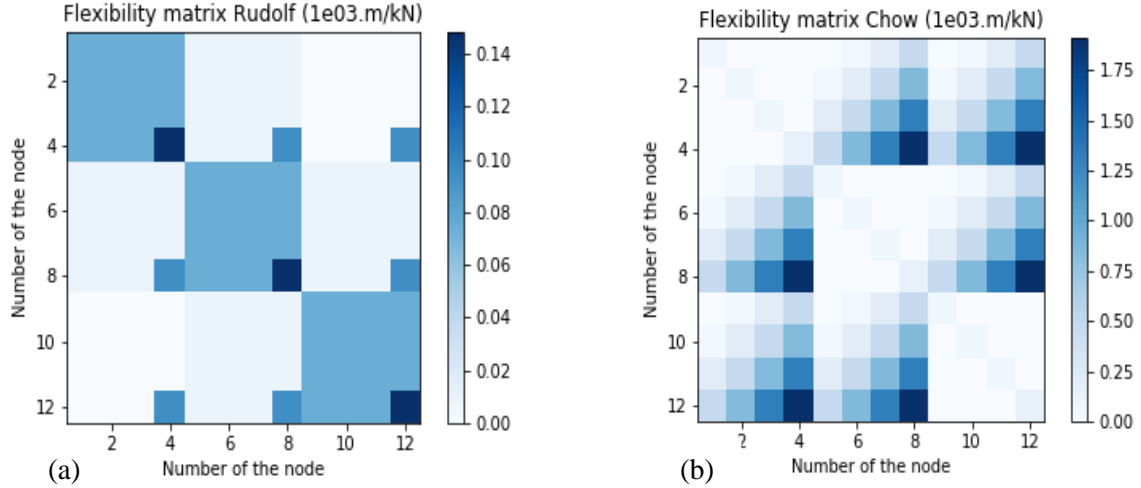


**Figure 3.8:** Flexibility matrix using the theories of (a) *Rudolf* (2005) [47] (b) *Chow* (1986) [7].

It can be observed that the coefficients after *Chow* (1986) [7] are about ten times higher than those used by *Rudolf* (2005) [47]. Furthermore, the influence of node 4 over node 8 is greater than over node 7, which itself is higher than over 6, etc., due to the greater distance separating the nodes. It has to be noted, however, that the influence of node 4 over node 12 is of the same order of magnitude than over the node 8, even if the node 12 is two times further than the node 8.

The flexibility coefficients after *Rudolf* (2005) [47] were implemented as they offer lower values of the coefficients. Indeed, it is shown in Section 3.2.4 that the influence radius and thus the influence coefficient are generally overrated. Moreover, the flexibility coefficients after *Rudolf* (2005) [47] depict the subject matter in a more comprehensive way.

It has to be mentioned that both solutions presented above are valid for linear soil behaviour, they only offer an approximation of the real interaction effects. Both authors proposed iterative methods to apply the total load step by step and thus take into account the non-linearity of the soil behaviour.

### 3.3.3 Soil stiffness

The calculation procedure of *Rudolf* (2005) [47] using a constant stiffness modulus of soil is extended by adopting a depth-dependent soil stiffness. Indeed, this stiffness modulus is not constant in the reality but grows with an increasing stress state. The subdivision of the model into different layers makes possible that a stress state and thus a modulus can be calculated for every layer.

*Von Soos and Engel* (2008) [49], among others, take into account the dependency of the stiffness modulus with the depth and hence expresses the stiffness of the soil as presented in Equation (3.23).

$$E_s = \nu_e \sigma_{ref} \left( \frac{\sigma}{\sigma_{ref}} \right)^{w_e} \quad (3.23)$$

$\sigma_{ref}$  reference pressure, usually set to 100 kPa,

$\nu_e$  dimensionless parameter that pilots the variation of the soil stiffness with depth (the product  $\nu_e \sigma_{ref}$  is the equivalent of  $E_{ref}$  in Grabe and Pucker (2011) [21]) and

$w_e$  dimensionless parameter comprised between 0 and 1 (corresponds to  $n$  in Grabe and Pucker (2011) [21]).

**Table 3.4:** Typical values of  $v_e$  and  $w_e$  for different soils adapted from [49].

	$w_e$	$v_e$
Medium plastic clay	30	0.9
Lightly plastic silt	110	0.6
Uniform fine sand	300	0.6
Well graded sand	600	0.55

The exponent  $w_e$  is according to experience comprised between 0.4 and 0.7 for sands and between 0.8 and 1.0 for plastic clay. Some typical values of these dimensionless parameters are given in Table 3.4. It has to be mentioned that the values of the stiffness modulus also vary from place to place within a homogeneous layer. This variation is not considered in the present study.

### 3.3.4 Loading cases

Contrary to the analytical procedure after *Rudolf* (2005) [47], the pile group is no longer assumed to be only subject to a central vertical load (see Section 3.2.1). The algorithm is modified so that a different vertical load can be applied to every pile. This facilitates the modelling of problems where the structure to support is not obviously symmetrical and where a part of the foundation is more loaded than the others.

To ensure a simple analytical calculation, vertical equivalent loads are used, to take into account the action of horizontal loads. Two load models are seen as equivalent if they generate the same loading state. An equivalent model is made possible by the means of a pair of loads directed in opposite directions (Figure 3.9). As seen in Section 2.1, the application of horizontal forces also increases the intensity of vertical forces. This loading case can now be considered more precisely by a modification of the distribution of the loads.

Following the same pattern, it can be assumed that bending moments applied on the structure lead to the apparition of an asymmetrical vertical loading. Bending moments can also be generated by the application of horizontal loads; in this case, it is referred to the equivalence presented in Figure 3.9.

**Figure 3.9:** Horizontal load equivalence with a pair of loads operating in opposite directions [47].

### 3.3.5 Geometrical parameters

The developed algorithm allows for more variation regarding the geometrical parameters such as the pile length and its position.

The code is indeed extended to give possibility to set a different pile length  $L_i$  for every pile. This is in particular useful for the optimisation of the foundation that will be achieved in Section 6.2. The graduation of the pile length constitutes a major improvement in the foundation design: piles subject to higher loads can be lengthened whereas other piles are shortened. This is, for example, the case with central axially loaded foundations: corner and edge piles can be designed shorter than the inner piles as they transfer a lower load to the ground.

The user is also enabled to set the position of a pile using its Cartesian coordinates, rather than only a constant pile spacing, which only permits the conception of rectangular and constantly spaced piled raft. Round CPRFs can, for example, be created. This solution concurs in the minimisation of the total cubature of CPRFs.

### 3.3.6 Differential settlement

The fact that a unique settlement is considered for the whole structure is a major limitation to the analytical method of *Rudolf* (2005) [47]. The assumption that the foundation slab is rigid prevents from conceiving a model that depicts the real settlement of the structure.

A differential settlement for each pile can easily be modelled by using a vector  $s^I$  of size “number of piles” instead of a scalar  $s^I$  and by creating a loop over the number of piles for each calculation of the settlement. The Equation (3.19) is therefore modified to consider the settlement as a vector (see Equation (3.24)).

$$\begin{aligned} s_i &= s_i^1 F_i \\ R_{b,i} &= R_{b,i}^1 F_i \\ R_{s,i,k} &= R_{s,i,k}^1 F_i \end{aligned} \quad (3.24)$$

It needs to be noted that the load was also transformed into a vector to take a distributed load into account as it has been explained in Section 3.3.4. The iteration procedure is therefore modified, and the simplified description of the calculation presented in Equation (3.24) can be divided into two different steps shown in Equations (3.25) and (3.26). Instead of calculating a unique incremental load for all the piles  $\Delta F$ , an incremental load  $\Delta F_i$  is necessary for each pile  $i$ , which increases the complexity of the iteration procedure. After each resolution of the equation of equilibrium, the results contained in the vector  $\mathbf{b}$  (see Equation (3.18)) are multiplied with the corresponding incremental load to obtain the incremental stress and settlement state of each pile, see Equation (3.25).

$$\begin{aligned} \Delta s_i &= b(s_i) \Delta F_i \\ \Delta R_{b,i} &= b(R_{b,i}) \Delta F_i \\ \Delta R_{s,i,k} &= b(R_{s,i,k}) \Delta F_i \end{aligned} \quad (3.25)$$

Then the stress and settlement state is set up by adding the existing state with the incremental values (Equation (3.26)). This iteration procedure is summarised in Figure 3.10, where the resistance-settlement curve of one pile is subdivided into the different incremental states.

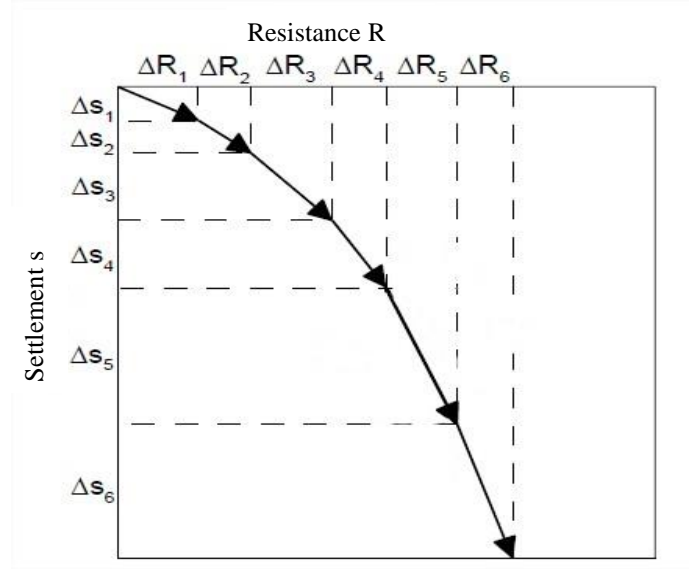


**Figure 3.10:** Resistance-settlement curve of one pile showing the schematic steps of the iteration procedure. Adapted from [47].

$$\begin{aligned}
 s_i &= s_i + \Delta s_i \\
 R_{b,i} &= R_{b,i} + \Delta R_{b,i} \\
 R_{s,i,k} &= R_{s,i,k} + \Delta R_{s,i,k}
 \end{aligned} \tag{3.26}$$

It should also be noted that the settlement differences are only affected by the variation of the load exerted on each pile. Indeed, as it has been shown in Equation (3.17), only the scalar settlement for the whole structure is affected by the group effect in the resolution of the equation of equilibrium. The settlement subject to a unit load, which is calculated by solving the equation of equilibrium of Equation (3.18) is then multiplied by the incremental load for each iteration. This settlement is thus affected by the variation of the load exerted on each pile. To study the influence of the loading distribution over the settlement, two different load cases are compared in Figure 3.11. The geometrical and soil parameters used for this comparison are those of the case study on pile groups that will be developed in Chapter 5.

Figure 3.12 compares the distribution of the pile resistances and of the differential settlement for a constantly and a linear distributed load. As it becomes visible, the settlement stays constant (18 cm) for a constantly distributed load of 5 MN, whereas the settlements are increasing for an increasing load (21 cm for a load of 6 MN) and inversely. The modified algorithm allows to model the differential settlement required by Eurocode 7.

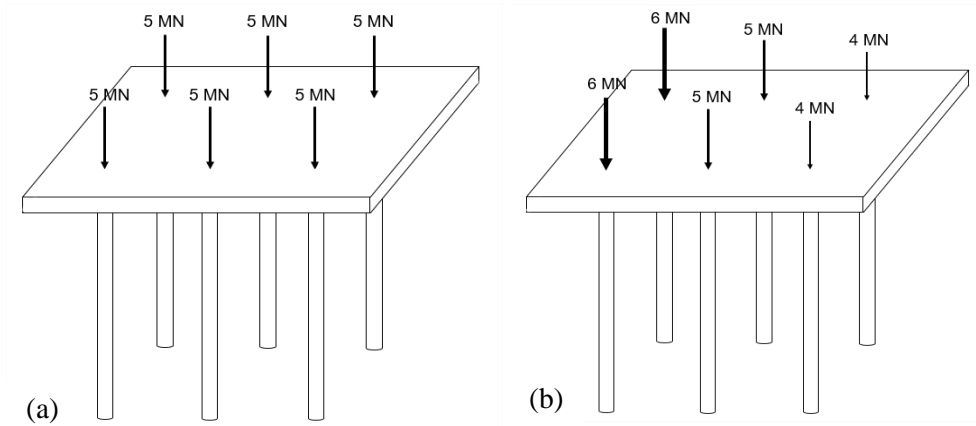


**Figure 3.11:** Distribution of a total load of 30 MN over six piles (a) constantly distributed load (b) linear distributed load.

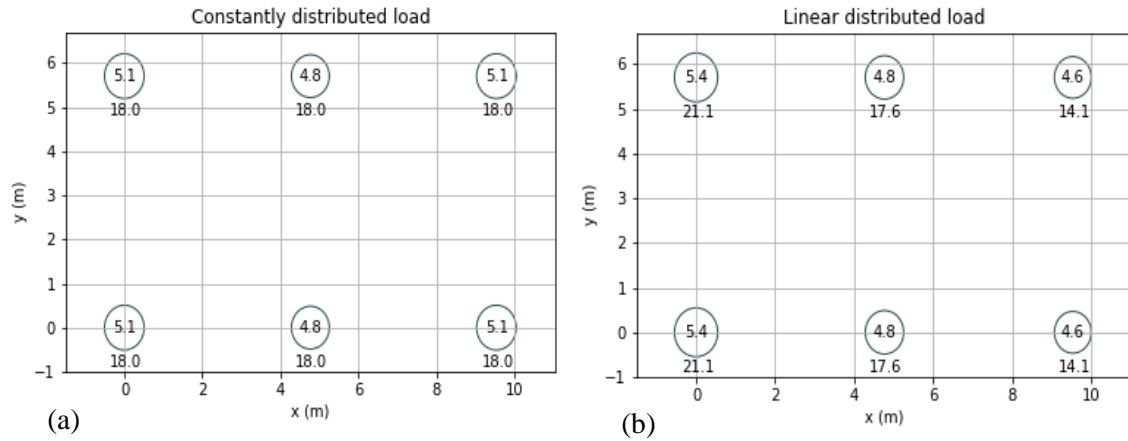


**Figure 3.12:** Distribution of the pile resistances (MN, inside the circles) and of the settlement (cm, below the circles) for a constantly distributed load (a) and a linear distributed load (b).

### 3.3.7 Object oriented programming

The developed code is object-oriented, meaning that the scripts are designed with objects that are interacting with each other. Indeed, the language Python is based on the concept of classes, whose instances are called “objects”.

The development of an object-oriented script is necessary for the optimisation, which will be presented in Chapter 6. Indeed, to code a problem in the optimisation library Pygmo, it is necessary to transfer the results of the object “pile group” to another class, which is defining the problem to optimise. The optimisation is therefore not possible without this type of programming. Moreover, the code is easily readable for a new user due to the numerous comments and the referencing of the different equations used. The structure of the code is also improved.

A major advantage of the object-oriented programming is its code reusability: the created objects can easily be reused in other programs. The code maintenance is also facilitated as the object oriented programs are easier to modify and maintain than non-object oriented ones. The legacy of the code must indeed be considered from its inception, either to improve its features easily in the future or to modify it to be compatible with more recent computers and software.

### 3.3.8 Workflow

The design approach is summarised in a workflow presented in Figure 3.14, where the major improvements and modifications made from the initial workflow of Rudolf (2005) [47] shown in Figure 3.3 are highlighted in red. Moreover, in order to better depict the implemented calculation procedure, the structure of the workflow has been slightly adapted.

Major improvements are made within the input of the calculation procedure. Indeed, this step gathers the various modifications made on the loading cases (differentiation of the vertical load for each pile  $V_i$ , introduction of horizontal loads  $H_i$  and bending moments  $M_i$ ), the pile length differences for each pile  $L_i$  and the user-defined geometry of the piles.

The stiffness of the soil is not constant anymore but depends on the stress state of the subsoil. Thus, the stiffness modulus must be updated for every stress state that is calculated. The soil stiffness is also implied in the calculation of the flexibility coefficients for the pile base  $f_b$  and for the pile shaft  $f_s$ , which must be updated according to the new stress state.

Moreover, the accuracy of the influence radius has an impact on the flexibility coefficients of the pile shaft  $f_s$ , which is modifying as a consequence the flexibility matrix  $A$ .

Differential settlement is taken into account for the calculation of every new settlement state, leading to the implementation of additional iterative loops over the number of piles. The iteration procedure is also modified as the incremental load is different for every pile. Therefore, the number of “major loops” as defined in Section 3.2.6 increases by a factor “number of piles”.

### 3.4 Limitations and drawbacks

In spite of these improvements and modifications, the developed algorithm still shows some limitations and drawbacks.

It should be noted that in the literature, no interaction between the radius of influence and the loading of the pile group has been taken into account so far. It might be assumed that the higher the loading, the longer the radius of influence, since the loading is influencing the soil in a larger extent and therefore could affect piles placed further away.

The Mohr-Coulomb failure criterion (MC) is a simple but effective failure criterion given in the state of the art (e.g. EC7 [20]). Other more advanced criteria like those of Lade-Duncan (LD) or Matsuoka-Nakai (MN) presented in Figure 3.13 would offer a high stress level of failure, but ask for different input parameters, which are difficult to derive from standard laboratory investigations. MN and LD yield surfaces are smoother versions of the MC yield surface. *Huber* (2013) [26] indicates that the choice of the constitutive failure criterion within a linear elastic, perfectly plastic constitutive model has a significant impact on the bearing capacity as well as on the failure probability of foundations.

Moreover, the horizontal loads and bending moments are not applied directly but modelled using equivalent loads, which is only an approximation. Indeed, a realistic equivalent should require a horizontal bedding as it is illustrated in Figure 3.9. However, this horizontal bedding is not implemented in the developed analytical calculation; therefore, the calculation developed in this thesis should be limited to the design of initial and tender projects and not for detailed planning.

The analytical method developed in this section and coded in a Python script only describes the load-bearing behaviour of pile groups, which can be extended for the design of combined piled raft foundations.

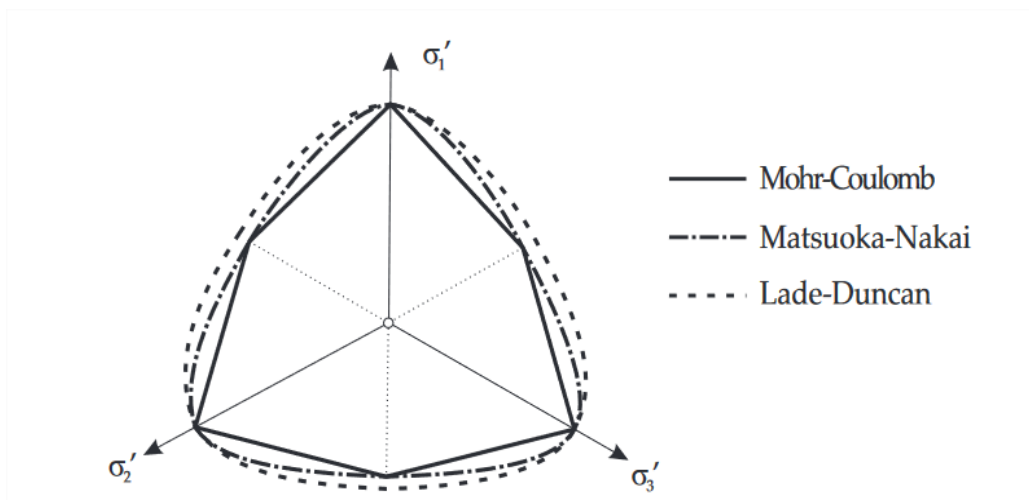


**Figure 3.13:** Failure criteria of Mohr-Coulomb, Matsuoka-Nakai and Lade-Duncan represented on the deviatoric plane [26].

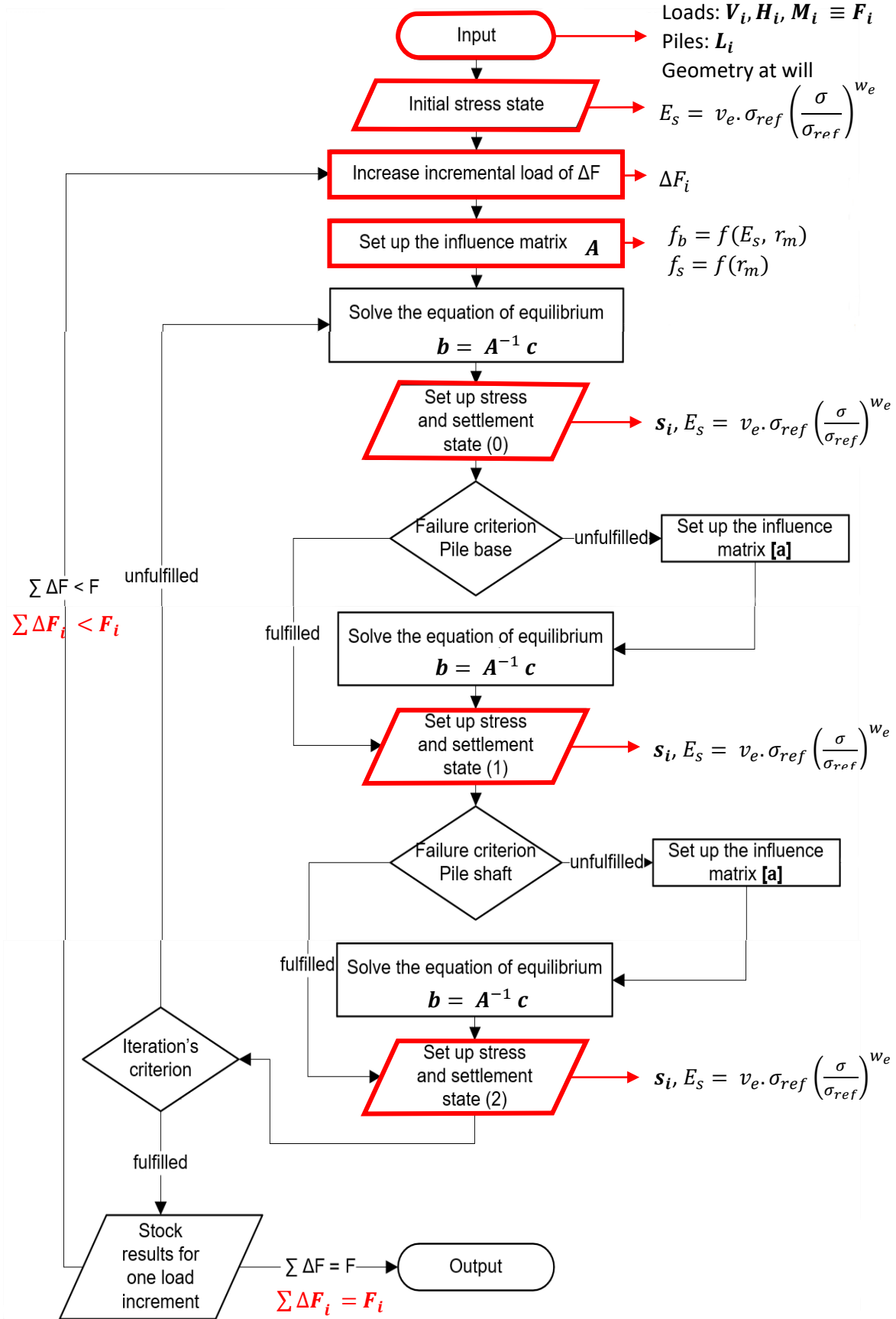


**Figure 3.14:** Pile group design workflow of the Python script inspired from Rudolf (2005) [47] and improvements (highlighted in red).





## 4 Design of combined piled raft foundation

### 4.1 Literature review on piled raft foundations

Numerous calculation methods can be chosen for the design and the calculation of CPRF. All of them are based on different modelling schemes. These modelling schemes combined with different boundary conditions and simplified assumptions lead to disparate results. Many of these methods are only suitable for a preliminary design of CPRFs or in very simple cases. Only numerical methods can depict correctly the reality [31]; resorting to these methods is thus necessary for the design of complex projects. Similar to the design of pile groups, three main methods of calculation can be described: empirical, analytic and numerical calculation methods. In addition, calculation methods with equivalent models were used in the nineties, in which the CPRF were substituted by deep shallow foundations or thick single piles. An overview of the existing calculation methods is presented in Table 4.1. The overview of the different methods, including their complexity presented in Table 3.1, is still valid for the design of combined piled raft foundations.

#### 4.1.1 Equivalent models

In equivalent methods, the CPRF is replaced by a strongly simplified foundation, commonly by a shallow foundation or a thick single pile. The calculation is then carried out for this substitute model. These methods can be separated into two main approaches: the equivalent raft method and the equivalent pier method.

In the equivalent deep shallow foundation (or equivalent raft method) proposed by *Poulos* (1993) [42], the action is applied on a virtual equivalent surface, which is situated at a specified depth under the CPRF. This surface is determined depending on the loading case and the initial geometry of the raft. The calculated settlement results from the settlement of the substituted surface, which takes the influence of the piles into account. The settlement of the equivalent surface is determined using the elasticity theory of shallow foundations in an elastic, isotropic half-space. This method has been modified by *Thaher* (1991) [51], who uses a semi-empirical approach. The load-bearing behaviour of the raft is described analytically (employing the stiffness modulus method) and the modelling of the piles follows an empirical approach.

In the case of the equivalent pile method according to *Poulos* (1993) [42], the pile group is replaced by an equivalent single pile, whose diameter and stiffness is calculated based on approximated formulas.

#### 4.1.2 Empirical methods

Empirical calculation methods are based on in situ measurements and model tests. The load-bearing capacity of a pile is deduced by means of correlations and tabled values referring to similar soils and similar geometrical configuration of piles. The results of laboratory and field tests also allow for the determination of the load-bearing behaviour of pile groups. Moreover, various empirical methods are taking into consideration the group effect using empirical approaches.

**Table 4.1:** Calculation methods for a combined piled raft (adapted from [47]).

Method	Approach	Remark
<b>Numerical</b>		
<i>Davis and Poulos</i> (1972)	FDM (Finite difference method), superposition	
<i>Butterfield and Banerjee</i> (1981)	BEM	
<i>Poulos</i> (1994)	BEM, superposition	Non-linear load-bearing behaviour
<b>Hybrid numerical (both BEM and FEM)</b>		
<i>O'Neil</i> (1981)	Hybrid model	
<i>Chow</i> (1986)	Modified hybrid model	
<i>El-Mossallamy</i> (1996)	Slab: FEM Group effect: BEM	Non-linear load-bearing behaviour
<b>Analytical</b>		
<i>Randolph</i> (1983)	Superposition	Linear-elastic
<i>El-Mossallamy</i> (1996)	Principle of path-independent support	
<i>Lutz</i> (2002)	Superposition	Linear-elastic
<i>El-Gendy et al.</i> (2006)	Hybrid, based on empirical values	Non-linear load-bearing behaviour
<i>Vrettos</i> (2006)	Superposition	Linear elastic, irregular geometry
<b>Empirical</b>		
	Correlation of the load-bearing behaviour of a single pile using laboratory and field tests.	
	Consideration of the group effect using empirical approaches.	
<b>Equivalent methods</b>		
<i>Thaher</i> (1991)	Modified deep shallow foundation	
<i>Poulos</i> (1993)	Deep shallow foundation ("equivalent raft method")	
<i>Poulos</i> (1993)	Thick single pile ("equivalent pile method")	

#### 4.1.3 Analytical methods

Two different approaches can be used for the analytical methods. One possibility is to begin the calculation studying exclusively a shallow foundation and to incorporate elements of deep foundations afterwards. The other possibility is to initiate the calculation with the deep foundation and add the elements of the shallow foundations (such as the slab) subsequently. For example, the load-bearing capacity of the raft is calculated by first neglecting the piles. If the loads exceed the bearing capacity of the raft, the remaining loads are divided among the piles [31]. Analytic methods often present the main

disadvantage that not all interaction effects are regarded. This approach is thus convenient as a first assessment.

It is not excluded that analytical methods make use of some empirical equations to model the load-bearing behaviour structural elements (see for instance *El-Gendy et al.* (2006) [18]). The frontier between these two calculation methods is not always clearly defined as most of the time geotechnical engineering is based on empirical constitutive laws.

One of the simplest analytical methods for the estimation of the load-bearing behaviour of CPRFs is the principle of path-independent support (“Prinzip der wegunabhängigen Stützung” in German), used for instance by *El-Mossallamy* (1996) [19]. As a first step, the maximal bearing capacity of the raft is determined by disregarding the load distribution in the pile group. Every pile constituting the group is then seen as an independent single pile with no consideration of the pile-pile interaction. The assumption is made that the settlement of the raft is so high that the ultimate bearing capacity of single piles is completely mobilised. The determination of the CPRF settlement equals the settlement of the raft under the previously determined loading case. This method presents the main disadvantage that pile-pile and pile-raft interactions are neglected.

Other analytical methods are predominantly based on the theory of elasticity. The approximation procedure of *Randolph* (1983) [45] is initially conceived for a single “pile with cap” and extended to piled raft foundations. The approach of *Randolph* (1983) [45] is based on the idea that the behaviour of CPRFs can be expressed in the form of a load-settlement relation summarised in Equation (4.1).

$$\begin{pmatrix} w_{pp} & w_{pc} \\ w_{cp} & w_{cc} \end{pmatrix} \begin{pmatrix} P_p \\ P_c \end{pmatrix} = \begin{pmatrix} w_p \\ w_c \end{pmatrix} \quad (4.1)$$

- $w_p$  pile group settlement,
- $w_c$  cap settlement,
- $w_{pp}$  settlement of the pile group under a unit load,
- $w_{cc}$  settlement of the cap under a unit load,
- $w_{cp}$  pile group settlement due to a unit load on the cap,
- $w_{pc}$  cap settlement due to a unit load on the pile group,
- $P_p$  loading of the pile group and
- $P_c$  loading of the pile cap.

The main diagonal contains variables that describe the load-settlement behaviour of the pile ( $w_{pp}$ ) and the cap ( $w_{cc}$ ) separately. Factors situated outside the main diagonal describe the interaction between elements of the CPRF. This matrix is often called “stiffness matrix” of the CPRF because the inverse of a settlement under unit load has the same unit as a stiffness. Under the condition of compatibility (or “reciprocal theorem” [37])  $w_{pc} = w_{cp}$ , it is possible to calculate the total stiffness of the CPRF  $k_{PR}$  as in Equation (4.2), where  $\alpha_{cp}$  is the pile-raft interaction factor.

$$k_{PR} = \frac{k_p + k_c (1 - 2\alpha_{cp})}{1 - \alpha_{cp}^2 \frac{k_c}{k_p}} \quad (4.2)$$

with  $\alpha_{cp} = \frac{w_{cp}}{w_{pp}}$ ,  $k_c = \frac{1}{w_{cc}}$  and  $k_p = \frac{1}{w_{pp}}$ .

For the determination of the load-settlement behaviour of the pile cap ( $w_{cc}$  or indirectly  $k_c$ ), formulas proposed by *Poulos and Davis* (1974) [43] are adopted.

As for the settlement of the pile group  $w_{pp}$ , the solution of *Randolph and Wroth* (1979) [46] presented in Section 3.1.2 is applied, where the settlement of the pile group is obtained by superposition of the settlement trough of every single pile. Another variant also proposed by *Randolph* (1983) [45] does not have recourse to a superposition method but uses a group effect whose interaction factors are introduced by *Poulos and Davis* (1974) [43].

Due to the symmetry of the stiffness matrix (Equation (4.1)) and using further approximations and simplifications together with a comparison with numerical simulations and empirical values, the interaction factor  $\alpha_{cp}$  can be estimated. This approximation enables to calculate simply the factor  $w_{cp}$  as presented in Equation (4.3).

$$w_{cp} = w_{pc} = w_{pp} \frac{\ln\left(\frac{r_m}{r_c}\right)}{\ln\left(\frac{r_m}{r_o}\right)} \quad (4.3)$$

$r_o$  pile radius,

$r_m$  radius of influence and

$r_c$  equivalent radius of the pile cap.

The load-settlement behaviour of the CPRF is then completely known. This analytical approach is the basis for various extended approaches. *Vrettos* (2006) [53] extends the approach of *Randolph* (1983) [45] to take into account a variable pile spacing and a different pile length for every pile. This method also allows for a differentiation of the load-bearing behaviour of edge piles from the one of inner piles.

In the modified approach of *Lutz* (2002) [37], the deduction of the stiffness matrix occurs using different formulas than those of *Randolph* (1983) [45]. The load-settlement behaviour of the cap described by  $w_{cc}$  is obtained using the formula of *Steinbrenner* (1934) [50]. The pile-raft interaction  $w_{pc} = w_{cp}$  is determined based on the properties of negative skin friction piles. Indeed, when the load is not directly applied to the pile but to the surrounding surface of the soil, it leads to the apparition of negative skin friction. *Lutz* (2002) [37] exploits the fact that the settlement of the subsoil due to surface loads must equal the settlement of the piles at the depth of the so-called “neutral layer”  $z_N$ . After introducing a calculation of this neutral layer, the interaction pile-raft is obtained for  $w_{cp} = w_{cc}(z = z_N)$ .

#### 4.1.4 Numerical methods

As far as numerical methods are concerned, the Finite Element Method (FEM) is the most commonly used. The advantages and disadvantages of numerical methods presented for pile groups are also valid for the design of CPRFs. These methods can simulate complex geometries as well as nonlinear constitutive equations. For three-dimensional models, a linear-elastic material behaviour is often applied to foundation elements, whereas the soil is modelled using elasto-plastic material behaviour. In comparison with calculation methods for pile groups, the numerical design of CPRF can be extended to the use of hybrid methods, which are combining both BEM and FEM in the same calculation method.

In the Boundary Element Method (BEM), elements of the foundation are numerically described and coupled to a medium using compatibility conditions. The medium, describing the subsoil, is often

defined as an elastic half-space. The major advantage of BEMs is that the deformation field can be described exclusively according to the discretisation of the boundary elements, as implemented for CPRFs in *Banerjee and Butterfield* (1981) [3]. It is possible to combine a BEM to model the pile group, as described in Section 3.1.3, together with a BEM to model shallow foundations, as presented in *Ohde* (1942) [39].

When using the Finite Difference Method (FDM), the differential equations adopted to describe the load-bearing behaviour of the CPRF are discretised, and the partial derivatives are varied over small finite elements whose mesh covers the whole system, as in *Davis and Poulos* (1972) [10].

As for the FEM, it has to be distinguished between 2D and 3D models. Two-dimensional models (usually axially symmetric) are not always able to produce satisfactory results, in particular for models using non-linear constitutive equations. This is due to the apparition of hoop tensions, which influence the results [37]. Nowadays, two-dimensional models are not often used and are replaced by three-dimensional models, which do not present those drawbacks and allows for more complex geometry.

## 4.2 Design procedure for PRF

As mentioned in Section 2.4, the design of piled raft foundations usually follows the German guidelines “Kombinierte Pfahl-Plattengründungen” (KPP-Richtlinie) from *Hanisch et al.* (2002) [24]. These guidelines present the state of the art of the CPRF design. The initial CPRF guideline published in 2002 and still considered as the reference for the design of CPRFs is making use of the global safety factor concept. This guideline has meanwhile been translated and published in English by the International Society for Soil Mechanics and Geotechnical Engineering [30]. This version is adapted to the current partial safety factor concept. Extended information about safety concepts can be found in Appendix B.

### 4.2.1 Area of application

The guidelines apply to the design, dimensioning, construction and testing of predominantly vertically loaded piled raft foundations. If the soil stratum below the foundation slab has a relatively low-stiffness (for instance in cases presenting soft, cohesive or organic soils), the guidelines do not apply. That is also the case for stratified ground with a stiffness ratio between the soil surface and the lowest layer of the structure greater than 10, or in cases with a piled raft coefficient  $\alpha_{PR}$  exceeding 0.9 [24].

Piled raft foundations have to be assigned to the Geotechnical Category 3 (GC 3) according to ÖNORM EN 1997-1 [23]. Indeed, due to the various interactions between foundation elements among each other as well as interactions with the subsoil, CPRFs present a very complicated load-bearing and deformation behaviour.

### 4.2.2 Calculation method requirements for PR design

Alongside the pile group effect, the contact pressure resistance influences the load-bearing behaviour of foundation piles in a combined piled raft significantly. Therefore, a requirement for a safe design of a piled raft is the use of a reliable calculation method. A method is said to be reliable if it can depict realistically and trustworthy the interdependency between the structure, the soil and the foundations [24]. The choice of the model to describe the material behaviour of soil has to be justified. Moreover, soil investigation on site and in laboratory is required since a sufficient knowledge of deformation and strength properties of the subsoil is needed.

To design a piled raft foundation, knowledge of the load-bearing behaviour of a single pile under similar ground conditions is also necessary. If no information of the external capacity of a single pile (defined in Chapter 2) under similar ground conditions is available, a pile test loading has to be performed following DIN 1054:1976 [13]. If no test loading is made, it is also possible to determine the external

capacity of the corresponding pile using empirical values after DIN 4014:1990 [15] and DIN 4026:1975 [16]. Requirements described in these codes have to be fulfilled before assigning the empirical values. The use of empirical values and its transferability to the planned CPRF have to be justified and proven [24]. The mathematical model used to design a piled raft has to be able to depict properly the shear action on the pile shaft as well as the compressive action on the pile base of the equivalent single pile.

### 4.2.3 Ultimate Limit State - ULS

The analysis of the Ultimate Limit State should eliminate the danger of damage to structures and human life. It aims at ensuring a sufficient load-bearing capacity and excludes any threat for humans. The verifications for the external and internal load-bearing capacity have to be performed to design a piled raft in ULS. Piled raft external and internal capacities are defined similarly to single piles (Section 2.1): internal capacity refers to the safety against piled raft single components' failure (pile, slab...). External capacity refers to the analysis of the safety against failure of the ground surrounding the pile while interacting with foundation elements.

#### 4.2.3.1 External bearing capacity in ULS

The two versions of the guidelines after *Hanisch et al.* (2002) [24] and after *Katzenbach and Choudhury* (2013) [30] differ slightly concerning the analysis of the external bearing capacity in ULS due to the introduction of the partial safety concept. The older approach is presented in Equation (4.4), whereas the new one is shown in Equation (4.6). The initial guideline of 2002 stipulates that a sufficient failure safety for the whole system is obtained under the condition

$$\eta \sum_{j=1}^m S_{k,j} \leq R_{1,tot,k} \quad (4.4)$$

- $\eta$  global safety factor,
- $m$  total number of actions,
- $S_{k,j}$  characteristic value of an action  $j$  and
- $R_{1,tot,k}$  characteristic value of the total resistance of a piled raft, ULS.

The value of the global safety factor  $\eta$  depends on the loading case (LC) after DIN 1054:1976 [13] Section 2.2 and has to be taken as follows:

$$\begin{aligned} \eta_{LC1} &= 2.00 \\ \eta_{LC2} &= 1.75 \\ \eta_{LC3} &= 1.50 \end{aligned} \quad (4.5)$$

$R_{1,tot,k}$  is calculated as the total resistance of a piled raft extracted from the calculated resistance-settlement curve (RSC) under a two times greater action as the one initially applied. If the failure appears for a smaller action than the double applied action,  $R_{1,tot,k}$  has to be set as the value of the resistance where the inflexion point of the RSC appears [24].

The approach presented above may be considered as obsolete since 2008, date after which the old codes were no longer applicable. The new safety concept is extended in *Katzenbach and Choudhury* (2013) [30]. The analysis of the external bearing capacity in ULS can be conducted following Equation (4.6).

$$E_d = E_{G,k} \gamma_G + E_{Q,k} \gamma_Q \leq \frac{R_{1,tot,k}}{\gamma_R} = R_{1,tot,d} \quad (4.6)$$

$E_d$	design value of the effect of actions,
$E_{G,k}$	characteristic value of the effect of a permanent action,
$E_{Q,k}$	characteristic value of the effect of a variable action,
$\gamma_G$	partial safety factor for a permanent action,
$\gamma_Q$	partial safety factor for a variable action,
$\gamma_R$	partial safety factor for a resistance and
$R_{1,tot,k}$	characteristic value of the total resistance of a piled raft, ULS.

The characteristic value of the total resistance is calculated similarly as in the global safety concept: it is equal to the load at which the settlement of the CPRF begins to increase drastically on the load-settlement curve [24].

If no realistic computational model is available to calculate  $R_{1,tot,k}$ , an alternative solution can be used in “simple cases”. For those cases, it is allowed to evaluate  $R_{1,tot,k}$  by means of the characteristic value of the base resistance of the foundation raft constituting the CPRF. Criteria for the “simple case” are:

- simple and uniform geometrical configuration of the CPRF (identical pile length and diameter, constant pile spacing and quadratic or round foundation raft),
- homogenous subsoil (approximately constant stiffness of the subsoil between the layers),
- central loads (concentrated in the centre of gravity) and
- dynamic loads negligible.

No proof of all single piles is needed, i.e. the analysis of the external bearing capacity of a CPRF is sufficient to prove the safety of the piles.

#### 4.2.3.2 Internal bearing capacity in ULS

As far as the material of the construction elements of the CPRF is concerned (e.g. foundation piles or foundation slab), it has to be designed against failure following the codes relative to this material. The analysis of the internal capacity has to be performed for every significant stressing condition. Following stressing conditions have to be analysed:

- piles: compression with deflection and shearing, tension during construction stages,
- slab: deflection, shearing, punching in the area of the load introduction and of the foundation piles.

To calculate stress resultants, characteristic quantities of the action have to be distributed among the pile group and the slab according to the piled raft coefficient  $\alpha_{PR}$ . The verification is then provided using these actions after DIN 1045:1988 [12] or Eurocode 2 [17]. The more unfavourable calculation result is chosen. If no detailed analysis is carried out, the piles have to be reinforced to the minimum amount. The schematic concept of the proof for the ULS is shown in Figure 4.1.

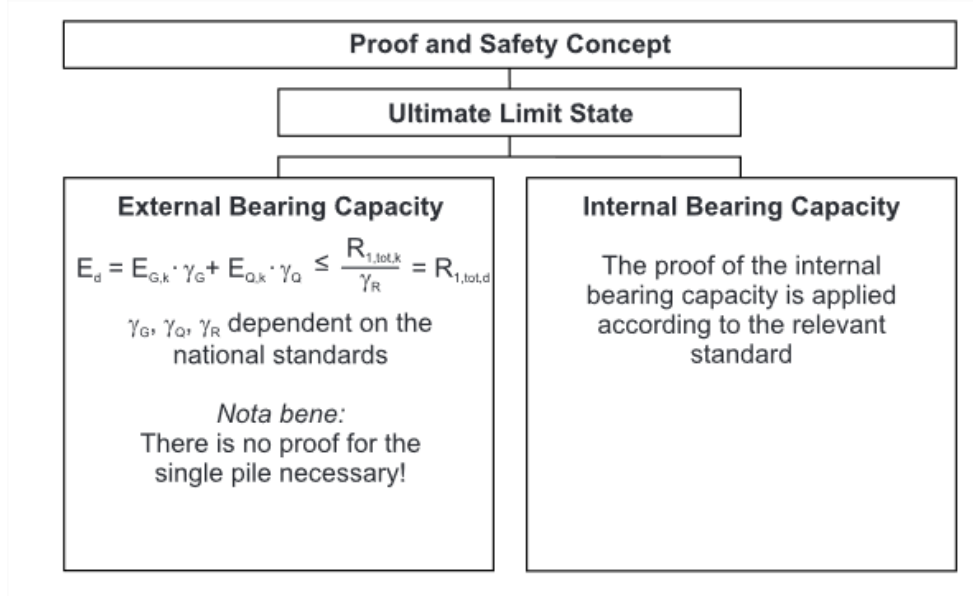


**Figure 4.1:** Proof and safety concept in the ULS after [30].

#### 4.2.4 Serviceability Limit State - SLS

The analysis of the Serviceability Limit State guarantees the long-term usability of the construction. It should ensure its functional reliability and prevent loss of service. This analysis focuses on the deformation of the structure. Absolute settlements, as well as differential settlements, have to be analysed. Similarly to the ULS, external and internal load-bearing capacities have to be verified to design a piled raft in the SLS.

##### 4.2.4.1 External bearing capacity in SLS

A sufficient failure safety is obtained under the condition

$$E_{2,d} = E_{2,k} \left( \sum_{j=1}^m S_{k,j} \right) \leq C_d \quad (4.7)$$

- $E_{2,d}$  design value of the action effect for SLS,
- $E_{2,k}$  characteristic value of the action effect for SLS,
- $S_{k,j}$  characteristic value of an action  $j$  and
- $C_d$  resistance property for SLS (settlement, crack width, etc.).

The parameter  $C_d$  is defined by the requirements of the planed piled raft or the influence of neighbouring structures. Limit values for the acceptable settlement  $s_2$  (or  $s_{SLS}$ ) and difference settlement  $\Delta s_2$  have to be fixed depending on the sensibility of the structure with deformation and settlement. The effect of the action  $E_{2,d}$  has to be determined under the onefold sum of the characteristic value of an action  $S_{k,j}$ .

The calculation of the resistance property  $C_d$  on the example of the settlement difference is shown in Figure 4.2. The characteristic settlement for the SLS  $s_{SLS}$  is read on the resistance-settlement curve of the piled raft and represents the allowed settlement of a structure. To consider the potential differential settlement between piles, the characteristic settlement has to be increased or reduced by a factor  $\Delta s_{SLS}$ . An estimation of  $\Delta s_{SLS} = 0.15 s_{SLS}$  is given in Katzenbach *et al.* (2016) [31] and should be adopted if no further analyses are made.



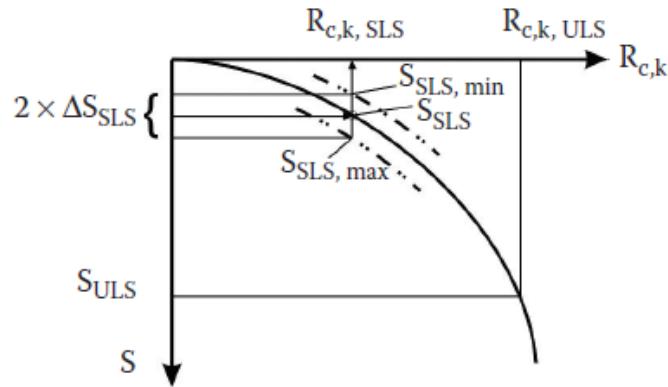


**Figure 4.2:** Determination of the expected differential settlement of a pile group [31].

#### 4.2.4.2 Internal bearing capacity in SLS

Following stressing conditions have to be verified:

- piles: crack width limitation,
- slab: crack width limitation, admissible deflection and settlement difference.

The schematic concept of the proof for the SLS is shown in Figure 4.3.

#### 4.2.5 Piled raft monitoring

The measurement-technology monitoring of a piled raft is an indispensable component of the partial safety concept (see Figure 4.4). It provides, during the construction phase and in the operating phase:

- the verification of the mathematical model and calculation approaches,
- an early recognisability of possible critical situations,
- a verification of the calculated settlement forecasts and
- the conservation of evidence.

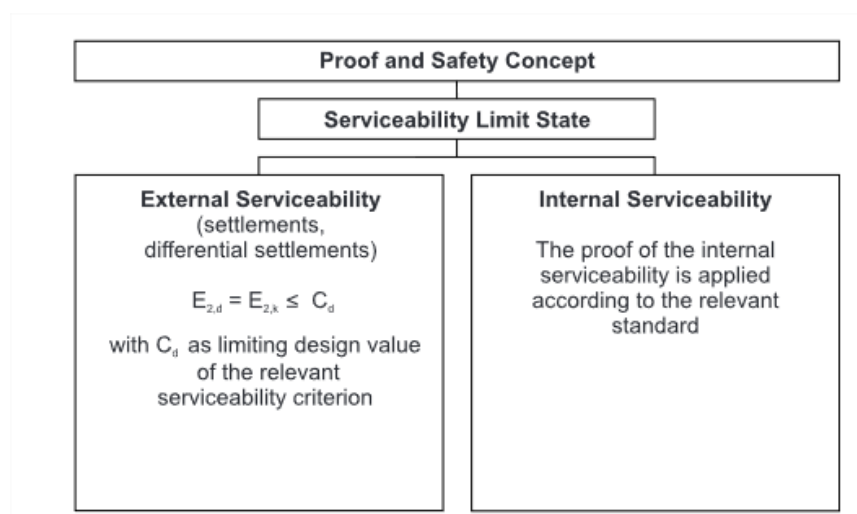


**Figure 4.3:** Proof and safety concept in the SLS [30].

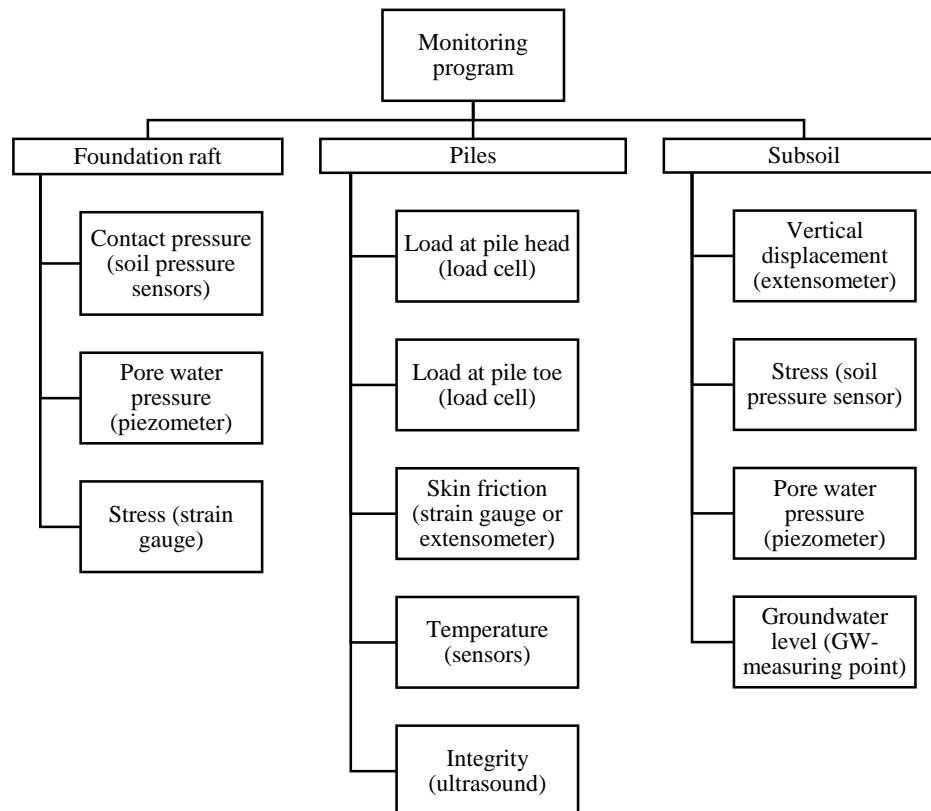


**Figure 4.4:** Monitoring of a CPRF, adapted from [31].

### 4.3 Adopted design approach

The adopted design of CPRFs is divided into two main steps: analytical calculation of a pile group and numerical simulation of the raft. The analytical design of a pile group has been presented in Section 3.3. It covers the analysis of the load-bearing behaviour, which takes into consideration pile-soil and pile-pile interactions. Raft-soil and pile-raft interactions have to be modelled to deliver a realist and trustworthy design approach.

#### 4.3.1 Modelling of the raft-soil interaction

Various methods exist to model the distribution of the contact pressure of raft foundations, which constitutes the basis for the modelling of the raft-soil interaction. Following calculation procedures are applicable [31]:

- distribution under rigid foundations according to *Boussinesq* (1885) [5],
- stress trapeze method,
- subgrade reaction modulus method,
- stiffness modulus method and
- numerical methods.

These procedures are sorted from the simplest to the most complex and realistic approaches. The theory according to *Boussinesq* (1885) [5] is, for example, only applicable for simple cases since it only offers a rough approximation of the contact pressure distribution. Foundation borders should theoretically support infinitely high tensions. The stress trapeze method (see Figure 4.5 (a)) is also suitable for simple cases and small foundations. In this method, the considered stresses are assumed to be linearly distributed along the foundation.

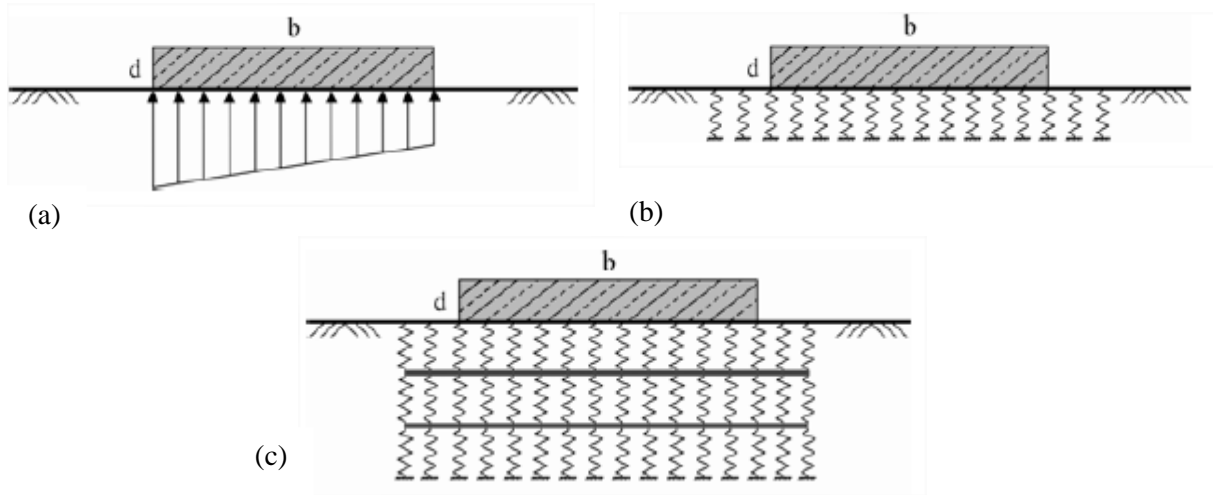


**Figure 4.5:** Different models of raft-soil interaction after [32]. (a) Stress trapeze method (b) Subgrade reaction modulus method (c) Stiffness modulus method.

More advanced methods are the subgrade reaction modulus and the stiffness modulus method (see Figure 4.5 (b) and (c)), which are usually sufficient for the analysis. As far as the subgrade reaction modulus method is concerned, the subsoil is seen as a system of independent springs, where a uniform load causes a uniform settlement of the structure [31]. The stiffness modulus method models the subsoil as an “elastic half-space with a system of connected springs” [31]. A uniform load causes a settlement trough. The methods presented so far are only approximate solutions. On the contrary, the most precise procedure is the numerical approach since it depicts more realistically the rigidity of the foundation as well as the non-linear behaviour of the subsoil.

The method chosen to analyse the raft-soil interaction in the present study is the subgrade reaction modulus method. This method is widely applied and offers the possibility to compare the obtained results with tested designs from the literature. Moreover, the limited complexity of this method makes it easier to implement than the stiffness modulus method.

The subgrade reaction modulus of the slab  $k_i$  can be calculated using numerical simulation. This is, for example, the case with the additional module RF-SOILIN of the software RFEM, employed to design a shallow foundation using the subgrade reaction modulus method. Another possibility to access the subgrade reaction modulus of a CPRF is by means of empirical tables. These values are based on the results of equivalent shallow foundations, which are combined with determined factors resulting of the monitoring of existing CPRFs [24].

#### 4.3.2 System rigidity

The contact pressure under a foundation slab mostly depends on the relation between the rigidity of the structure and the rigidity of the subsoil. To proceed in a realistic analysis of the contact pressure, it is necessary to investigate the rigidity of the whole system. The knowledge of the distribution of the contact pressure is also conditioning the determination of internal forces such as deformations and bending moments. The system rigidity  $K$  of a rectangular spread foundation according to Kany (1974) [29] is expressed in Equation (4.9), derived from the general definition of this parameter presented in Equation (4.8). This parameter offers a value for the appreciation of the raft-soil interaction.

$$K = \frac{\text{structure stiffness}}{\text{subsoil stiffness}} \quad (4.8)$$

$$K = \frac{1}{12} \frac{E_{PR}}{E_s} \left( \frac{h}{l} \right)^3 \quad (4.9)$$

$E_{PR}$  modulus of elasticity of the slab,  
 $E_s$  stiffness modulus of the subsoil,  
 $h$  height of the shallow foundation and  
 $l$  length of the shallow foundation.

For a circular shallow foundation, the length of the foundation  $l$  adopted for rectangular geometries is replaced by the diameter of the circular foundation in Equation (4.9).

Different systems will be compared in Chapter 6. It is necessary to use a standard parameter to lead these comparisons. *Kany* (1974) [29] introduced limit values of the system rigidity  $K$  to differentiate between limp and rigid foundations. These values are presented in Table 4.2.

**Table 4.2:** Type of foundation according to the system rigidity. Adapted from [31].

System rigidity $K$	Type of foundation
$K \geq 0.1$	Rigid foundation
$0.001 \leq K < 0.1$	Intermediate area
$K < 0.001$	Limp foundation

For limp foundations, the contact pressure presents the same distribution as the load applied on the structure, as illustrated in Figure 4.6 (a). On the contrary, for rigid foundations, higher stresses appear on the edge of the structure. A constant loading of the foundation leads to a non-linear distribution of the contact pressure (Figure 4.6 (b)).

Depending on the thickness of the foundation, and thus on its rigidity, shallow foundations can be conceived with or without reinforcement, even if reinforced foundations should be favoured due to their greater robustness. The thickness of the reinforced concrete slab depends on the bending moments as well as on the punching (local failure due to punctual loading). A thicker slab may permit to avoid the introduction of shear reinforcement. This is why a difficult choice has often to be made: decrease the volume of the foundation to save costs on concrete utilisation but introduce other solutions such as reinforcement, or increase the volume of the foundation and save reinforcement costs.

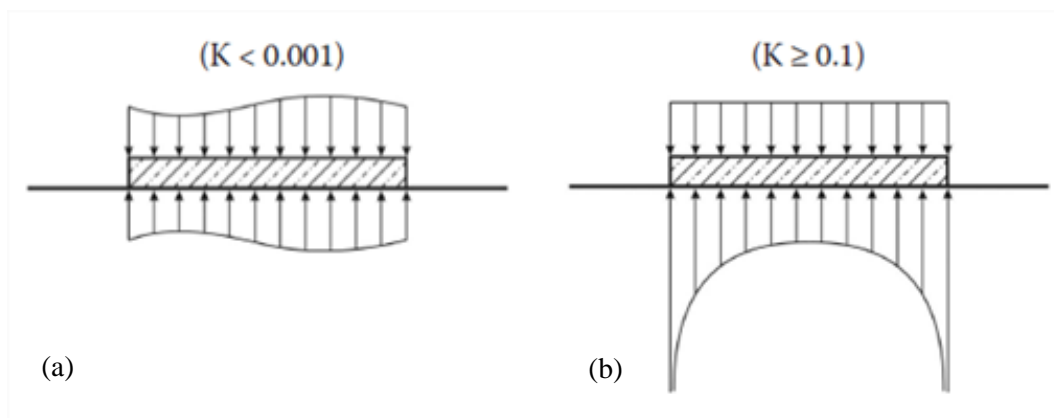


**Figure 4.6:** Contact pressure distribution for limp (a) and rigid (b) shallow foundations after [31].

### 4.3.3 Workflow

To compensate the main disadvantage of analytic methods mentioned in Section 4.1 – some interactions are disregarded in pure analytic methods –, a hybrid calculation method making use of a numerical calculation of the slab is carried out. The output parameters of the analytical calculation, i.e. the spring stiffness  $C_i$  of each pile, become the input parameters for the numerical calculation.

A workflow of the adopted hybrid design approach is presented in Figure 4.7. The main input parameters of the analytical method are the total load  $F_i$ , the pile length  $L_i$ , the pile radius  $r_i$  and the pile spacing  $d_x$ ,  $d_y$  in two dimensions. Given those elements and the geotechnical parameters, the algorithm calculates the settlement and the resistance of the piles. The spring stiffness of each pile  $C_i$  can thus be determined. In combination with the subgrade reaction modulus of the slab  $k_i$ , the CPRF is modelled in RFEM. The resistances  $R_i$  are modified due to the influence of the foundation slab, which also transfers loads into the ground. Moreover, it is made possible to access the piled raft coefficient  $\alpha_{PR}$  (see Equation (2.10)), which indicates the part of the total action transferred by the piles.

The loads carried by the piles, calculated with RFEM, become the input loads of the analytical calculation of a pile group in Python. This load is lower than the initial one because of the influence of the slab, which transfers a part of the load directly into the ground. Using this updated load distribution, the spring stiffness of each pile is calculated anew and transmitted to RFEM.

The introduction of an iterative procedure between Python and RFEM is necessary since the first evaluation alone does not correctly depict the pile-raft interaction. In fact, only the influence of the pile group is considered after the first iteration using the analytical calculation in Python. The piled raft coefficient  $\alpha_{PR}$  equals one since only the pile group is supporting loads. Moreover, the spring stiffness of each pile is low due to the high settlement occurring by neglecting the influence of the raft. If the spring stiffness of each pile is small, a large part of the load is supported by the slab during the next RFEM calculation. Thus, for the second iteration, the value of  $\alpha_{PR}$  is at its lowest (see Figure 4.8).

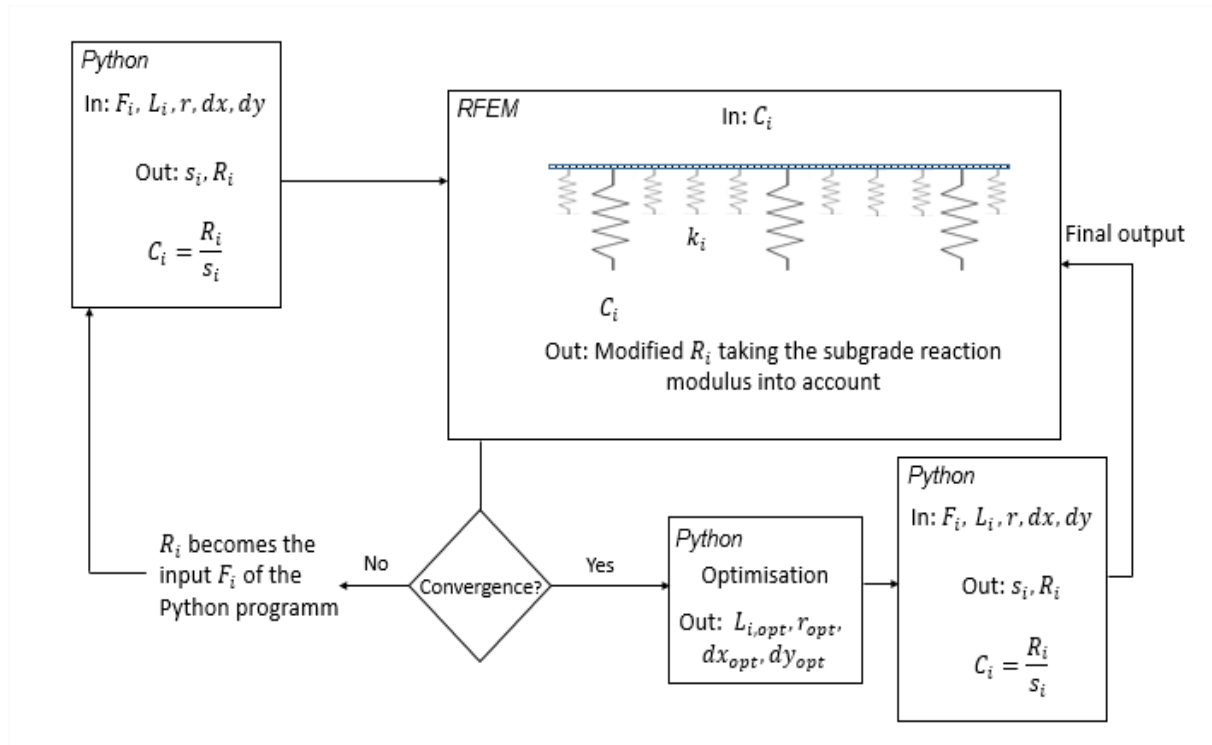


**Figure 4.7:** Workflow of the adopted hybrid design approach of CPRFs.

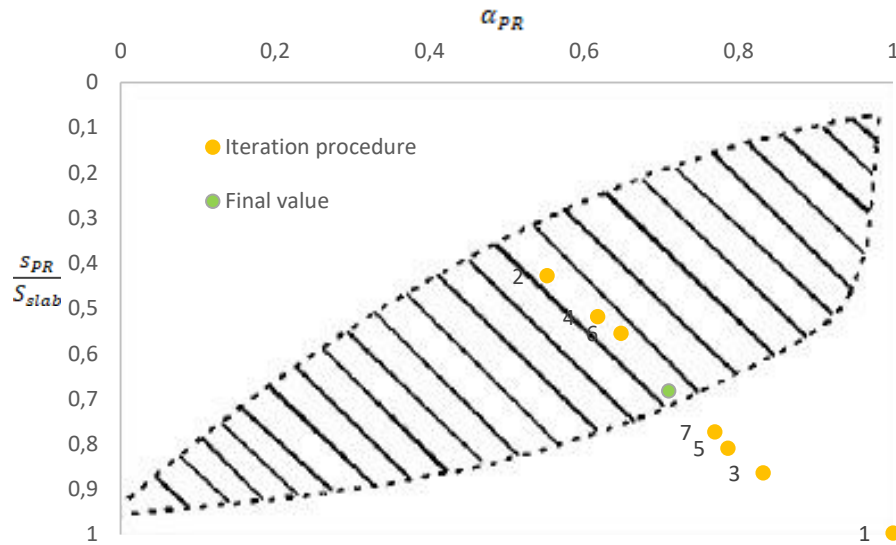


**Figure 4.8:** Evolution of the piled raft coefficient during the iterative procedure (design of CPRF guideline example 1 version 3).

Since a large part of the load is carried by the slab, only the limited amount of the loads carried by the piles are transferred to Python for the next iteration step. Following a similar scheme, this leads to higher spring stiffness due to the lower settlements. If spring stiffnesses of the piles are more significant, the part borne by the slab is smaller, which means that the piled raft coefficient  $\alpha_{PR}$  increases in comparison with the preceding iteration. The iteration steps are repeated until a convergence is found. To get a more comprehensive overview of the explained iteration process, the successive values of the piled raft coefficient  $\alpha_{PR}$  obtained during the iteration procedure for the design of the first example of the CPRF guideline version 3 are shown in Figure 4.8. This calculation is detailed in Section 5.2.

The optimisation process, appearing on the workflow Figure 4.7 if a convergence value is found, is developed in Chapter 6. New, optimised values of pile length, pile diameter and pile spacing are calculated. These values are used to determine the final spring stiffness of each pile. The final design of the CPRF is then obtained after the final simulation with RFEM.

#### 4.4 Limitations and drawbacks

A major limitation of this design approach is the fact that the transfer of the calculated loads and spring stiffnesses is not automated. The interface between RFEM and other software using the additional module RF-COM is only accessible with given programming languages such as Visual Basic, Visual Basic for Applications (VBA) and Visual C++. The direct communication between RFEM and Python is not currently possible.

It should also be noted that the calculation of the subgrade reaction modulus of the slab is not always straightforward. The values obtained using empirical approaches are often valid for a given soil or a defined geometry. Therefore, these values are not directly transferable to different projects. Moreover, the subgrade reaction modulus method disregards the influence of surrounding contact pressures.

To evaluate the efficiency and the reliability of the developed solution, a comparison with tested examples coming from the literature is carried out.

## 5 Case studies on pile groups and piled raft foundations

To compare and validate the results of the developed design approach, a case study has been carried out. It compares several typical configurations of pile groups and piled raft foundations with the state of the art. The CPRF guideline offers a wide range of examples to compare the different types of foundations. Four different variants are presented to design foundations of a multi-span bridge crossing a valley (problem 1 in the CPRF guideline, *Hanisch et al.* (2002) [24]). The first variant is a simple shallow foundation, the second one is a pile group made of twelve piles embedded in talus material, the third one presents the design of a CPRF with six piles and the last one is a pile group of six piles embedded in the rock. The focus is on the comparison of the obtained results with the second and third examples mentioned above. The geometrical and soil parameters adopted for those studies are presented Table 5.1 and Table 5.2 respectively.

**Table 5.1:** Geometrical parameters of different pile groups for the benchmark study on pile groups.

Pile group parameters	Guidelines 1.2 and 1.3	End bearing	Skin friction
Pile diameter $D$ [m]	1.5	0.9	0.9
Pile length $L$ [m]	15	9	9
Load $F$ [MN]	30	3	10 / 15
Pile layers	8	6	6
Total number of layers	9	9	9

**Table 5.2:** Soil parameters of different standard soils for the benchmark study on pile groups.

Soil parameters	Well graded sand (guidelines 1.2 and 1.3)	Uniform fine sand	Clay
Poisson's ratio $\nu$ [-]	0.25	0.3	0.45
Friction angle $\varphi$ [°]	25	35	18
Specific weight of the soil $\gamma'$ [kN/m <sup>3</sup> ]	10	11	7
Cohesion $c$ [kN/m]	5	0	5
$w_e$ [-]	0.55	0.6	110
$v_e$ [-]	400	300	1
Secant modulus, pile top [MPa]	10	7	1
Secant modulus, pile base [MPa]	48.1	44.6	6.2

## 5.1 Pile groups

The case study on pile groups is carried out using the second example of the CPRF guideline (referred to in this chapter as “Guideline 1.2”) as well as other standard case studies, such as pile groups predominantly making use of the end bearing or the skin friction to transfer loads to the ground. The analytical design approach used for the design of pile groups is presented in Section 3.3.

### 5.1.1 Guideline 1.2

The second version of the first problem presents a pile group made of twelve piles constantly spaced whose parameters are summarised in Figure 5.1. This 3×4 pile group is subject to a central load of 30 MN. The position and numbering of the piles are shown in Figure 5.2 with  $a$  representing the pile spacing and  $D$  the diameter of the piles. As mentioned in Hanisch *et al.* (2002) [24], the admissible settlement of the bridge foundation is fixed to  $s_{adm} = 4$  cm considering the requirements of the superstructure. Using the algorithm developed in Python, an analytical calculation is carried out. The resistance-settlement curve (RSC) can be displayed for every pile. As discussed in Section 2.1, the total resistance of a pile  $R_{pile,k}(s)$  can be divided into two components, the resistance of the shaft  $R_{s,k}(s)$  and the resistance of the base  $R_{b,k}(s)$ . These components are represented separately to get a better overview of the load transmission mechanism. The pile group has a symmetrical geometry and the structure is centrally loaded, one can therefore limit the study to three representative piles whose RSCs are shown in Figure 5.3, 5.4 and 5.5: one inner pile (pile number 5), one edge pile (pile number 4) and one corner pile (pile number 3). The resistance-settlement curve of every pile is therefore known.

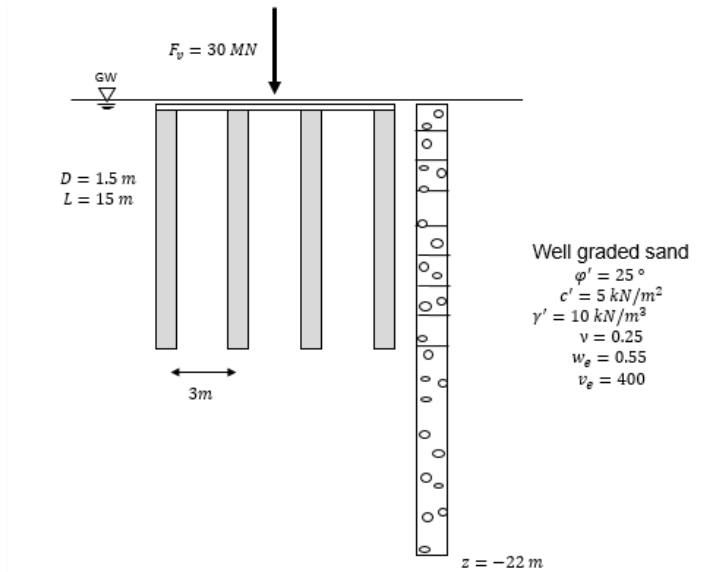


**Figure 5.1:** Illustration of the major parameters used in the benchmark “Guideline 1.2”.

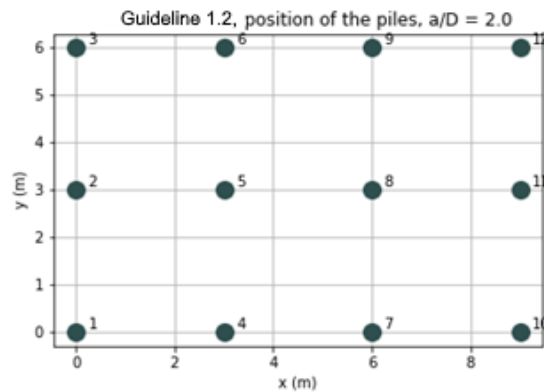


**Figure 5.2:** Position of the piles for the benchmark “Guideline 1.2” with  $a$  pile spacing and  $D$  pile diameter.



The results obtained using the analytical calculation implemented in Python are compared with the reference solution from *Hanisch et al. (2002)* [24], obtained by means of numerical simulation (FEM model).

One observes that the shapes of the RSCs are similar in both calculation methods within an initial area. It should be noted that the shape of the RSC for the edge pile is coinciding with the shape of the corner pile to a large extent. However, the area in which the flat branch of the RSC begins to show a steeply sloping branch appears for a higher settlement in the case of the edge pile than for the corner pile (compare Figure 5.3 and Figure 5.4). In other words, the corner pile presents signs of failure for a lower settlement than the edge pile. This phenomenon also occurs in the numerical calculation.

The transition area of the pile shaft resistance appears for a larger settlement in the numerical calculation than in the analytical calculation. This could be explained by an oversimplified model of the stress state in the subsoil implemented in the analytical approach [47]. Another factor influencing the behaviour of the pile shaft resistance is the yield criterion of the soil. The difference of shaft resistance may also be because the Modified Cap Model of Drucker-Prager adopted in *Hanisch et al. (2002)* [24] exhibits a stiffer soil behaviour than the Mohr-Coulomb failure criterion used in the developed calculation [47]. This appearance is most striking when it comes to inner piles (Figure 5.5), whereas corner and edge piles only display limited discrepancies between the two models

The pile base resistance presents approximately the same curve for the different piles of the group, for the analytical as well as for the numerical approaches. The values obtained with both methods largely correspond to one another. The values obtained analytically are slightly smaller due to the depth-dependant stiffness modulus of soil implemented in the calculation. Moreover, when a pile section fails, this results in the occurrence of an inflexion point in the RSC of the base resistance (see for example Figure 5.3, orange curve) and a steeper slope appears. If one section breaks down, other sections are indeed loaded more strongly to compensate the lack of bearing capacity induced by the failed part since remaining parts still have bearing reserves. This behaviour does not appear in the FEM approach because the failure criterion is different. Here, the analytical calculation offers a more realistic modelling of the failure mechanism.

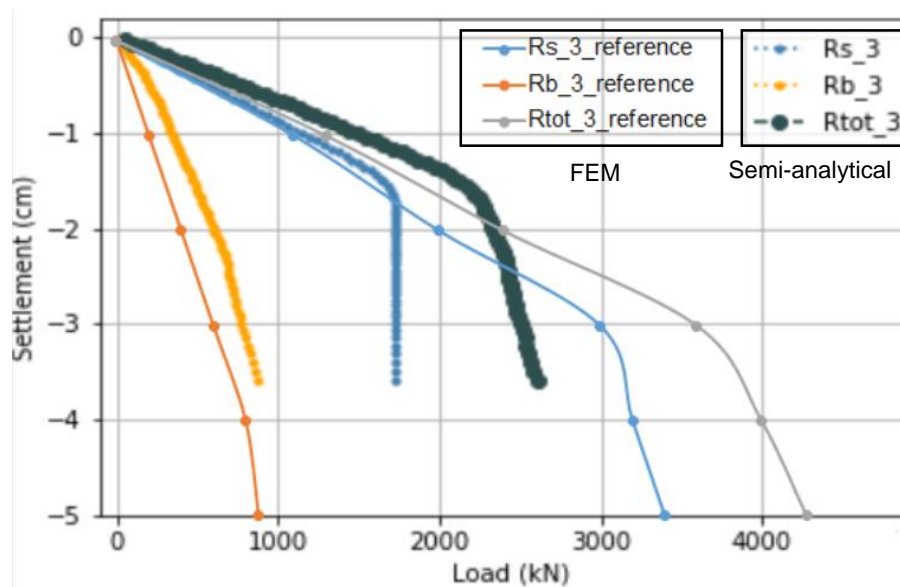


**Figure 5.3:** Comparison of the RSCs for the corner pile obtained with an analytical calculation and with a numerical simulation (reference design from *Hanisch et al. (2002)* [24]).

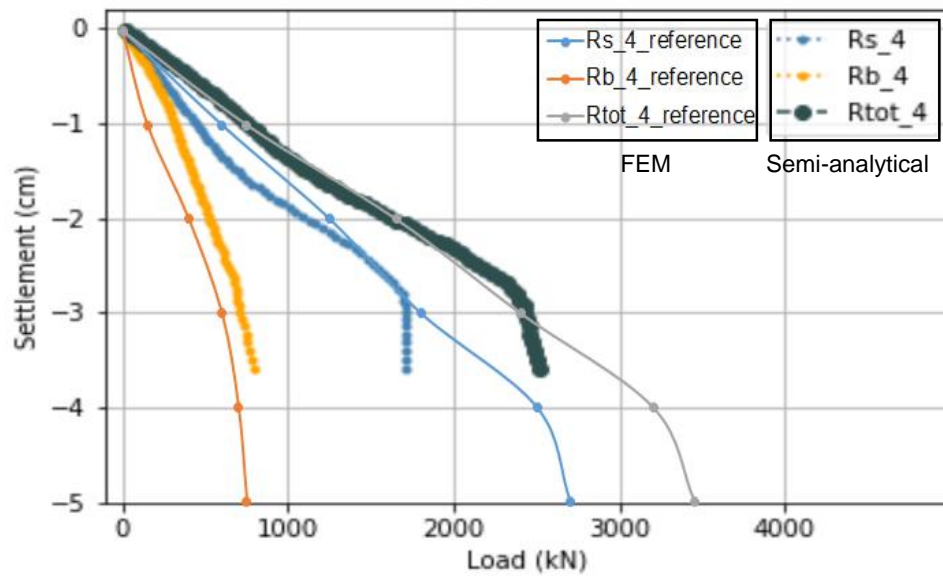


**Figure 5.4:** Comparison of the RSCs for the edge pile obtained with an analytical calculation and with a numerical simulation (reference solution from *Hanisch et al. (2002)* [24]).

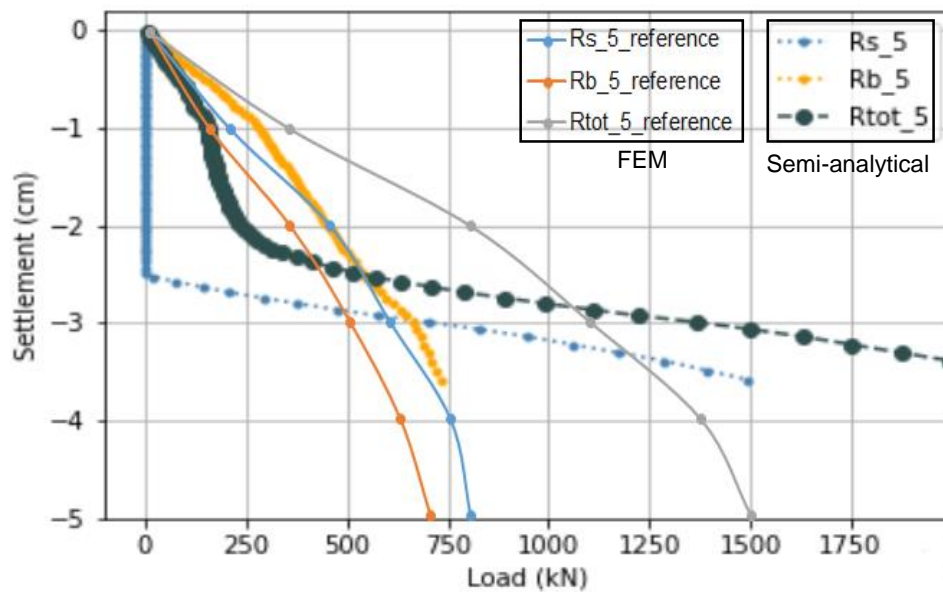


**Figure 5.5:** Comparison of the RSCs for the inner pile obtained with an analytical calculation and with a numerical simulation (reference solution from *Hanisch et al. (2002)* [24]).

The inner pile Figure 5.5 does not display coinciding shapes between the two models because of the influence of the pile shaft resistance. For small settlements, the RSC of the inner pile resistance exhibits a steep slope whereas RSCs of other piles are quite moderate. After the inflexion point, this behaviour is inverted; the slope is flatter regarding the inner pile. The reference solution of *Hanisch et al. (2002)* [24] does not contain an inflexion point – the slope is relatively constant with an increasing settlement.

The results of the settlement and the resistance of each pile for both design approaches are presented in Figure 5.6. A reason that could explain the different load-bearing behaviour of the piles for a similar settlement is the different mobilisation of the skin friction occurring in each pile. Indeed, the inner piles are “protected” by the outer piles, preventing the skin friction from being activated. This is mostly the

case for the numerical simulation, where the outer resistances are two to three times higher than the inner resistances.

Contrary to the FEM calculation, pile resistances are distributed in a fairly uniform way when following the analytical method, even if the tendency is maintained. This difference can be explained by the impact of the group effect, which is more significant for the analytical approach and counterbalances the shielding of the outer piles over the inner piles. Indeed, the inner piles are directly surrounded by more piles than the edge or corner piles, leading to an increased group effect. The differences between the two models are highlighted in Table 5.3.

Moreover, the analytical calculation provides bigger settlements of the foundation regarding the reference solution. As briefly mentioned above, those differences might lie in the fact that the applied failure criteria are different (Mohr-Coulomb for the analytical calculation and Drucker-Prager for the numerical calculation). However, it should be mentioned that EC7 stipulates that the use of the Mohr-Coulomb's failure criterion is also admitted. In addition, the stiffness of the soil differs, the developed analytical approach adopts an increasing stiffness modulus with the depth whereas the numerical calculation simplifies the model with a constant stiffness modulus of soil. Finally, one could note that the FEM model takes the influence of the pile cap into account, which transfer slightly less than 10% of the total load directly into the ground according to *Hanisch et al.* (2002) [24]. This is not the case for the semi-analytical calculation where the pile cap is not involved in the load transfer mechanism.

The coefficient of earth pressure at rest  $K_0$  also differs between the two models. The developed semi-analytical model adopts the simplified approach conceived by *Jaky* (1944) [28] shown Equation (5.1) where  $\varphi$  is the friction angle. With the given friction angle of  $25^\circ$ , the coefficient of earth pressure at rest amounts to 0.42, while the 3D FEM model uses a constant coefficient of 0.50 as presented in *Hanisch et al.* (2002) [24].

$$K_0 = 1 - \sin(\varphi) \quad (5.1)$$

Moreover, a limitation of the maximal stress is applied in the 3D FEM model. The principal stresses are limited by a cap with an associated flow rule in the hydrostatic stress range. This is, however, not decisive in the developed design approach, as the failure criterion is only applied along the shaft and for the pile base.

The proof of external serviceability is adduced for both design approaches as the settlement of 3.6 cm calculated with the analytical calculation as well as the settlement of 3.0 cm obtained with the reference solution are lower than the admissible settlement of 4.0 cm.

**Table 5.3:** Highlights of the differences between the two models.

Parameters	Developed semi-analytical model	3D FEM reference model [24]
Failure criterion	Mohr-Coulomb	Drucker-Prager
Maximal stress	unlimited	limited (Cap Model)
Dilatancy $\Psi$	considered	not considered
Earth pressure at rest $K_0$	after <i>Jaky</i> (1944) [28]	direct field tests
Stiffness modulus $E_s$	depth-dependant	constant

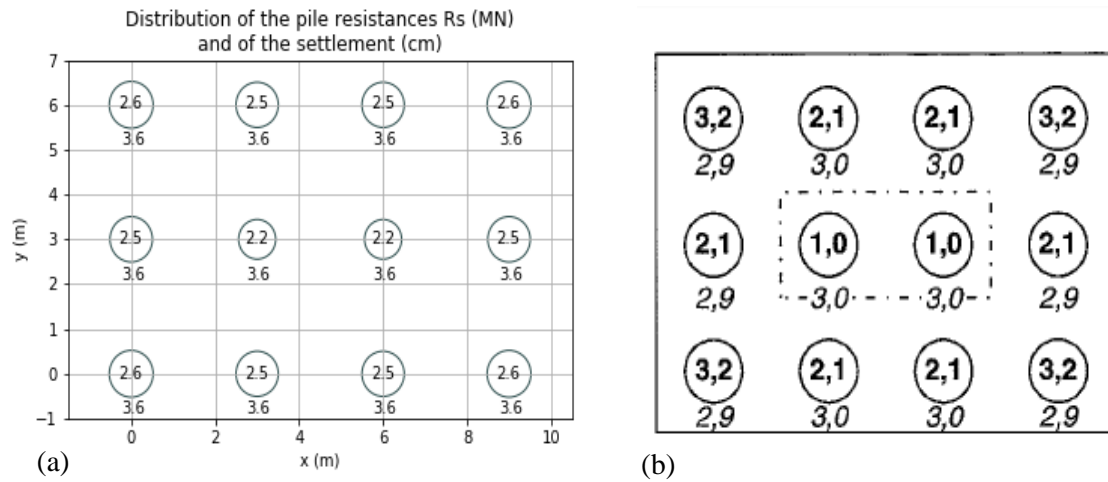


**Figure 5.6:** Comparison of the results obtained for the benchmark “Guideline 1.2” (a) analytical calculation (b) FEM model from Hanisch et al. (2002) [24]. Pile resistance inside the piles (MN), settlement under the piles (cm).

### 5.1.2 End bearing pile and skin friction pile

As mentioned in Section 2.1, resistance-settlement curves generally present shapes specific to the resistance predominantly used by a pile to transfer loads to the ground. This is why the two major types of piles are compared in this subchapter: the “skin friction” piles and the “end-bearing” piles. The geometrical as well as geotechnical parameters used for this study are referred to in Table 5.1 and Table 5.2. The end bearing pile is presented in Figure 5.8 and the skin friction pile in Figure 5.7. To model the end bearing problem, the upper part of the pile is embedded in a soil with a poor bearing capacity such as clay, whereas the lower part of the pile is embedded in soil with a superior bearing strata such as a uniform fine sand (see Figure 5.8). This modelling of the subsoil is simply inverted to obtain a skin friction problem, where a uniform fine sand is present above clay strata (Figure 5.7).

According to Kempfert et al. (2012) [34], one should observe a pronounced curvature of the load displacement curve for a pile subject to shaft resistance (skin friction pile) since the limit value of the skin friction is reached at relatively small pile displacements. For end-bearing piles, however, RSCs present a less pronounced curvature because the base resistance increases up to very large settlements. Those affirmations are confirmed by the analytical approach developed in this thesis. Indeed, the modification of curvature is smoother after the inflexion point of the end bearing pile Figure 5.9 than after this of the skin friction pile Figure 5.10. Moreover, the remarks made on the RSCs for the benchmark “Guideline 1.2” are still confirmed for these two problems.

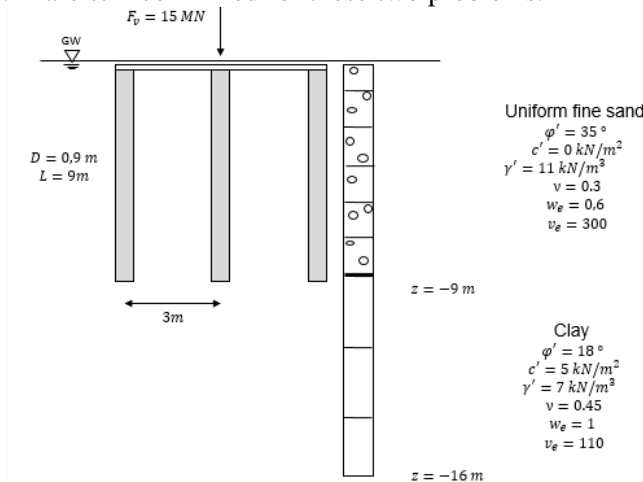


**Figure 5.7:** Illustration of the major parameters of the benchmark “skin friction pile”.

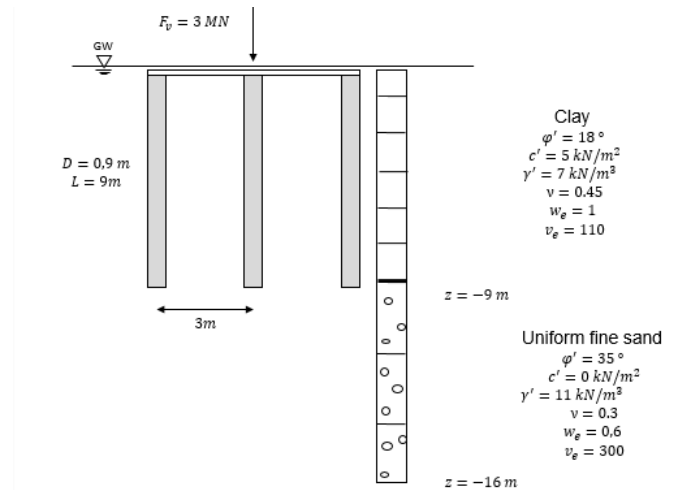


**Figure 5.8:** Illustration of the major parameters of the benchmark "end bearing pile".

In regard to the end bearing problem Figure 5.9, it is remarkable that the resistance of the inner pile (pile 5) is almost only constituted of the base resistance, the skin friction having a limited influence. That is why the inner pile resistance displayed in Table 5.4 is approximately three times lower than the resistance of the surrounding piles. Here, the phenomenon of shielding of the inner pile by the outer piles mentioned by *Hanisch et al. (2002)* [24] is clearly visible: the skin friction is not activated at low settlements.

Such differences are also visible in the skin friction problem in Figure 5.10. Indeed, one observes substantial differences between the pile resistances for a small loading (10 MN), whereas for a more significant load (15 MN), the pile resistances are more or less constantly distributed (Table 5.4). When the applied load becomes too high, the protecting effect of the outer piles is arguably not sufficient anymore; instead, the skin friction is activated for every pile.

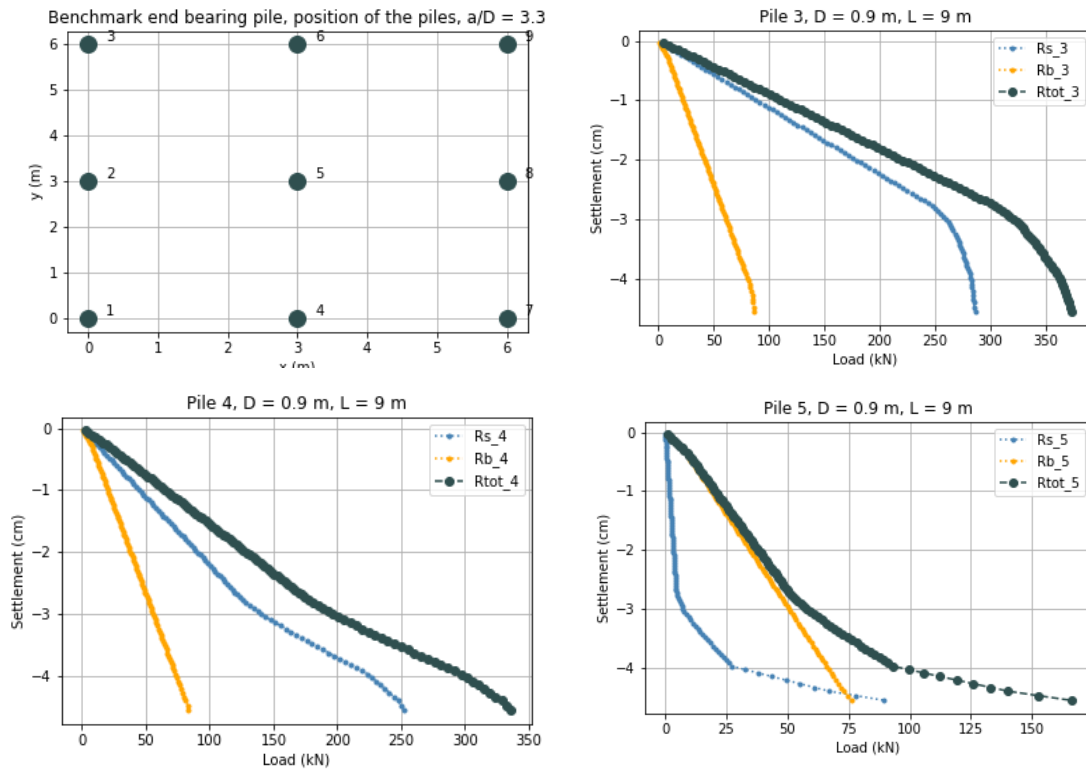


**Figure 5.9:** Position of the end-bearing piles and load-settlement curve for the corner pile (pile number 3), edge pile (number 4) and inner pile (number 5).

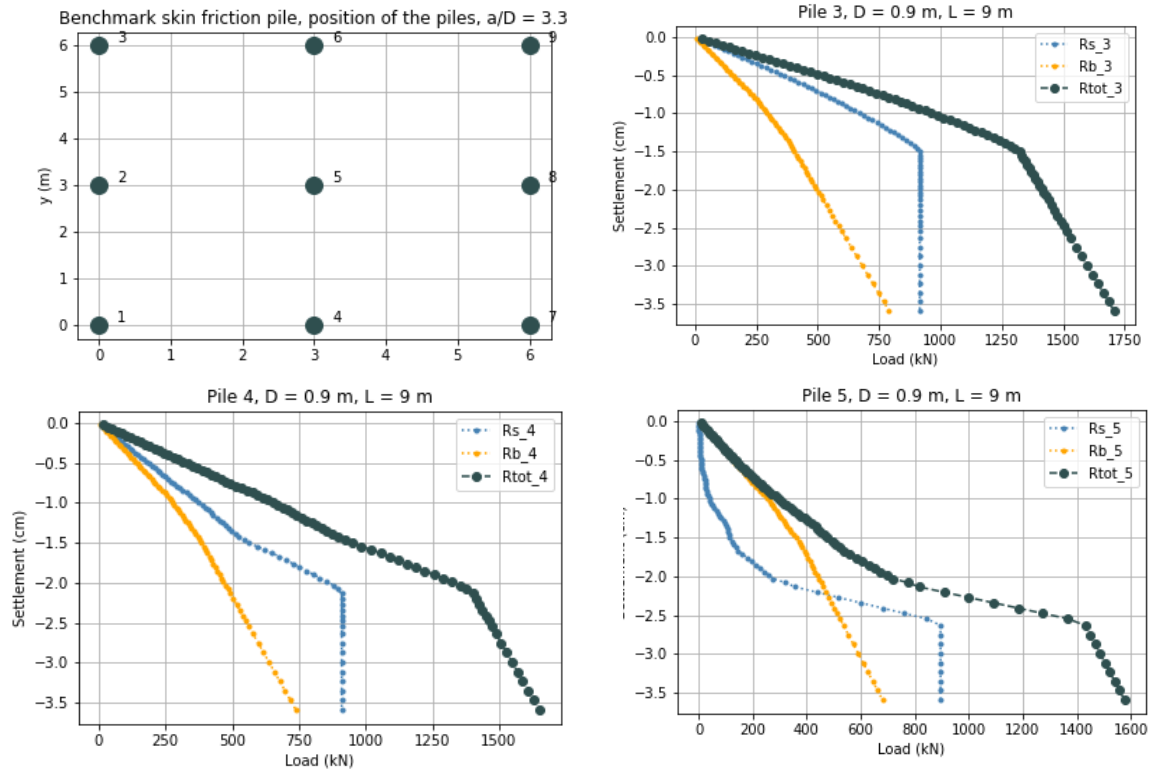


**Figure 5.10:** Position of the skin friction piles and load-settlement curve for the corner pile (3, top right), edge pile (4, bottom left) and inner pile (5, bottom right). Total load of 15 MN.

**Table 5.4:** Results obtained for the benchmark end bearing and skin friction pile.

	End bearing	Skin friction	
	3 MN	10 MN	15 MN
Settlement [cm]	4.56	1.6	3.59
Inner pile [MN]	0.17	0.51	1.57
Edge pile [MN]	0.33	1.03	1.65
Corner pile [MN]	0.37	1.34	1.71

Finally, *Katzenbach et al.* (2016) [31] mention that for a pile group predominantly making use of the base pressure to transfer loads to the ground, the foundation can be modelled and calculated analogically to a deep raft foundation. For a skin friction pile group, however, the determination of the settlement is much more complex and the recourse to a numerical calculation should be considered.

## 5.2 Combined piled raft foundation

The case study on combined piled raft foundation is carried out using the third example of the CPRF guideline example 1 (referred to in this chapter as “Guideline 1.3”). The geometrical and soil parameters adopted for the example “Guideline 1.3” are the same as those used for the example “Guideline 1.2” and are referenced in Table 5.1 and Table 5.2. Only the number of piles is modified, i.e. twelve piles for the pile group instead of six piles for the combined piled raft foundation (see Figure 5.11). The contribution of the slab is now taken into account in the adopted model. As mentioned in Section 5.1.1 the admissible settlement of the bridge foundation is fixed to  $s_{adm} = 4$  cm considering the requirements of the superstructure.

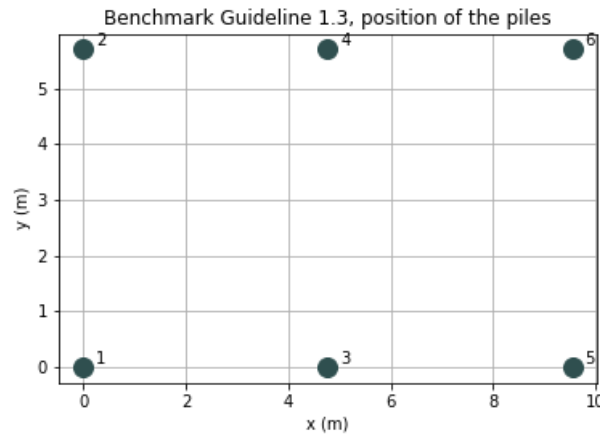


**Figure 5.11:** Position of the piles for the benchmark “Guideline 1.3”.

The combined piled raft is modelled as presented in Section 4.3, combining a semi-analytical calculation of the pile group with a numerical calculation of the slab (hybrid method). This design approach is compared with the FEM model of *Hanisch et al.* (2002) [24] presented in the CPRF Guideline.

The adopted subgrade reaction modulus is derived from a numerical simulation conceived by *Hanisch et al.* (2002) [24]. To obtain a reliable comparison, both models use the same subgrade reaction modulus calculated for a rigid slab. However, the spring stiffness for each pile as well as the yield criterion adopted are different.

Table 5.5 contains empirical values of the ratio  $k_{s, \text{CPRF}}/k_{s, \text{shallow}}$  between the subgrade reaction modulus of the CPRF and the equivalent shallow foundation, which permits to calculate the subgrade reaction modulus of the CPRF. In Table 5.5,  $a$  represents the pile spacing and  $D$  the diameter of the piles. Those ratios are valid for the pre-dimensioning of CPRF in stiff cohesive soils and they mostly depends on the rigidity of the raft and on the stiffness of the subsoil. Upper limit values are valid for flexible rafts, while lower limit values are applicable to rigid rafts.

Combining those empirical values and the subgrade reaction modulus of the equivalent shallow foundation calculated in *Hanisch et al.* (2002) [24], one obtains the subgrade reaction modulus of the rigid CPRF, which is presented Figure 5.12. Results are graded from a lower modulus in the inner area to a higher modulus in the outer part.

Given that for CPRFs a part of the action is applied directly near the surface of the soil strata, the expected settlement should tend to exceed the one of 3.0 cm obtained with a pile group in the “Guideline 1.2”, as explained in *Hanisch et al.* (2002) [24].

**Table 5.5:** Empirical values for the determination of the subgrade reaction modulus under a CPRF in cohesive soils. Adapted from [24].

Subgrade reaction modulus ratio		
$k_{s, \text{CPRF}}/k_{s, \text{shallow}}$		
Pile axis spacing	Inner area	Border area
$a/D = 3.0$	0.1 - 0.2	0.8 - 0.9
$a/D=6.0$	0.2 - 0.7	0.8 - 0.9

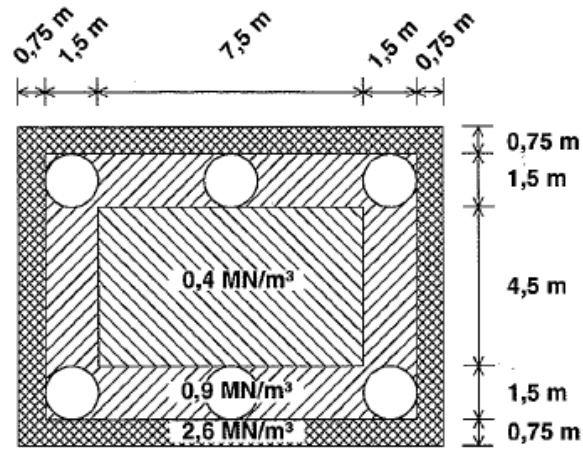


**Figure 5.12:** Subgrade reaction modulus for the CPRF of the “Guideline 1.3” according to [24].

The resistance-settlement curves are obtained with the help of the Python script, where the input loads are derived using the convergence procedure described in Section 4.3. Those input loads are presented in Table 5.6. The modification of the piled raft coefficient occurring during the process is shown in Figure 4.8. The remaining part of the initial load of 30 MN is directly carried out by the foundation slab.

Resistance-settlement curves for the corner pile and for the edge pile are shown in Figure 5.13 and Figure 5.14. Both are compared with the reference solution. It can be observed that the general shapes of the RSCs coincide with the reference solution. However, the area in which the flat branch of the RSC begins to sink into a steeply sloping branch appears, in the case of the numerical simulation, for a higher settlement than with the hybrid approach (around 4 cm for the numerical simulation in comparison with 1.5 to 2 cm for the hybrid approach).

It can also be noted that, similarly to pile groups, the transition area begins for a lower settlement for the corner pile than for the edge pile. The corner pile presents signs of failure before the edge pile. This behaviour also occurs in the case of the numerical calculation, but for a greater settlement. At equivalent settlements, the CPRF obtained by numerical simulation can thus carry higher loads than the hybrid design. The results of the simulation are presented in Figure 5.15.

**Table 5.6:** Input parameters for the determination of the resistance-settlement curves obtained with the convergence procedure.

	Load [kN]
Corner pile (1,2,5,6)	3447
Edge pile (3,4)	3393
Total load applied	20574



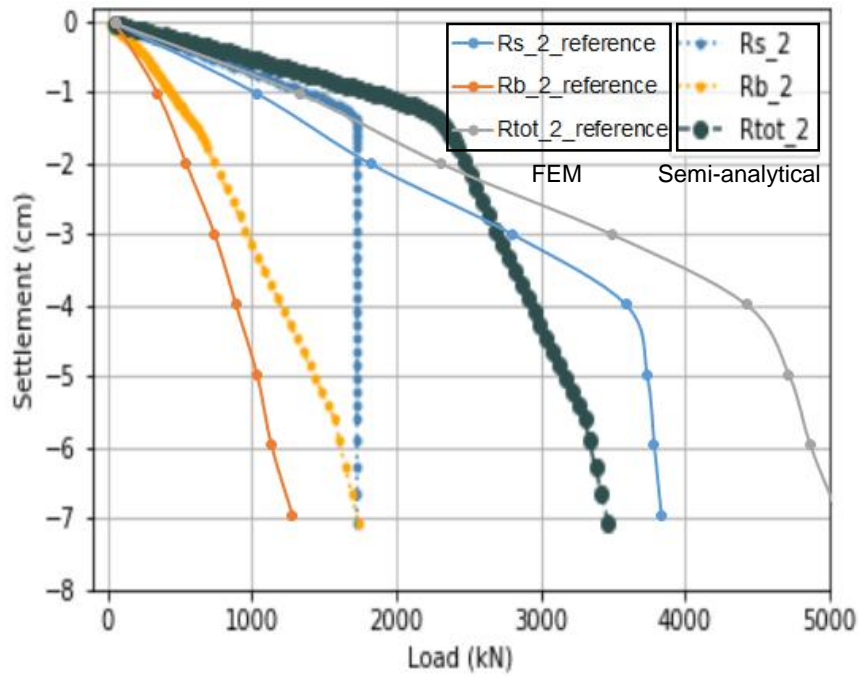


**Figure 5.13:** Comparison of the RSCs for the corner pile obtained with the developed design approach and with a numerical simulation (reference solution from *Hanisch et al. (2002)* [24]).

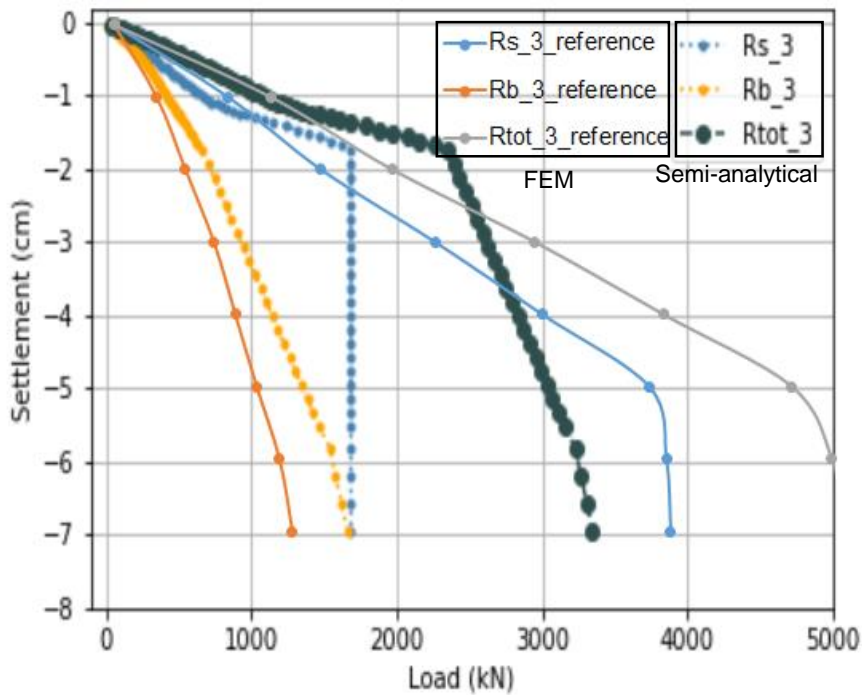


**Figure 5.14:** Comparison of the RSCs for the edge pile obtained with the developed design approach and with a numerical simulation (reference solution from *Hanisch et al. (2002)* [24]).

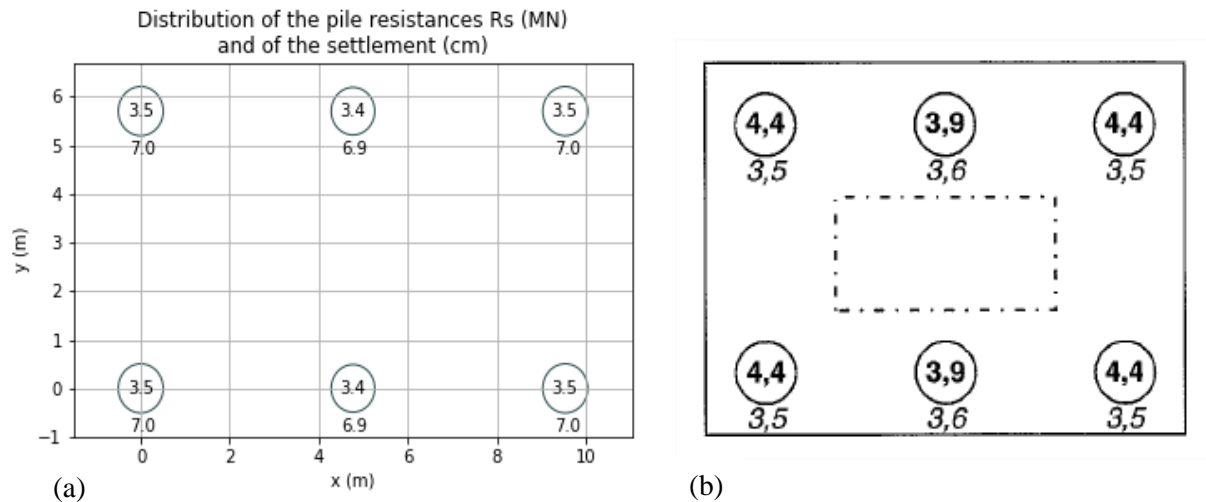


**Figure 5.15:** Comparison of the results for the benchmark "Guideline 1.3" (a) developed design approach (b) FEM model from Hanisch et al. (2002) [24]. Pile resistance inside the piles (MN), settlement under the piles (cm).

The final spring stiffness for the corner pile amounts to 49.4 MN/m and, for the edge pile, to 48.6 MN/m. The final design of the CPRF is finally obtained with the help of RFEM in Figure 5.16, providing detailed results of the semi-analytical calculation Figure 5.15 (a).

Given that a larger part of the total load is carried by the slab in the hybrid calculation (see Figure 5.17 comparing the piled raft coefficient of the two different approaches), the obtained pile resistances are expectedly smaller. However, the settlements are almost twice as high in the hybrid method as in the reference solution. This difference can be explained with the same arguments than those used for the pile group design, which were highlighted in Table 5.3. The introduction of a more complex constitutive equation of soil in the semi-analytical calculation such as the Hardening Soil Model could improve the quality of the results.

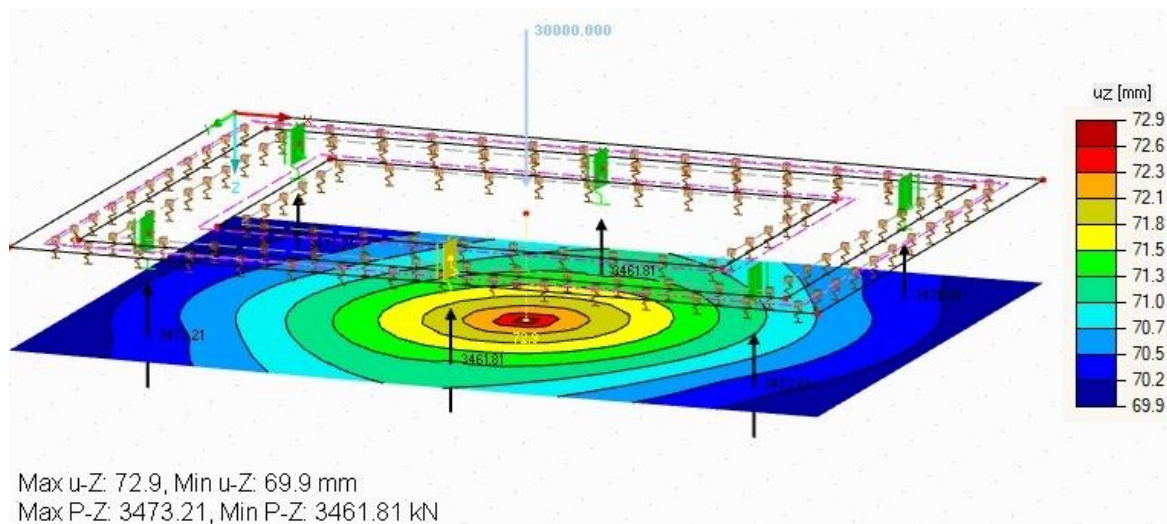


**Figure 5.16:** Final calculation in RFEM using the final spring stiffness calculating with a semi-analytical approach.

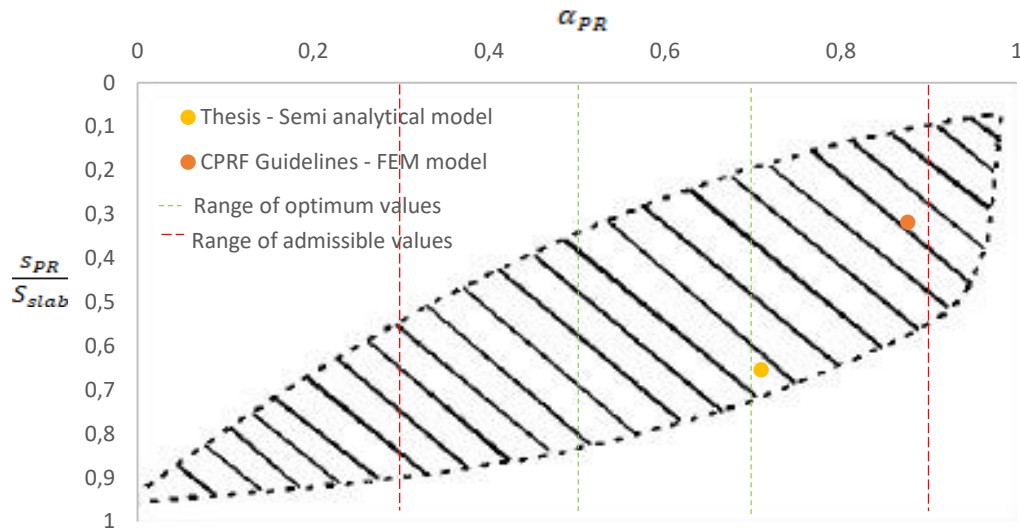


**Figure 5.17:** Comparison of the piled-raft coefficient  $\alpha_{PR}$ .

To better compare the two models, one finally calculates their piled raft coefficients. According to *Hanisch et al.* (2002) [24], CPRFs with a coefficient  $\alpha_{PR}$  between 0.3 and 0.9 have been put into practice. Related to technical and economic aspects, a CPRF coefficient  $\alpha_{PR}$  between 0.5 and 0.7 can be considered as ideal [31]. Those limit values are represented in Figure 5.17 together with the piled raft coefficients of the two approaches. It can be said that the developed approach offers an amelioration of the piled raft coefficient, but, at the same time, increases the settlement.

The settlement calculated with the design approach developed in this thesis lies above the admissible value of the settlement  $s_{adm} = 4$  cm, whereas this value is not exceeded in the reference solution. The foundation of the bridge pillar as CPRF with the given geometrical parameters designed following the developed method is therefore not possible. Further optimisation of these parameters is necessary.

In a nutshell, the analytical approach for the design of pile groups 3.3 provides satisfactory results and a good approximation of the numerical results for edge and corner piles. However, the pile shaft resistance of the inner pile presents discrepancies with the numerical calculation due to the influence of the group effect in the semi-analytical calculation. The hybrid method presented in 4.3 enables to optimise the piled raft coefficient but simultaneously increases the settlement, which can lead to a problem for the design of CPRF.

To reduce costs while designing a safe structure, it is necessary to optimise the design of the foundations. An optimisation method applicable to pile groups and CPRFs is therefore proposed in the next chapter of this thesis.



# 6 Optimisation of pile groups and piled raft foundations

## 6.1 Optimisation method

### 6.1.1 Problem

Optimisation procedures are sorted into two main groups of problems: those with single objective and those with multiple objectives. A general mathematical problem of optimisation is described as follows:

$$\text{Find: } x \in A = [\text{lower boundary, upper boundary}]$$

$$\text{To minimise: } f(x) \in \mathbb{R}^{n_{obj}}$$

$$\text{Subject to: } c_e(x) = 0$$

$$\text{And } c_i(x) \leq 0$$

where  $x$  is called *decision vector* or *chromosome*,  $c_e \in \mathbb{R}^{n_{ec}}$  represents the equality constraints (with  $n_{ec}$  the number of equality constraints),  $c_i \in \mathbb{R}^{n_{ic}}$  the inequality constraints (with  $n_{ic}$  the number of inequality constraints),  $A$  is the box-bounds and  $n_{obj}$  is the number of objectives to minimise. Such a problem is expressed in various other forms, for instance:

$$\min (f(x) \in \mathbb{R}^{n_{obj}} \mid x \in A, c_e(x) = 0, c_i(x) \leq 0) \quad (6.1)$$

In most cases, the problem of optimisation revolves around minimisation, but sometimes optimisation requires maximisation. In the latter case, one expresses the maximisation problem as an equivalent of the minimisation problem as follows:

$$\max f(x)_{x \in A} = -\min (-f(x))_{x \in A} \quad (6.2)$$

In this context, “equivalent” means here that the solutions are the same and that the optimal values are of opposite sign. An optimisation method can be used for both minimisation and maximisation problems.

As mentioned in *Chase et al. (2009)* [6], there is rarely a single optimal solution of a multi-objective problem if the objectives conflict. That is often the case for applied engineering projects, where the best performance at the lowest price is sought: improving the performance often leads to increasing costs. In this case, a multi-objective optimisation should be performed, commonly called Pareto optimisation, providing multiple solutions representing a trade-off between the objectives. Further details are to be found in Section 6.1.3 regarding, for example, the non-dominated sorting in multi-objective optimisation.

To benchmark the performance of multi-objective Pareto optimisation methods, special problems, or test functions, were created containing some obstacles or difficulties in order to converge to the Pareto

front. This is the case of the ZDT family of functions presented in *Zitzler et al. (2000)* [54], named after its authors Zitzler, Deb and Thiele, which is conceived for two-objective problems.

The first ZDT function (box constrained continuous problem in  $n$  dimensions, with  $n > 1$ ) is used to test the developed Python scripts. The first ZDT function is expressed as follows:

$$\begin{aligned} x &\in [0,1] \\ f_1(x) &= x_1 \\ f_2(x) &= g(x) \left[ 1 - \sqrt{\frac{x_1}{g(x)}} \right] \text{ where } g(x) = 1 + 9 \frac{\sum_{i=2}^n x_i}{n-1} \end{aligned} \quad (6.3)$$

It has been decided to use this test function in two dimensions,  $g$  is then simply expressed as  $g(x) = 1 + 4.5 x_2$ .

The Pareto optimal front is well known analytically and formed for  $g(x) = 1$  [54]. This enables to study precisely the convergence of the solution to the Pareto front precisely. A metric is for example defined and introduced by *Izzo and Biscani (2017)* [27]. This convergence metric allows measuring a “distance” of a population from the analytical Pareto front (more precisely the average distance of each individual of the input population). A distance of zero indicates that the optimal front is reached.

### 6.1.2 Population

A population is a storage for candidate solutions to some problem, sometimes called individuals. A population contains a problem and a number of decision vectors together with their fitness vectors. The fitness function determines the quality of the solution, that is to say their concordance with the objective function.

The best individual that has ever been part of a population is called “champion” and is not necessarily currently part of the population. The champion can only be extracted in single objective problems; in multi-objective problems, the notion of solution is better expressed using non-dominated fronts (see the following section).

### 6.1.3 Algorithm

A large number of algorithms were created to solve the general problem presented above. Sorting them is complex due to the considerable number of parameters defining each algorithm. Algorithms can be deterministic or stochastic. A deterministic algorithm is an algorithm which, given an input, will always produce the same output and execute the same sequence. On the contrary, stochastic optimisation methods are optimisation methods that generate and use random variables.

#### 6.1.3.1 Iterative methods

Iterative methods differ according to whether they evaluate Hessians, gradients, or only function values. Evaluating Hessians and gradients improves the convergence but at the same time increases the computational cost of each iteration. The well-known Newton’s method approximate, for example, Hessians using finite differences whereas the Gradient descent’s method uses gradient evaluations.

These methods present some disadvantages, for example the fact that the objective function must be smooth enough to be differentiable, or even two times differentiable for the Hessian matrix. In civil engineering, the mathematical properties of the objective functions are often not well-known and it may even be difficult to express the objectives explicitly. Furthermore, initial conditions must be given to

initiate the iterative process, and this choice can drastically influence the result. Moreover, the convergence is slow and can lead to a suboptimal solution. That is why other algorithms were developed.

### 6.1.3.2 Combinatorial optimisation

A combinatorial optimisation consists of finding an optimal object from a finite set of objects. It concerns problems where at least a part of the box bound contains discrete values. They are often used in the Constraint Composite Graph theory or in the Game theory.

### 6.1.3.3 Heuristics and metaheuristics

To solve more complex problems and to avoid the disadvantages of the iteration methods mentioned above, techniques were created to determine decision vectors that are not strictly optimal, but that give a good approximation of the minima or maxima, and which converge in a reasonable time. This enables to solve problems that would otherwise require too much time. A huge advantage of these methods is that they make few or no assumptions about the problem being optimised and are able to search very large spaces of candidate solutions. Heuristic algorithms are stochastic as they need random parameters to evolve.

Heuristics algorithms will be used to optimise CPRFs, and in particular some genetic algorithms, themselves member of the family of the evolutionary algorithms. An evolutionary algorithm uses the concept of biological evolution, based on the notions of variation (recombination, reproduction, mutation, etc.) and selection. In each generation, or iteration of the algorithm, new candidate solutions are created by a variation of the individuals of the former generation. Then, some individuals are selected to become parents in the next generation based on their fitness. If the decision vectors with the best fitness are systematically chosen, the process is said to be elitist and leads to a quicker convergence. Acting so, one takes the risk to push aside bad decision vectors that could have produced extremely good ones by reproduction in the next generations.

As mentioned above, genetic algorithms are part of the larger class of the evolutionary algorithms. Their general process is summarised in Figure 6.1.

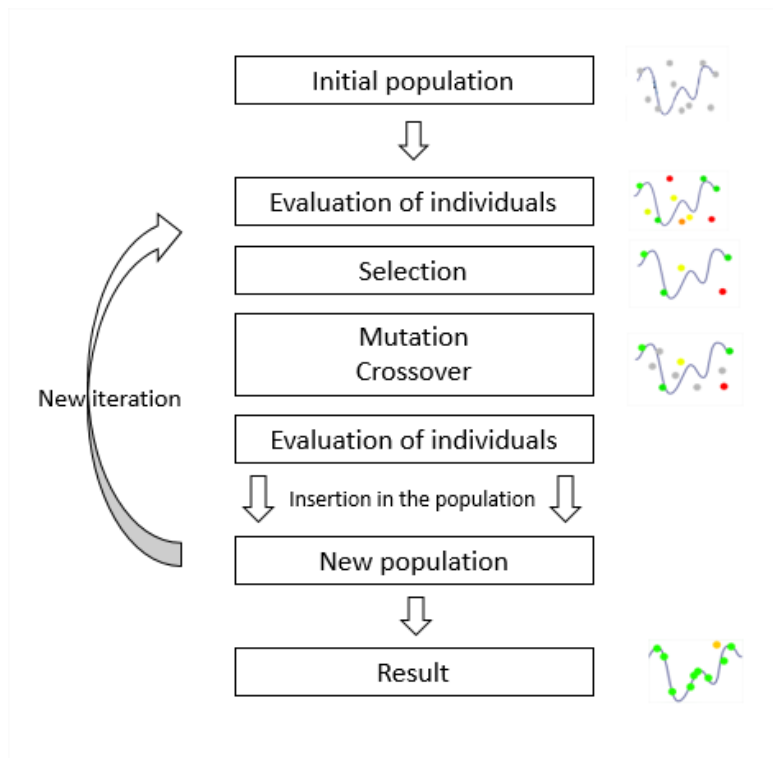


**Figure 6.1:** Simplified process of a genetic algorithm.

However, such algorithms do not guarantee an optimal solution is ever found. It is only established that none of the obtained solutions dominates the others. The notion of non-dominated sorting is a common technique to sort designs in a multi-objective optimisation study. As explained in *Chase et al. (2009)* [6], one individual dominates another if it is better regarding one objective and not worse regarding all other objectives.

Figure 6.2 summarises the major types of algorithm available to solve single and multi-objectives problems.

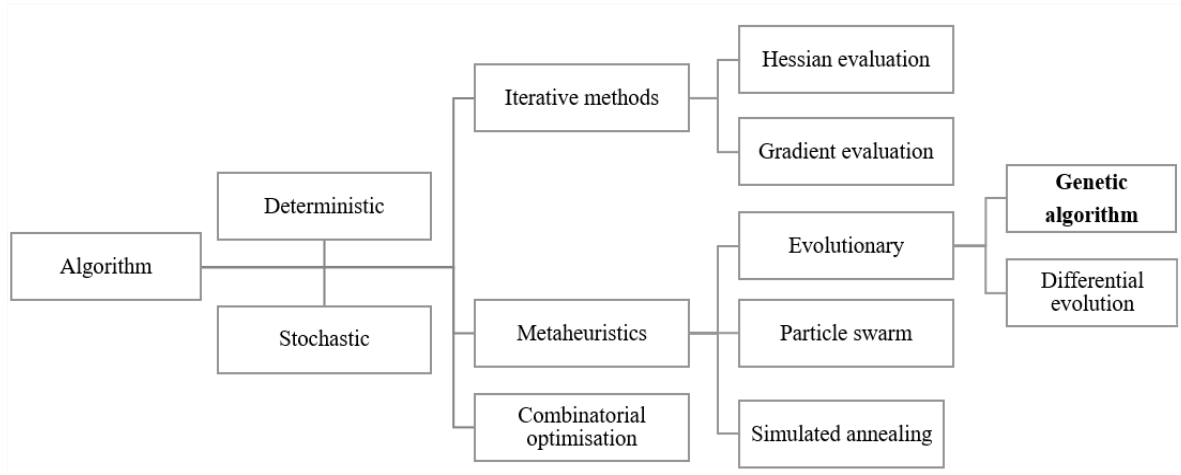


**Figure 6.2:** Simplified sorting of the main families of algorithms.

#### 6.1.3.4 Some examples

Algorithms were chosen within the pygmo library to study the CPRFs because of their robustness and the large documentation available. They constitute a solid benchmark to test against.

The Non-dominated Sorting Genetic Algorithm-II (NSGA-II) is a solid and popular multi-objective algorithm. As indicated in its name, it is part of the genetic algorithms whose general process is shown in Figure 6.1. The speciality of the NSGA-II is the use of crowding distance comparison and non-dominated selection to select the next generation that will be evaluated (see Figure 6.3 and *Deb et al. (2002)* [11]). The total population  $R_t$  (of size  $2n$ ) formed by  $P_t$  and  $Q_t$ , is sorted using the non-dominating method. The population contained in the best front set  $F_1$  is selected first to create the new population  $P_{t+1}$ . In the example in Figure 6.3, the last set  $F_3$  would lead to an oversized population  $P_{t+1}$ . We thus sort the solutions of  $F_3$  using the crowded-comparison. Solutions which are far away (called “not crowded”) from other solutions are given a higher preference during the selection. This is done in order to make a diverse solution set and avoid a crowded solution set.  $P_{t+1}$  of size  $n$  is then used for selection, crossover and mutation to create  $Q_{t+1}$ , and so on.

The NSGA-II algorithm needs some input parameters to run. These are the number of generations to evolve, the size of the population, the crossover probability, called  $cr$ , and the mutation probability, called  $m$ . The default values given by the Python library used to solve the optimisation problem are  $cr = 0.95$  and  $m = 0.01$ . Note that the conditions  $cr \in [0,1[$  and  $m \in [0,1]$  have to be fulfilled. These default values are in accordance with the values generally seen in genetic algorithms. The crossover probability is chosen high (usually 0.8 - 0.9) and the mutation far smaller (around 0.005 - 0.01) [6]. A high crossover rate gives a global search capability to the algorithm, which enables to search within the whole box bound of the problem. The low mutation rate helps to explore the local vicinity of the possible solutions, also called local search capability.



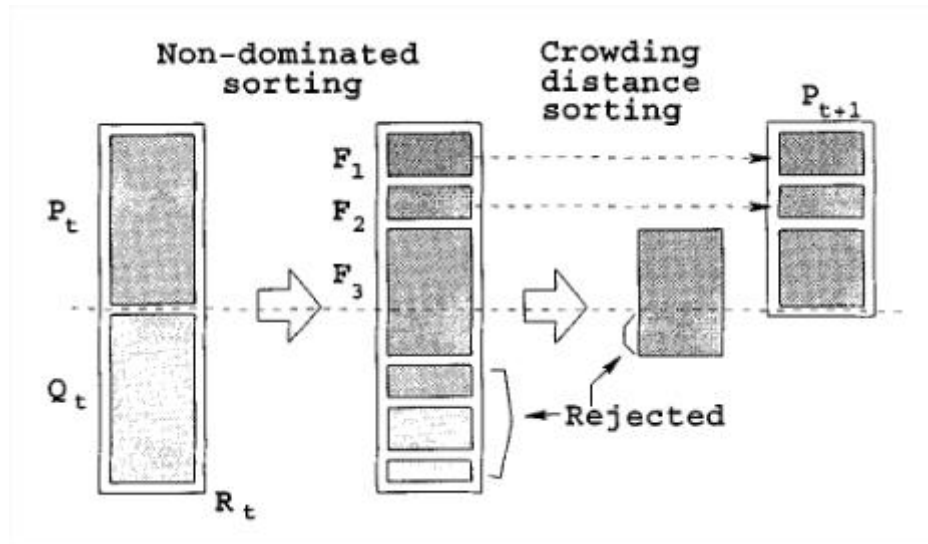


**Figure 6.3:** NSGA-II Procedure, illustration taken from [11].

According to *Izzo and Biscani* (2017) [27], the Multi Objective Evolutionary Algorithm by Decomposition (MOEAD) is a very successful optimisation algorithm. The main idea of this algorithm is the decomposition of the optimisation problem into different scalar subproblems, which are optimised simultaneously. Each subproblem is optimised exploiting only information from its several neighbouring subproblems since neighbouring subproblems should have close optimal solutions [35]. This enables a lower computational complexity at each generation than other algorithms, such as the non-dominated sorting genetic algorithm. The population is then composed of the best solution found for each subproblem. Different methods were developed to decompose the optimisation problem. The most commonly used are the Weighted Sum approach, the Tchebycheff approach and the boundary intersection approach. More details on these methods can be found in *Li* (2007) [35]. These three possibilities of decomposition are selectable in pygmo, together with a mutation rate to create an offspring.

As further developed in a benchmark study in Appendix C.2, the MOEAD turns out to be inapplicable for the present optimisation problem. Indeed, the algorithm tends to favour one objective over the other; it exaggerates the impact of the volume reduction over the settlement objective. That is why the NSGA-II is predominantly chosen for the present study.

## 6.2 Optimisation of pile groups

The optimisation of pile groups is a complex engineering task as the problem to solve cannot be expressed in a simple and straightforward way but in a complex semi-analytical calculation. The properties of the objective functions are not known, and one cannot make statements about the steadiness of the functions, their convexity, the number of maxima, etc. The lack of information about some precise mathematical functions (which are normally available for standard optimisation problems) makes the use of evolutionary algorithms necessary. One does not need to make mathematical assumptions about the problem to optimise.

The foundation of a bridge pillar is optimised, consisting of a  $4 \times 3$  pile group subject to an axial centrally load of 30 MN. One takes as reference the initial design coming from the CPRF Guideline and presented in Section 5.1.1 “Guideline 1.2”. The optimisation method is coded in a Python script and included in Appendix A.2.

### 6.2.1 Design parameters

Different design parameters are optimised in this study, chosen to meet the needs of the optimisation. The pile spacing is modelled by means of two parameters, one over the length of the foundation raft, the other over its width. Therefore, rectangular configurations of the pile group can be optimised. The possibilities of the optimisation stay limited to rectangular configurations since only numerical values (i.e. the distance between two piles in two directions) can be varied, and a randomly generated position of the pile in a grid is not carried out.

One standard radius is adopted for all the piles and varied during the optimisation. This assumption is made for practical reasons. On the construction site, usually one drilling machine is available, which is able to drill piles of standard diameter. The construction of piles, each one of which having different diameters would not be easily accomplishable on site. Therefore, the study is limited to one radius parameter.

Concerning the pile length, a different parameter is adopted for every pile; twelve length parameters are therefore necessary. In total, fifteen parameters are contained in the decision vector: twelve for the pile lengths, two for the pile spacing and one for the pile radius.

### 6.2.2 Objective functions

The foundation must be configured so that the smallest settlement is reached. This objective is often achieved by increasing the number of piles or lengthening them, which leads to a larger volume of the foundation and thus to higher costs. The present problem to optimise is therefore multi-objective: improving an objective function worsens other aspects of the problem.

Material and manufacturing costs as well as construction costs of the foundation elements are strongly simplified and supposed proportional to the volume of the foundation. The costs are a direct function of the volume. No difference in the costs between the construction of the piles and the construction of the raft is taken into account in a first approximation.

The optimisation problem is composed of the objective functions presented in Equations (6.4) and (6.5), where  $\alpha$  is the proportionality factor between the costs and the volume of the foundation and  $x$  the decision vector generated within a box-bound. The lower and upper boundaries of the decision vectors are defined in Section 6.2.3.

$$f_1(x) = s_{max}(x) \quad (6.4)$$

$$f_2(x) = V_{\text{foundation}}(x) = \alpha \text{ costs} \quad (6.5)$$

### 6.2.3 Constraints and box boundaries

For this optimisation problem, no equality or inequality constraints are considered. Nevertheless, the design parameters are only varied within physically meaningful limits, which are presented in Table 6.1.

### 6.2.4 Results

The optimisation is performed using the NSGA-II algorithm, which appears to be the most suitable in comparison to other tested algorithms. The crossover rate  $cr$  amounts to 0.95 and the mutation rate  $m$  to 0.01. A sufficient amount of individuals and generations are chosen to obtain a satisfactory result according to the simulations realised in an academic benchmark (see Appendix C.1).

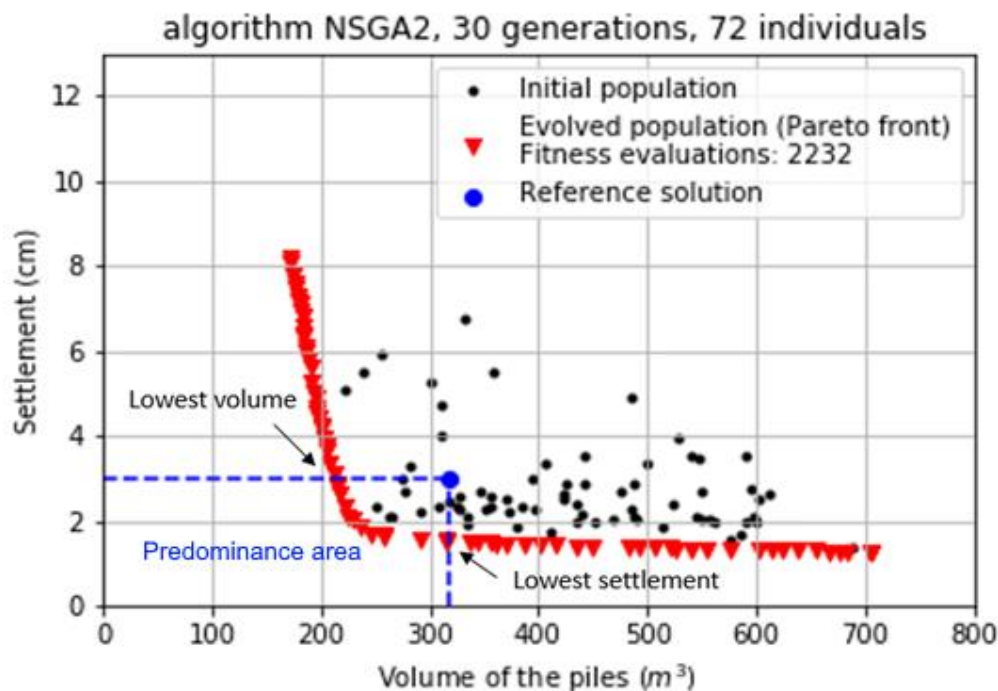
**Table 6.1:** Boundaries of the design parameters for the optimisation of the “Guideline 1.2”.

Designation	Minimum value [m]	Maximal value [m]
Pile length	10	25
Pile radius	0.6	1
Pile spacing (length)	1.5	6
Pile spacing (width)	1.5	6

Figure 6.4 represents the investigated solutions of the objective functions, where the initial population is displayed with black dots and the evolved population (in red) forms the final Pareto front, i.e. the optimal set of solutions. The optimal set of solutions is not necessarily the set of decision vectors of the last iteration of the genetic algorithm.

For each point of the Pareto front, none of the two objective functions can be improved without worsening the other one. It is not possible, for any of the red triangles forming the Pareto front in Figure 6.4, to improve the settlement without simultaneously increasing the volume of the foundation, respectively to reduce the volume without increasing the settlement.

The reference solution of *Hanisch et al.* (2002) [24] is plotted as a blue dot. The blue dotted lines delimit a predominance area, which contains all the solutions that are improving the initial reference design in terms of both settlement and volume. The intersection of the dotted blue line with the Pareto front constitutes two specific optimal solutions: the “lowest settlement” and “lowest volume” solution. The lowest volume (or volume optimum) solution is the solution that presents, for the same settlement as the reference solution, the lowest volume; and inversely for the lowest settlement solution. The settlement and volume optima solutions are presented in Table 6.3. The geometrical parameters of the foundation for the reference solution and for both optima solutions are contained Table 6.2.

**Figure 6.4:** Fitness of the objective functions plotted in the objective space, settlement over the volume of the piles (Pareto front highlighted in red).

**Table 6.2:** Parameters of the original chosen design and of the lowest volume and lowest settlement solutions, mean values for the length of each standard pile; values are given in meters.

	Reference	Lowest volume	Lowest settlement
Length corner pile	15	17.55	22.13
Length edge pile	15	15.66	19.38
Length inner pile	15	11.55	19.45
Pile diameter	1.5	1.20	1.28
Pile spacing (length)	3	5.99	5.98
Pile spacing (width)	3	5.97	5.88

**Table 6.3:** Lowest volume and lowest settlement solution referring the original chosen design.

	$s$ [cm]	$\Delta s$ [%]	$V$ [m <sup>3</sup> ]	$\Delta V$ [%]
Reference solution	3.00	-	318	-
Volume optimum	3.12	+4.0	212	<b>-33.3</b>
Settlement optimum	1.51	<b>-49.7</b>	316	-0.6

The initial design of the pile group could be optimised successfully. The pile volume has been reduced by 33% for a comparative settlement, and the settlement has been diminished by 50% for the same volume.

### 6.3 Optimisation of CPRFs

The foundation of a bridge pillar consisting of a 3×2 CPRF subject to an axial centrally load of 30 MN is optimised. One takes the initial design coming from the CPRF Guideline and presented in Section 5.2 “Guideline 1.3” as reference.

Design parameters and objective functions are the same as those presented for the optimisation of pile groups in Section 6.2. It has to be noted that the number of design parameters is smaller for the optimisation of CPRFs since the number of piles used is lower. The decision vectors contain nine parameters: six for the piles, two for the pile spacing and one for the pile radius.

#### 6.3.1 Rigidity

In this optimisation study, two types of foundations are compared, one foundation presenting a rigid raft and the other a more flexible raft. One determines the type of foundation in relation to the thickness of the slab presented in Equation (6.6), derived from Equation (4.9).

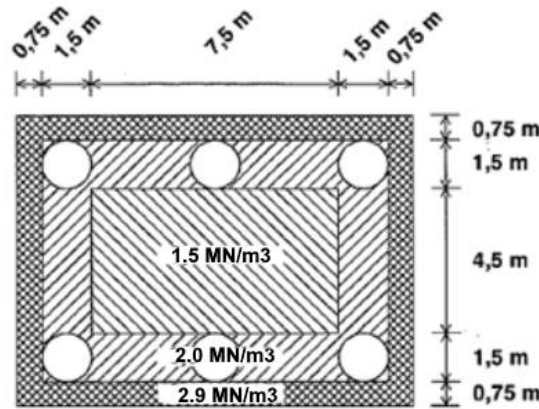
$$h = \sqrt[3]{12K \frac{E_s}{E_{PR}}} l \quad (6.6)$$

where  $E_s$  is calculated as the mean value of the stiffness of the subsoil and equals 40 MPa. The chosen material for the slab of the CPRF is a concrete of strength class C25/30 whose modulus of elasticity  $E_{PR}$  amounts to 32 GPa. The length of the pile  $l$  is 12 m.

**Table 6.4:** Limit thickness of the slab for the benchmark “Guideline 1.3”.

System rigidity $K$	Type of foundation	Thickness of the slab [m]
$K \geq 0.1$	Rigid foundation	$h \geq 1.4$
$0.001 \leq K < 0.1$	Intermediate area	$0.3 < h \leq 1.4$
$K < 0.001$	Limp foundation	$h < 0.3$

The thickness of the rigid slab is set to two meters and the thickness of the intermediate foundation to one meter following the desired categories of Table 6.4. The study of a limp foundation leads to inapplicable results since a slab thinner than 30 cm is not able to carry the required loads for the given geometrical parameters of the piles. The adopted subgrade reaction modulus for the rigid foundation is the one already calculated Section 5.2 and presented in Figure 5.12. For the subgrade reaction of the intermediate slab, however, it is necessary to calculate a new reaction modulus since the ratios presented in Table 5.5 depend on the rigidity of the desired foundation. Combining those empirical values and the subgrade reaction modulus of the equivalent shallow foundation calculated in *Hanisch et al. (2002)* [24], one obtains the subgrade reaction modulus of the intermediate CPRF presented in Figure 6.5.

**Figure 6.5:** Subgrade reaction modulus for the CPRF of the example “Guideline 1.3”, intermediate slab. Adapted from [24].

### 6.3.2 Box boundaries

The box boundaries of the decision vectors generated in this optimisation problem are introduced in Table 6.5. The minimum values are of special importance. Indeed, for a given generation of the algorithm, if one randomly generated decision vector is set up with all the design parameters at their minimum values, the unfavourable geometry could lead to a breakdown of the foundation. The minimum values are then chosen so that none of the generations leads to a possible failure of the CPRF.

**Table 6.5:** Boundaries of the design parameters for the optimisation of the CPRF “Guideline 1.3”.

Designation	Minimum value [m]	Maximum value [m]
Pile length	12	22
Pile radius	0.72	1.2
Pile spacing (length)	3.5	5
Pile spacing (width)	3.5	6

### 6.3.3 Results

The NSGA-II algorithm is used with the same crossover and mutation ratio as for the optimisation of pile groups. Figure 6.6 represents the investigated solutions of the objective functions for both CPRFs. The dotted red and orange lines are nonlinear regressions of the optimal decision vectors extending the Pareto fronts for values that could not be covered by the optimisation.

The reference solution of *Hanisch et al. (2002)* [24] for the CPRF is plotted as a blue point and the predominance area formed as presented in Section 6.2. As the dotted blue lines delimiting this area cross the two Pareto fronts, each foundation design possesses both lowest volume and settlement solutions. The lowest settlement solution (obtained when the volume of the piled raft is fixed to the volume of the reference solution) for both foundation designs are coinciding to a large extent. That is not the case for the lowest volume solution: the CPRF presenting the thinner foundation slab enables a more significant reduction of the volume of the whole piled raft.

Due to the symmetry of the structure and given the axial central load, one can restrict the study of the piles to two standards piles enumerated in Figure 6.7: the edge piles are referenced to as “1” and the corner piles as “2”.

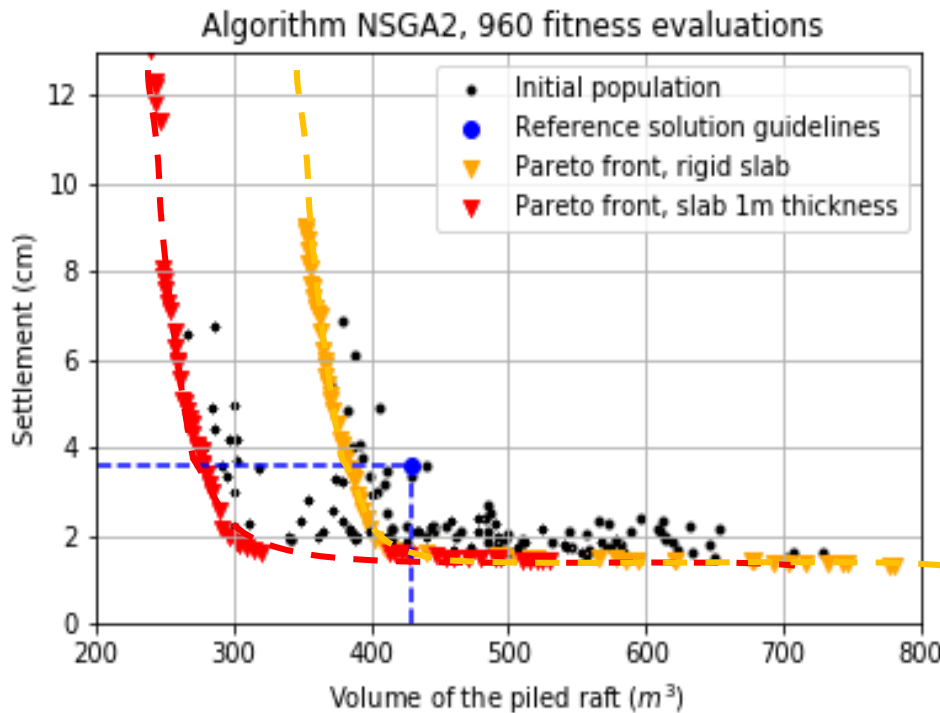


**Figure 6.6:** Pareto fronts for a rigid slab (in orange) and for an intermediate slab (in red) obtained for 960 iterations.

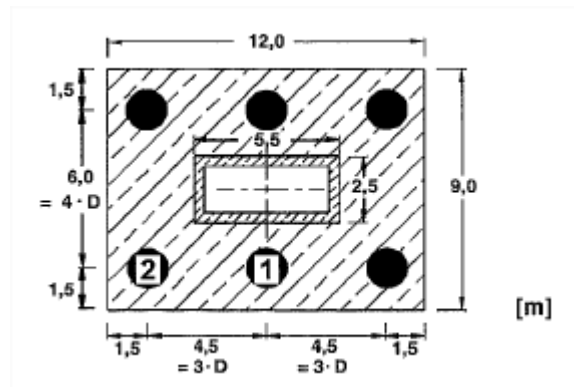


**Figure 6.7:** Pile numbering and geometrical parameters for the reference design [24].

The geometrical parameters obtained for the lowest volume solution of both foundations are presented in Table 6.6 and those for the lowest settlement solution in Table 6.7.

It can be noted that the piles of the volume optimum are shorter than the piles of the settlement optimum. This is particularly visible for the rigid CPRF, where both corner and edge piles are three meters longer for the optimum settlement than for the optimum volume. As a general rule, the optimised piles are longer than those of the reference solution. The obtained pile lengths are coherent since a pile lengthening reduces the settlement but increases the volume; it is logical that the optimum settlement presents longer piles whereas the optimum volume tends to reduce their length.

Moreover, optimised piles are longer than the reference piles since the hybrid design approach exhibits higher settlements than the reference solution (Section 5.2) for equal geometrical parameters. To obtain at least the same settlements as the reference, longer piles are necessary. Lowest settlement solutions (Table 6.7) for the two CPRF designs display different geometrical parameters but achieve approximately the same result, as shown in Figure 6.6. The CPRF with an intermediate slab presents shorter piles but a larger pile diameter than the foundation with a rigid slab. The pile spacing obtained is similar for the two designed foundations as well as for the reference solution.

Settlement and volume optima solutions for both foundation types referring the original chosen design are compiled in Table 6.8. A reduction of the settlement of 55% has been reached for both chosen designs referring the initial solution of *Hanisch et al.* (2002) [24]. The CPRF adopting an intermediate slab has led to the largest reduction of the volume (37%). To get a better overview of the obtained geometrical parameters, an illustration of the different designs is presented in Figure 6.8 for the settlement optimum. The three piled raft foundations have the same volume, whereas the settlements of the two optimised designs are 55% smaller than the one of the reference design.

**Table 6.6:** Parameters of the original chosen design and of the lowest volume solution, mean values of the length for each standard pile. Values are given in meters.

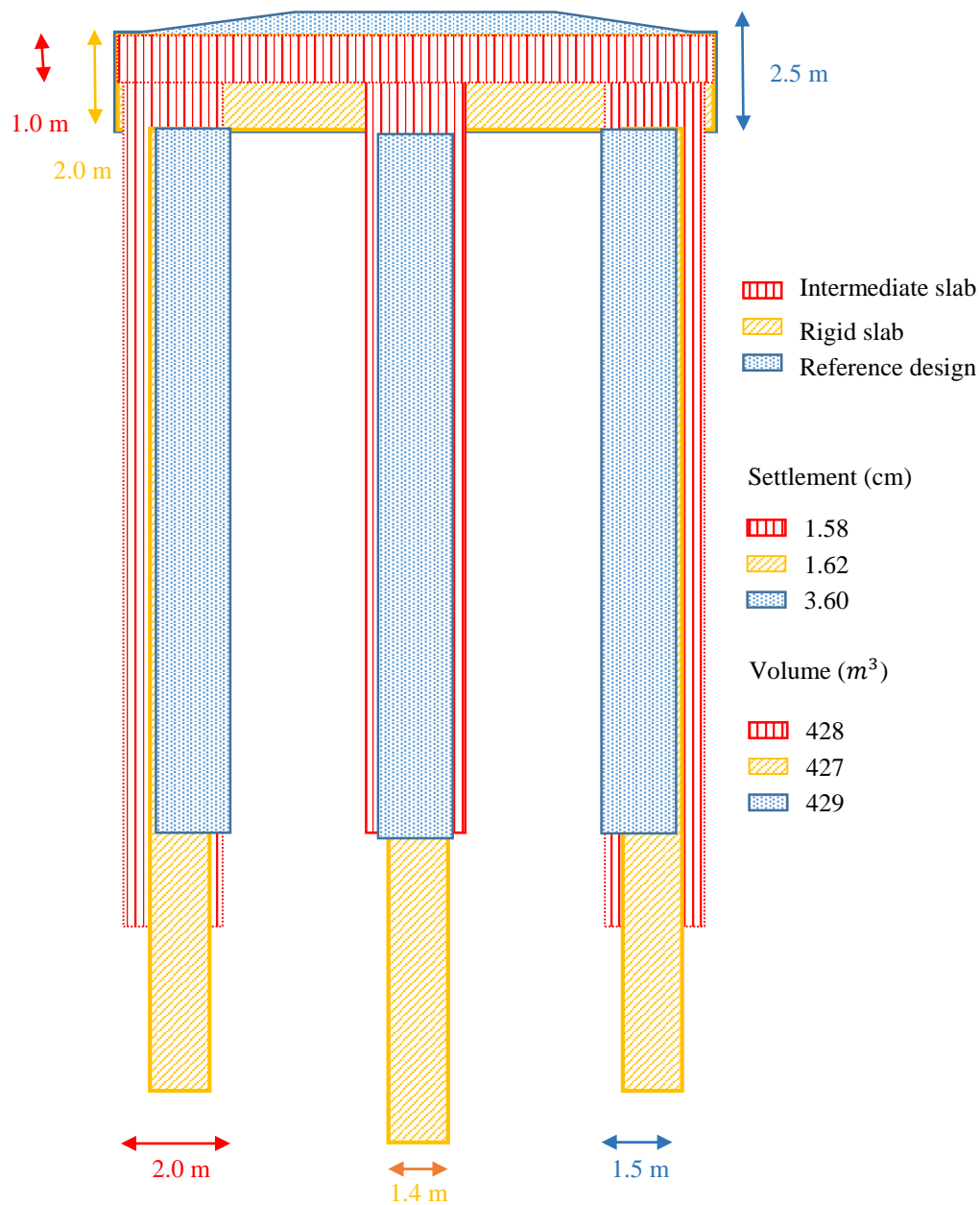
	Reference	Rigid slab	Intermediate slab
Length corner pile (2)	15	17	17
Length edge pile (1)		18	16.5
Pile diameter	1.5	1.4	1.4
Pile spacing (length)	4.5	4.65	4.5
Pile spacing (width)	6	5.9	5.8
Slab thickness	2.2	2	1

**Table 6.7:** Parameters of the original chosen design and of the lowest settlement solution, mean values of the length for each standard pile. Values are given in meters.

	Reference	Rigid slab	Intermediate slab
Length corner pile (2)	15	20.5	18
Length edge pile (1)		21.6	16.5
Pile diameter	1.5	1.4	2
Pile spacing (length)	4.5	4.8	4.9
Pile spacing (width)	6	5.7	5.8
Slab thickness	2.2	2	1

**Table 6.8:** Lowest volume and lowest settlement solution referring the original chosen design.

		s [cm]	$\Delta s$ [%]	V [m <sup>3</sup> ]	$\Delta V$ [%]
<b>Reference solution</b>		3.60	-	429	-
<b>Volume optimum</b>	Rigid slab	3.51	-2.5	383	<b>-10.7</b>
	Intermediate slab	3.62	+0.5	272	<b>-36.6</b>
<b>Settlement optimum</b>	Rigid slab	1.62	<b>-55.0</b>	427	-0.5
	Intermediate slab	1.58	<b>-56.1</b>	428	-0.2

**Figure 6.8:** Illustration of the optimised CPRFs in comparison with the reference design for the lowest settlement solution.



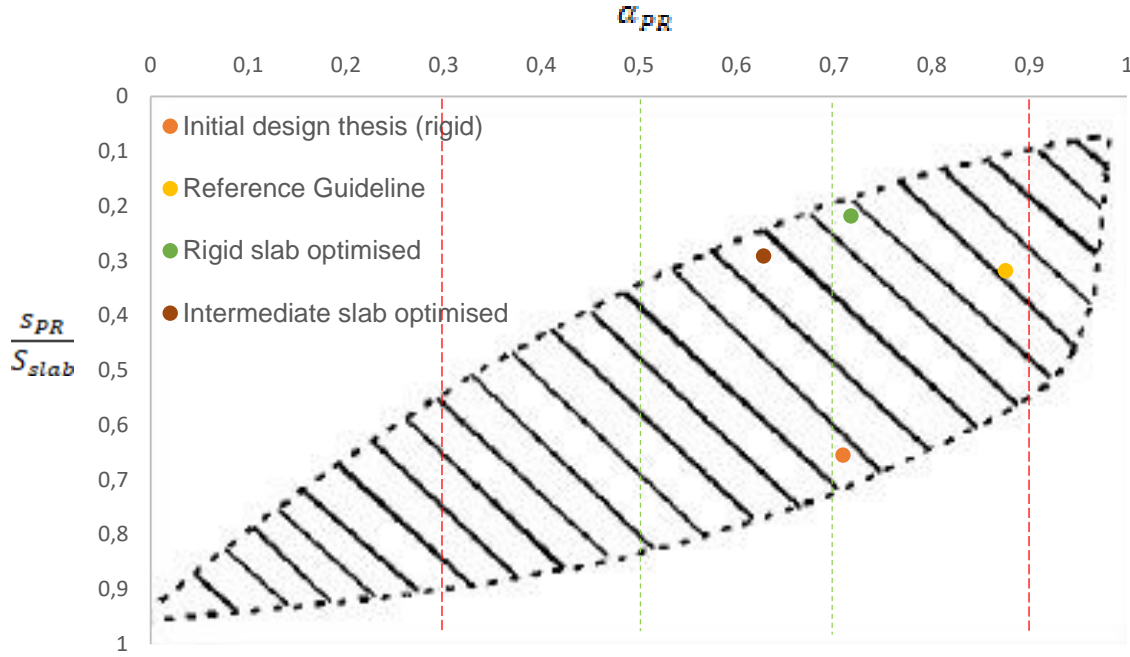


**Figure 6.9:** Piled-raft coefficients for different designs of the “Guideline 1.3”.

The piled raft coefficients of the different designs are summarised in Figure 6.9, where the same limit values are presented in Section 5.2: admissible values are delimited by the red lines and optimum values by the green ones. The settlement of the shallow foundation used to calculate the ratio  $s_{PR}/s_{slab}$  comes from the numerical simulation of the CPRF guideline example 1 version 1 “Guideline 1.1” of *Hanisich et al.* (2002) [24].

The initial design of the thesis presented in Section 5.2 adopts a rigid slab, together with the “Reference guideline” solution of *Hanisich et al.* (2002) [24]. Both designs are not optimal, the first one presenting a too high settlement and the second one transferring a too large load component by means of the piles, as shown by the piled raft coefficient approaching 0.9 in Figure 6.9. On the contrary, the two optimised solutions present satisfactory results. The optimised CPRF with a rigid slab presents lower settlements than the reference solution and its piled raft coefficient approaches the optimal area. The optimised CPRF with an intermediate flexible slab has even been able to reach a piled raft coefficient in the optimal area for a slightly higher settlement than the optimised CPRF with a rigid slab.

Moreover, the proof of external serviceability is added for both optimised designs as the settlements of 1.6 cm respectively 1.58 cm calculated with the geometrical parameters of the settlement optima are lower than the admissible settlement  $s_{adm} = 4$  cm.

## 6.4 Limitations and drawbacks

A major limitation of the current optimisation method is that the influence of the slab (interaction raft-soil and interaction raft-pile) is not taken into account during the evolution of the genetic algorithm. Indeed, the genetic algorithm works with the results of the analytical algorithm developed in Python and does not communicate directly with RFEM. The different Pareto fronts obtained therefore present, to a large extent, the same shape up to a translation of the curve corresponding to the difference of the volume of the slab.

Moreover, only rectangular pile configurations can be investigated. In contrast to the initial design where the piles can be positioned according to their Cartesian coordinates and form an arbitrary geometry, the

optimisation of such an arbitrary geometry is not possible. Indeed, the genetic algorithm needs to optimise values and cannot directly “optimise” a point defined by its coordinates.

One can call attention to the fact that the reinforcement is not taken into consideration in the foundation. There are no special costs for the reinforcement of the raft or the piles.

It has to be noted that the cost of the foundation is considered as proportional to the volume of the piled raft. This is equivalent to the introduction of a constant price per running meter, independent of the depth of the pile. Moreover, no influence factor is introduced between the volume of the slab and the volume of the piles, even if the costs are not the same for those elements. The producibility of the foundation is not considered in the optimisation, the assumption that the costs are directly proportional to the volume of the piled raft is strong and does not truly depict the reality. That is why the results of this optimisation have to be considered as a theoretical design study.

## 7 Summary and conclusions

Combined piled raft foundations are composite foundation systems combining the bearing capacity of a foundation raft with the one of the piles. Elements of the foundation exercise a mutual load-bearing effect and present reciprocal interactions (pile-pile and pile-raft) as well as interactions with the subsoil (pile-soil and raft-soil). In a CPRF system, the piles are employed as a measure to limit the settlements of a high loaded footing.

To the present day, a generally established and applicable analytical approximation procedure for CPRFs does not exist. This thesis presents a simplified method for the design of pile groups and of combined piled raft foundations based on a semi-analytical approach. This new design approach enables a rapid and robust approximation of the load-bearing behaviour of the structure, where the local boundary conditions can be easily adapted. An algorithm capable of creating an optimised design covering geotechnical as well as structural aspects is developed. This contribution also focuses on a multi-objective optimisation in practical applications using evolutionary algorithms. Based on a case study, it is shown that the required concrete masses for the piles and the raft of the CPRF can be significantly reduced.

This approximation procedure is based on sophisticated approaches, such as a non-homogeneous subsoil and a stress dependency of the soil stiffness. The model divides CPRF into a pile group and a footing, which is elastically bedded on the subsoil and on the pile group. The load-settlement curve for each pile is iteratively calculated for each load increment considering the mutual interaction between each pile. The interaction is considered by using a so-called influence radius in a simplified and load-independent way. Moreover, the load-settlement behaviour of each pile is derived on the basis of the Mohr-Coulomb failure criterion on the base and along the shaft of each pile. The developed algorithm offers an evolved design but remains straightforward and easy to handle.

In the proposed model the resulting load-settlement curves are used to calculate the equivalent spring stiffness for each pile. These spring stiffnesses and an estimated bedding of the raft on the subsoil are used as an input for iterative simulations using the standard design software RFEM, in which the CPRF raft is simulated as a bedded plate. Using this iterative simulation approach, one can calculate relatively fast the complex soil structure interaction of a CPRF foundation. The significant advantage of this new semi-analytical model is its high calculation speed, which is required for an efficient use of optimisation algorithms.

This approximation procedure can be applied to the design of foundations within the tender phase or to preliminary designs, when a good approximation model for the determination of the load-bearing behaviour is necessary but the recourse to numerical simulations is not compulsory. For the final dimensioning or within the execution phase, additional 3D FE calculations should be carried out since the model satisfies a simplified approach method and does not truly depict all the related effects.

In Chapters 3 and 4, different design approaches for pile groups respectively for combined piled raft foundations were presented, which thus contribute to a better understanding of deep foundation designs. In particular, the development of the script was described and the resulting improvements were compared to the initial analytical procedure of *Rudolf* (2005) [47]. The developed semi-analytical calculation method for CPRF was described in Chapter 4.

The basics of deep foundations were outlined in Chapter 2 and shall help to develop an understanding of their way of transferring loads to the subsoil and the particularities of the different existing systems. Moreover, they help interpret results of case studies presented in Chapter 5 to test the efficiency and the reliability of the developed solution by referring to tested examples from the literature. These case studies showed the application of the developed calculation method and shall guide the reader to a comprehensive understanding of the presented approaches.

Moreover, an overview of multi-objective optimisation problems was presented in Chapter 6. A newly developed way of optimisation using genetic algorithms was put forth. The semi-analytical calculation was optimised using mathematical algorithms to minimise the volume of necessary material as well as the settlement of the foundation, leading to a set of optimal solutions.

The results obtained by means of the simplified procedure are in good concordance with numerical calculations even if they do not entirely coincide due to the use of different models, boundary conditions and assumptions. It has been shown that the major advantages of CPRFs are a lower settlement of the whole structure as well as a reduction of the volume of material used in comparison with deep foundations, leading to optimised costs and a better economic viability.

Engineering design often relies on constant arrangement and symmetry of structures. However, such constant configurations are generally not very cost-effective. Moreover, the load-transfer capacity of elements of the foundation is rarely completely exploited. That is why an optimisation of deep foundations is of great advantage. By using the multi-objective optimisation library pygmo, better and more cost-effective results have been achieved compared to the reference solution from *Hanisch et al.* (2002) [24]. Based on the obtained results, it is arguable that the pile lengths are an effective measure to reduce the settlements of the CPRF in combination with a flexible raft. Concerning the overall need for concrete masses for the raft and for the piles, the obtained solutions show a significant reduction of required concrete. The settlement by identical volume has been reduced by 50% for pile groups and by 55% for CPRFs (for both rigid and more flexible slabs) in comparison with findings presented in the literature. However, these results have to be considered as theoretical design studies, since the producibility of the foundation as well as its internal bearing capacity have not been examined.

It has further been shown that by means of an optimisation procedure, a direct relation between costs and settlement can be established and displayed in the form of a Pareto front. This facilitates the evaluation of possible cost saving measures with a concrete insight into the increased risks following those savings. The representation of a Pareto front enables a rapid cost-benefit analysis when a limit settlement concerning the serviceability must be stated. This optimisation procedure presents a new perspective for constructors and planners, which opens the way for more cost-effective and thus competitive solutions in foundation design and the optimisation of complex problems in civil engineering.

The proposed and applied design model of the current paper could be further improved with the help of the following suggestions. An interface for the automated transmission of the results between RFEM and the Python algorithm should be developed. This would allow for a more efficient iteration procedure regarding CPRF design. Moreover, the use of both FEM programs Plaxis 3D and RFEM could lead to a more precise and trustworthy design than the use of RFEM solely. Moreover, an interface between the Python script and Plaxis 3D could be developed. Finally, additional studies should be conducted regarding constitutive equation of soils, such as the Hardening Soil Model with Small Strain Stiffness (HS-Small). The implementation of such models would improve the quality of the CPRF design.

# References

- [1] Adam, D. 2016. Skriptum zur Vorlesung Grundbau und Bodenmechanik. Kapitel 19: Ausblick Eurocode 7. Technische Universität Wien.
- [2] Anaconda Inc 2017. Conda user guide. [Online] <https://conda.io/docs/>. (2017).
- [3] Banerjee, P.K. and Butterfield, R. 1981. Boundary Element Method in Engineering Science. McGraw-Hill.
- [4] Banerjee, P.K. and Driscoll, R.M. 1976. Three dimensional analysis of raked pile groups. Proc. Instn. Civ Engrs. 2, 61 (1976), 653–671.
- [5] Boussinesq, J.V. 1885. Application des potentiels à l'étude de l'équilibre et du mouvement des solides élastiques. Gauthier-Villard.
- [6] Chase, N., Rademacher, M. and Goodman, E. 2009. A Benchmark Study of Multi-Objective Optimization Methods. Red cedar technology.
- [7] Chow, Y.K. 1986. Analysis of vertically loaded pile groups. International journal for numerical and analytical methods in geomechanics, vol. 10, 59-72.
- [8] Chow, Y.-K. 1987. Three Dimensional Analysis of Pile Groups. Journal of Geotechnical Engineering. 113, 6 (1987), 637–651.
- [9] Cooke, R.W. 1974. The settlement of friction pile foundations. Proc. Conf. Tall Buildings. 3. Kuala Lumpur. 1–16.
- [10] Davis, E.H. and Poulos, H.G. 1972. The analysis of pile raft systems. The Australian Geomechanics Journal, vol. 2 (1), 21-27.
- [11] Deb, K., Pratap, A., Agarwal, S. and Meyarivan 2002. A fast and elitist multiobjective genetic algorithm: NSGA-II. IEEE transactions on evolutionary computation, 6 (2). 182–197.
- [12] DIN 1045:1988-07 Tragwerke aus Beton, Stahlbeton und Spannbeton.
- [13] DIN 1054:1976-11 Baugrund - Zulässige Belastung des Baugrundes.
- [14] DIN 1054:2005-01 Baugrund - Zulässige Belastung des Baugrundes.
- [15] DIN 4014:1990-03 Bohrpfähle - Herstellung, Bemessung und Tragverhalten.
- [16] DIN 4026:1975-08 Rammpfähle - Herstellung, Bemessung und zulässige Belastung.
- [17] DIN EN 1992-1-1 Bemessung und Konstruktion von Stahlbeton und Spannbetontragwerken.
- [18] El-Gendy, M., Hanisch, J. and Kany, M. 2006. Empirische nichtlineare Berechnung von Kombinierten Pfahl-Plattengründungen (KPP). Bautechnik 83, Heft 9. Verlag für Architektur und technische Wissenschaften GmbH & Co. KG.
- [19] El-Mossallamy, Y. 1996. Ein Berechnungsmodell zum Tragverhalten der Kombinierten Pfahl-Plattengründung. Mitteilungen des Institutes und der Versuchsanstalt für Geotechnik der TU Darmstadt, Heft 36.
- [20] Eurocode 7 2005. Entwurf, Berechnung und Bemessung in der Geotechnik - Teil 1: Allgemeine Regeln.

- [21] Grabe, J. and Pucker, T. 2011. Beitrag zum Entwurf und zur Ausführung von kombinierten Pfahl-Plattengründungen. Bautechnik. 88, 12 (2011), 828–835.
- [22] Guo, W.D. and Randolph, M.F. 1997. Vertically loaded piles in non-homogenous soils. International Journal for Numerical and Analytical Methods in Geomechanics, vol. 21, 507–532.
- [23] Handbuch EC7-1 2011. Handbuch Eurocode 7 – Geotechnische Bemessung, Band 1. Allgemeine Regeln, 1. Auflage. Berlin. Beuth Verlag.
- [24] Hanisch, J., Katzenbach, R. and König, G. 2002. Kombinierte Pfahl-Plattengründungen. Ernst & Sohn.
- [25] Hettler, A. 1986. Setzungen von vertikalen, axial belasteten Pfahlgruppen in Sand. Bauingenieur 61, 417 - 421.
- [26] Huber, M. 2013. Soil variability and its consequences. Mitteilung 69 des Instituts für Geotechnik, Universität Stuttgart.
- [27] Izzo, D. and Biscani, F. 2017. Pagmo & pygmo. [Online] Consulted on: 16 february 2018. <https://esa.github.io/pagmo2/index.html>. (2017).
- [28] Jaky, J. 1944. The coefficient of earth pressure at rest . s.l. : J. Soc. Hung. Eng. Arch. (Magyar Mernok es Epitesz-Egylet Kozlonye). (1944), 355–358.
- [29] Kany, M. 1974. Berechnung von Flächengründungen. Berlin. Band 2, 2. Auflage, Ernst & Sohn Verlag.
- [30] Katzenbach, R. and Choudhury, D. 2013. Combined Piled-Raft Foundation Guideline. Darmstadt. International Society for Soil Mechanics and Geotechnical Engineering.
- [31] Katzenbach, R., Leppla, S. and Choudhury, D. 2016. Foundation systems for high rise structures. CRC Press.
- [32] Katzenbach, R., Leppla, S. and Ramm, H. 2012. Die Kombinierte Pfahl-Plattengründung (KPP) – eine innovative, kostenoptimierte Gründungstechnologie. Zurich. Referat im Rahmen der Fachveranstaltung Baugrund-Bauwerk-Interaktion: Optimierung der Foundation und Bemessung nach dem Stand der Technik.
- [33] Kempfert, H.G. 2012. Empfehlungen des Arbeitskreises „Pfähle“ (EA-Pfähle). 2. Auflage, Deutschen Gesellschaft für Geotechnik e.V.
- [34] Kempfert, H.-G. 2009. Pfahlgründungen. In: Grundbautaschenbuch, 7. Auflage, Teil 3, Kapitel 3.2. Verlag Ernst & Sohn, 73–277.
- [35] Li, H. and Zhang, Q. 2007. MOEA/D: A Multiobjective Evolutionary Algorithm Based on Decomposition. IEEE Transactions on evolutionary computation, vol 11 (6).
- [36] Liu, P. 1996. Untersuchungen zur Berechnung der Pfahlsetzung mit der FDM. TH Darmstadt (unveröffentlicht). Fachbereich Bauingenieurwesen.
- [37] Lutz, B. 2002. Beitrag zur Modellierung des Tragverhaltens Kombiniierter Pfahl-Plattengründungen (KPP) unter Verwendung geotechnischer Messungen. Mitteilung des Institutes und der Versuchsanstalt für Geotechnik der Technischen Universität Darmstadt, Heft 63.
- [38] Mindlin, R.D. 1936. Force at a point in the interior of a semi-infinite solid. 195–202.
- [39] Ohde, J. 1942. Die Berechnung der Sohldruckverteilung unter Gründungskörpern. Springer-Verlag Berlin.

- [40] O'Neil, M.W. 1981. Field study of pile group action. Offices of Research & Development, Materials Divisions. (1981).
- [41] Poulos, H.-G. 1994. An approximate numerical analysis of pile-raft interaction. s.l. : Research. University of Sydney, Australia.
- [42] Poulos, H.G. 1993. Settlement prediction for bored pile groups. Rotterdam: Proc. 2nd Int. Geot. Sem on Deep foundation on Bored and Auger Piles, Ghent. 1–4.
- [43] Poulos, H.G. and Davis, E.H. 1974. Elastic solutions for soil and rock mechanics. John Wiley & Sons, New York.
- [44] Poulos, H.G. and Davis, E.H. 1980. Pile foundations analysis and design. John Wiley & Sons, New York.
- [45] Randolph, M.F. 1983. Design of piled raft foundations. CUED/D-Soils TR, vol. 163.
- [46] Randolph, M.F. and Wroth, C.P. 1979. A simple approach to pile design and the evaluation of pile tests. Behavior of Deep Foundations: ASTM Special Technical Publication. 670, (1979), 484–499.
- [47] Rudolf, M. 2005. Beanspruchung und Verformung von Gründungskonstruktionen auf Pfahlrosten und Pfahlgruppen unter Berücksichtigung des Teilsicherheitskonzeptes. Schriftenreihe Geotechnik, Universität Kassel, Heft 17.
- [48] Skempton, A.W. 1953. Diskussionbeitrag. Zürich, Proc. 3 ICSMFE, Band 3, 127.
- [49] von Soos, P. and Engel, J. 2008. Eigenschaften von Boden und Fels – ihre Ermittlung im Labor. In: Grundbau Taschenbuch, Teil 1: Geotechnische Grundlagen. K.J. Witt, ed. Ernst & Sohn Verlag, 7. Edition.
- [50] Steinbrenner, W. 1934. Tafeln zur Setzungsberechnung. Die Straße, 121–124.
- [51] Thaher, M. 1991. Tragverhalten von Pfahl-Platten Gründungen im bindigen Baugrund, Berechnungsmodelle und Zentrifugen Modellversuche. Serie Grundbau, Schriftenreihe des Institutes für Grundbau, Wasserwesen und Verkehrswesen, Ruhr-Universität, Heft 15. Bochum.
- [52] Van Impe, W.F. and De Clerq, Y. 1994. Ein Interaktionsmodell für Pfahlplattengründungen. s.l. Geotechnik 17, 61-73.
- [53] Vrettos, C. 2006. Ein Näherungsverfahren zur Berechnung von Pfahl-Plattengründungen mit unregelmäßiger Geometrie.
- [54] Zitzler, E., Deb, K. and Thiele, L. 2000. Comparison of Multiobjective Evolutionary Algorithms: Empirical Results. Evolutionary Computation 8 (2). 173–195.





# Table of figures

<b>Figure 1.1:</b> Development of recent high-rise buildings in Frankfurt am Main, after [1].	15
<b>Figure 1.2:</b> Workflow representing the methodology followed during the master thesis.	16
<b>Figure 2.1:</b> Characteristic resistance-settlement curve (RSC) of a single pile [1].	20
<b>Figure 2.2:</b> Pile denomination within a group (adapted from [6]).	21
<b>Figure 2.3:</b> Nomogram showing the influence of the soil type and the group geometry of a bored pile group for a cohesive soil (group of soil “cohesive II” according to Table 2.1) [6].	23
<b>Figure 2.4:</b> Nomograms showing the influence of the group size for the determination of the mean settlement of a pile group in a cohesive soil (group of soil “cohesive II” according to Table 2.1) [6].	23
<b>Figure 2.5:</b> Soil-structure interaction after [2].	24
<b>Figure 2.6:</b> Combined piled-raft foundation as a geotechnical structure, pile and raft resistances [2].	24
<b>Figure 2.7:</b> Settlement of a CPRF depending on the piled raft coefficient $\alpha_{PR}$ , adapted from [2].	25
<b>Figure 3.1:</b> (a) Stress state of an infinitesimal volume [18] (b) Shear stress distribution on the pile shaft in radial direction [19].	29
<b>Figure 3.2:</b> Dependency on the influence radius with influence coefficients (a) Cross-section through the pile group (b) Plan view of a pile group. Adapted from [3].	33
<b>Figure 3.3:</b> Workflow representing the main steps of the procedure of [3].	37
<b>Figure 3.4:</b> Representation of the influence radius using different empirical models.	38
<b>Figure 3.5:</b> Radiuses of influence represented with their origin at the pile 1.	39
<b>Figure 3.6:</b> Calculation of the flexibility coefficients after Mindlin (1936) [26] in [23].	40
<b>Figure 3.7:</b> Position of the nodes for a two dimensional pile group study.	40
<b>Figure 3.8:</b> Flexibility matrix using the theories of (a) <i>Rudolf</i> (2005) [3] (b) <i>Chow</i> (1986) [11].	41
<b>Figure 3.9:</b> Horizontal load equivalence with a pair of loads operating in opposite directions [3].	42
<b>Figure 3.10:</b> Resistance-settlement curve of one pile showing the schematic steps of the iteration procedure. Adapted from [3].	44
<b>Figure 3.11:</b> Distribution of a total load of 30 MN over six piles (a) constantly distributed load (b) linear distributed load.	44
<b>Figure 3.12:</b> Distribution of the pile resistances (MN, inside the circles) and of the settlement (cm, below the circles) for a constantly distributed load (a) and a linear distributed load (b).	45
<b>Figure 3.13:</b> Failure criteria of Mohr-Coulomb, Matsuoka-Nakai and Lade-Duncan represented on the deviatoric plane [28].	46
<b>Figure 3.14:</b> Pile group design workflow of the Python script inspired from <i>Rudolf</i> (2005) [3] and improvements (highlighted in red).	47
<b>Figure 4.1:</b> Proof and safety concept in the ULS after [40].	56
<b>Figure 4.2:</b> Determination of the expected differential settlement of a pile group [1].	57
<b>Figure 4.3:</b> Proof and safety concept in the SLS [40].	57
<b>Figure 4.4:</b> Monitoring of a CPRF, adapted from [1].	58
<b>Figure 4.5:</b> Different models of raft-soil interaction after [45]. (a) Stress trapeze method (b) Subgrade reaction modulus method (c) stiffness modulus method.	59
<b>Figure 4.6:</b> Contact pressure distribution for limp (a) and rigid (b) shallow foundations after [1].	60
<b>Figure 4.7:</b> Workflow of the adopted hybrid design approach of CPRFs.	61
<b>Figure 4.8:</b> Evolution of the piled raft coefficient during the iterative procedure (design of CPRF guideline example 1 version 3).	62
<b>Figure 5.1:</b> Illustration of the major parameters used in the benchmark “Guideline 1.2”	64

<b>Figure 5.2:</b> Position of the piles for the benchmark “Guideline 1.2” with $a$ pile spacing and $D$ pile diameter. ....	64
<b>Figure 5.3:</b> Comparison of the RSCs for the corner pile obtained with an analytical calculation and with a numerical simulation (reference design from <i>Hanisch et al. (2002) [2]</i> ). ....	65
<b>Figure 5.4:</b> Comparison of the RSCs for the edge pile obtained with an analytical calculation and with a numerical simulation (reference solution from <i>Hanisch et al. (2002) [2]</i> ). ....	66
<b>Figure 5.5:</b> Comparison of the RSCs for the inner pile obtained with an analytical calculation and with a numerical simulation (reference solution from <i>Hanisch et al. (2002) [2]</i> ). ....	66
<b>Figure 5.6:</b> Comparison of the results obtained for the benchmark “Guideline 1.2” (a) analytical calculation (b) FEM model from <i>Hanisch et al. (2002) [2]</i> . Pile resistance inside the piles (MN), settlement under the piles (cm). ....	68
<b>Figure 5.7:</b> Illustration of the major parameters of the benchmark “skin friction pile”. ....	68
<b>Figure 5.8:</b> Illustration of the major parameters of the benchmark “end bearing pile”. ....	69
<b>Figure 5.9:</b> Position of the end-bearing piles and load-settlement curve for the corner pile (pile number 3), edge pile (number 4) and inner pile (number 5). ....	69
<b>Figure 5.10:</b> Position of the skin friction piles and load-settlement curve for the corner pile (3, top right), edge pile (4, bottom left) and inner pile (5, bottom right). Total load of 15 MN. ....	70
<b>Figure 5.11:</b> Position of the piles for the benchmark “Guideline 1.3”. ....	71
<b>Figure 5.12:</b> Subgrade reaction modulus for the CPRF of the “Guideline 1.3” according to [2]. ....	72
<b>Figure 5.13:</b> Comparison of the RSCs for the corner pile obtained with the developed design approach and with a numerical simulation (reference solution from <i>Hanisch et al. (2002) [2]</i> ). ....	73
<b>Figure 5.14:</b> Comparison of the RSCs for the edge pile obtained with the developed design approach and with a numerical simulation (reference solution from <i>Hanisch et al. (2002) [2]</i> ). ....	73
<b>Figure 5.15:</b> Comparison of the results for the benchmark “Guideline 1.3” (a) developed design approach (b) FEM model from <i>Hanisch et al. (2002) [2]</i> . Pile resistance inside the piles (MN), settlement under the piles (cm). ....	74
<b>Figure 5.16:</b> Final calculation in RFEM using the final spring stiffness calculating with a semi-analytical approach. ....	74
<b>Figure 5.17:</b> Comparison of the piled-raft coefficient $\alpha PR$ . ....	75
<b>Figure 6.1:</b> Simplified process of a genetic algorithm. ....	79
<b>Figure 6.2:</b> Simplified sorting of the main families of algorithms. ....	80
<b>Figure 6.3:</b> NSGA-II Procedure, illustration taken from [50]. ....	81
<b>Figure 6.4:</b> Fitness of the objective functions plotted in the objective space, settlement over volume of the piles (Pareto front highlighted in red). ....	83
<b>Figure 6.5:</b> Subgrade reaction modulus for the CPRF of the “Guideline 1.3”, intermediate slab. Adapted from [2]. ....	85
<b>Figure 6.6:</b> Pareto fronts for a rigid slab (in orange) and for an intermediate slab (in red) obtained for 960 iterations. ....	86
<b>Figure 6.7:</b> Pile enumeration and geometrical parameters for the reference design [2]. ....	86
<b>Figure 6.8:</b> Illustration of the optimised CPRFs in comparison with the reference design for the lowest settlement solution. ....	88
<b>Figure 6.9:</b> Piled-raft coefficients for different designs of the “Guideline 1.3”. ....	89
<b>Figure B.1:</b> Representation of the global and partial safety concepts. ....	117
<b>Figure C.1:</b> Influence of the number of generations on the convergence of the genetic algorithm (a) 2 iterations (b) 4 iterations (c) 10 iterations. ....	119
<b>Figure C.2:</b> Influence of the population size on the convergence of the genetic algorithm (a) 12 individuals (b) 32 individuals (c) 60 individuals. ....	120
<b>Figure C.3:</b> Convergence to the optimal Pareto front for 30 generations and 40 individuals. ....	121
<b>Figure C.4:</b> Application of the MOEAD algorithm on the benchmark “Guideline 1.2” (a) 15 generations, 48 individuals (b) 80 generations, 100 individuals. ....	121

## Table of charts

<b>Table 2.1:</b> Characterisation of the soil depending on the stiffness modulus. Adapted from [6].	22
<b>Table 3.1:</b> Overview of different calculation methods, design of pile groups, adapted from [12].	27
<b>Table 3.2:</b> Calculation methods for a pile group (adapted from [3]).	28
<b>Table 3.3:</b> Empirical models for the influence radius $rm$ (adapted from [3]).	34
<b>Table 3.4:</b> Typical values of $v_e$ and $w_e$ for different soils adapted from [27].	42
<b>Table 4.1:</b> Calculation methods for a combined piled raft (adapted from [3]).	50
<b>Table 4.2:</b> Type of foundation according to the system rigidity. Adapted from [1].	60
<b>Table 5.1:</b> Geometrical parameters of different pile groups for the benchmark study on pile groups.	63
<b>Table 5.2:</b> Soil parameters of different standard soils for the benchmark study on pile groups.	63
<b>Table 5.3:</b> Highlights of the differences between the two models.	67
<b>Table 5.4:</b> Results obtained for the benchmark end bearing and skin friction pile.	70
<b>Table 5.5:</b> Empirical values for the determination of the subgrade reaction modulus under a CPRF in cohesive soils. Adapted from [2].	71
<b>Table 5.6:</b> Input parameters for the determination of the resistance-settlement curves obtained with the convergence procedure.	72
<b>Table 6.1:</b> Boundaries of the design parameters for the optimisation of the “Guideline 1.2”.	83
<b>Table 6.2:</b> Parameters of the original chosen design and of the lowest volume and lowest settlement solutions, mean values for the length of each standard pile; values are given in meters.	84
<b>Table 6.3:</b> Lowest volume and lowest settlement solution referring the original chosen design.	84
<b>Table 6.4:</b> Limit thickness of the slab for the benchmark “Guideline 1.3”.	85
<b>Table 6.5:</b> Boundaries of the design parameters for the optimisation of the CPRF “Guideline 1.3”.	85
<b>Table 6.6:</b> Parameters of the original chosen design and of the lowest volume solution, mean values of the length for each standard pile. Values are given in meters.	87
<b>Table 6.7:</b> Parameters of the original chosen design and of the lowest settlement solution, mean values of the length for each standard pile. Values are given in meters.	87
<b>Table 6.8:</b> Lowest volume and lowest settlement solution referring the original chosen design.	88
<b>Table B.1:</b> Partial factors on actions following two different sets of partial factors (from [7]).	117



# Appendix A Python Codes

## A.1 Analytical calculation of a pile group

```
1  # -*- coding: utf-8 -*-
2  """
3  Created on Wed Jan 24 16:38:19 2018
4  @author: Corentin
5  """
6  import numpy
7
8  import matplotlib
9
10 import matplotlib.pyplot as plt
11
12 class PileGroup(object):
13     """This class calculates the load-settlement curve of a pile group based on
14     Rudolf (2005), 'Beanspruchung und Verformung von Gründungskonstruktionen
15     auf Pfahlrosten und Pfahlgruppen unter Berücksichtigung des Teilsicherheits
16     konzeptes' E.1 Quellcode Berechnungsverfahren Bruchkriterium 'MC'"""
17     __name__ = 'Calculation of a pile group foundation'
18
19
20     def __init__(self):
21         """NB: Pile lengths, pile radius and pile spacing are directly given in
22         the method's arguments to meet the needs of pygmo"""
23         self.plot_fig = True # Boolean running the final plot of the figures
24         """Geometry of the piles"""
25         # Radius of the pile [m]
26         self.npx = 4
27         # Number of piles in x direction
28         self.npy = 3
29         # Number of piles in y direction
30         self.np = self.npx * self.npy
31         # Total number of piles
32         """Load"""
33         self.Fv = numpy.array([30000, 30000, 30000, 30000, 30000, 30000, 30000,
34                                30000, 30000, 30000, 30000, 30000])
35         # len(self.Fv) must be egal to self.np:
36         print(numpy.mean(self.Fv))
37         # Total vertical Load [kN]
38         """Underground"""
39         self.n_layer = 8
40         # Number of layers up to the pile base
41         self.n_bottom = 9
42         # Number of layers up to the model bottom
43         self.n_elem_b = 5
44         # Virtual failure pile base(eq (7.20 & 7.21))
45         # The concordance between analytical and FEM results is good for
46         # self.n_elem_b = 5, see p.84
47         # self.z = numpy.array([0, 1.5, 2.5, 4, 7, 9, 11, 13, 15, 22])
48         self.z_bottom = 22
49         self.nu = numpy.array([0.25, 0.25, 0.25, 0.25, 0.25, 0.25, 0.25, 0.25,
50                                0.25])
51         # Poisson's ratio [-]
52         self.phi = numpy.array([25, 25, 25, 25, 25, 25, 25, 25, 25])
53         # Friction angle(°)
```

```

54     self.gamma = numpy.array([10, 10, 10, 10, 10, 10, 10, 10, 10])
55     # Specific weight of the soil (below groundwater table) [kN/m3]
56     self.cohes = numpy.array([5, 5, 5, 5, 5, 5, 5, 5, 5])
57     # Cohesion [kN/m]
58     self.psi = self.phi-30
59     # Dilatancy(°)
60     self.psi[numpy.where(self.psi < 0)] = 0
61     # Dilatancy values cannot be negative
62     self.K0 = 1-numpy.sin(numpy.deg2rad(self.phi))
63     # Coefficient of earth pressure at rest [-]
64
65     """Iteration method"""
66     self.n_iter_tot = 80
67     # Number of iterations
68     self.f_iter = 10
69     # Number of iterations, failure criterion pile base.
70     """Secant modulus' modification with the depth
71     see K.J. Witt, Grundbau Taschenbuch Teil 1, 7. Auflage, pp.124-125"""
72     self.sigma_ref = 100
73     # Reference pressure [kN/m2], set to 100kN/m2,
74     self.ve = 400
75     # Coefficient that pilots the modification of the modulus with
76     # depth, ve * sigma_ref corresponds to the "E_ref" in Grabe and Pucker,
77     # Beitrag zum Entwurf und zur Ausführung von KPP.
78     self.we = 0.55 # Coefficient that pilots the modification of the
79     # modulus with depth, is comprised between 0 and 1 and corresponds to n
80     # in Grabe and Pucker
81     #Examples:
82     # - Lightly plastic silt
83     #     we = 110
84     #     ve = 0.6
85     # - Well graded sand
86     #     we = 600
87     #     ve = 0.55
88     # - Uniform fine sand
89     #     we = 300
90     #     ve = 0.6
91
92     self.settlement()
93     self.volume()
94
95 def volume(self, decision_vect = [15, 15, 15, 15, 15, 15,
96                                15, 15, 15, 15, 15, 15, 0.75, 3, 3]):
97     """ Calculates the volume of all piles in m3 with given default values
98     for pile length, pile radius and pile spacing
99     NB: decision_vect = [lp[0], ... lp[np], rp, dx, dy]
100     with
101     lp: pile length [m]
102     rp: pile radius [m]
103     dx: pile spacing, x direction [m]
104     dy: pile spacing, y direction [m]"""
105     V = 0
106     for i in range(self.np):
107         V += numpy.float(
108             numpy.pi*decision_vect[self.np]**2*decision_vect[i])
109     # Volume of the piles (m3). dtype = float is necessary to compute the
110     # problem using the pygmo library
111     print('lp_1 = %s' %decision_vect[0])
112     print('lp_2 = %s' %decision_vect[1])
113     print('lp_3 = %s' %decision_vect[2])
114     print('lp_4 = %s' %decision_vect[3])
115     print('lp_5 = %s' %decision_vect[4])
116     print('lp_np = %s' %decision_vect[self.np-1])
117     print('rp = %s' %decision_vect[self.np])
118     print('dx = %s' %decision_vect[self.np+1])

```

```

119         print('dy = %s' %decision_vect[self.np+2])
120         print('V = %s' %V)
121         return(V)
122
123
124
125     def settlement(self, decision_vect = [15, 15, 15, 15, 15, 15,
126                                         15, 15, 15, 15, 15, 15, 0.75, 3, 3]):
127         """ Calculates the settlement (cm) of the pile group with given
128         default values for pile length, pile radius and pile spacing
129         NB: decision_vect = [lp[0], ... lp[np], rp, dx, dy]
130         with
131         lp: pile length [m]
132         rp: pile radius [m]
133         dx: pile spacing, x direction [m]
134         dy: pile spacing, y direction [m]"""
135
136     %% Initialisation
137     x = numpy.zeros(self.np)
138     # x coordinate of each pile [m]
139     y = numpy.zeros(self.np)
140     # y coordinate of each pile [m]
141     r = numpy.zeros((self.np,self.np))
142     # Distance between two piles
143     rm = numpy.zeros(self.np)
144     # Influence radius for each pile
145     z_pile = numpy.zeros((self.np,self.n_layer+1))
146     # Depth of each pile layer
147     fs = numpy.zeros ((self.np,self.np,self.n_layer))
148     # Coefficients of influence for the pile shaft
149     fb = numpy.zeros ((self.np,self.np))
150     # Coefficients of influence for the pile mantel
151     a = numpy.zeros(((self.n_layer+1)*self.np+1,
152                     (self.n_layer+1)*self.np+1))
153     # Concatenation of the coefficients of influence, see equation (7.11)
154     c = numpy.zeros(((self.n_layer+1)*self.np+1)) # see equation (7.11)
155     Es = numpy.zeros(self.n_layer)
156
157     """Failure criterion of the pile base"""
158     # NB: index f could refer to "failure"
159     sigma_z0_pile = numpy.zeros(self.np)
160     # Vertical stress, pile bottom
161     fsigma_z0_pile = numpy.zeros(self.np)
162     fsigma_x0_pile= numpy.zeros(self.np)
163     fy = 0
164     fx = numpy.zeros (self.f_iter)
165     fr = numpy.zeros (self.f_iter)
166     fc = numpy.zeros(self.np)
167     fz = numpy.zeros(self.np)
168     # cf CHOW, Analysis of vertical loaded pile groups, eq (15), (1986)
169     fR1 = numpy.zeros((self.np,self.f_iter))
170     fR2 = numpy.zeros((self.np,self.f_iter))
171     fsigma_x = numpy.zeros((self.np,self.f_iter))
172     # Vertical stress for the pile base failure
173     fsigma_z = numpy.zeros((self.np,self.f_iter))
174     # Horizontal stress for the pile base failure
175     ftau_xz = numpy.zeros((self.np,self.f_iter))
176     # Shear stress for the pile base failure
177     fsigma_1 = numpy.zeros((self.np,self.f_iter))
178     # Principal stress 1 for the pile base failure
179     fsigma_3 = numpy.zeros((self.np,self.f_iter))
180     # Principal stress 3 for the pile base failure
181     MC_base = numpy.zeros((self.np,self.f_iter))
182     # Expression of the MC's failure criterion pile base
183     n_failure_b = numpy.zeros(self.np)

```

```

184         # Number of elements under the pile base where the failure
185         # occurred (eq (7.20 & 7.21))
186
187         """Failure criterion of the pile shaft"""
188         sigma_z1_s = numpy.zeros((self.np,self.n_layer))
189         # Vertical stress in the middle of each soil layer
190         sigma_x1_s = numpy.zeros((self.np,self.n_layer))
191         # Horizontal stress in the middle of each soil layer
192         tau_s = numpy.zeros((self.np,self.n_layer))
193         # Shear stress for the pile shaft failure
194         sigma_z1_s_buffer = numpy.zeros(self.np)
195         # Buffer
196         sigma_1_s1 = numpy.zeros((self.np,self.n_layer))
197         # Principal stress 1 for the pile shaft failure
198         sigma_3_s1 = numpy.zeros((self.np,self.n_layer))
199         # Principal stress 3 for the pile shaft failure
200         MC_shaft = numpy.zeros((self.np,self.n_layer))
201         # Expression of the MC's failure criterion pile shaft
202         Failure_s = numpy.zeros((self.np,self.n_layer))
203         # "Boolean" used to test the failure criterion of the shaft
204
205         """Storage of the results"""
206         dFv = numpy.zeros(self.np)
207         # Incremental load
208         Rb = numpy.zeros(self.np)
209         # Final load base
210         Rb1 = numpy.zeros(self.np)
211         # Load in the base during the first passage within one increment
212         Rb2 = numpy.zeros(self.np)
213         # Load in the base during the second passage within one increment
214         Rs = numpy.zeros((self.np,self.n_layer))
215         # Final load shaft
216         Rs1 = numpy.zeros((self.np,self.n_layer))
217         # Load in the shaft during the first passage within one increment
218         Rs2 = numpy.zeros((self.np,self.n_layer))
219         # Load in the shaft during the second passage within one increment
220         s_tot = numpy.zeros(self.np)
221         # Total settlement
222         s1 = numpy.zeros(self.np)
223         # Settlement during the first passage within one increment
224         s2 = numpy.zeros(self.np)
225         # Settlement during the second passage within one increment
226         delta_Rs = numpy.zeros((self.np,self.n_layer))
227         # Incremental stress state for the pile shaft
228         delta_Rb = numpy.zeros(self.np)
229         # Incremental stress state for the pile base
230         Rs_tot = numpy.zeros(self.np)
231         # Total pile shaft load (sum of all the layer loads)
232
233         """Matrix to plot the results"""
234         Rb_plot = numpy.zeros((self.np,self.n_iter_tot))
235         Rs_tot_plot = numpy.zeros((self.np,self.n_iter_tot))
236         R_tot_plot = numpy.zeros((self.np,self.n_iter_tot))
237         s_tot_plot = numpy.zeros((self.np,self.n_iter_tot))
238     %% Geometrical conditions
239     """Set up the depth of each pile"""
240     for i in range (self.np):
241         z_pile[i] = numpy.linspace(0,decision_vect[i],self.n_layer+1)
242     """Set up the position of each pile"""
243     for i in range(self.npx):
244         # Piles in x direction
245         for j in range(self.npy):
246             # Piles in y direction
247             n_pile = j+i*self.npy
248             # Number of the considered pile

```



```

249         x[n_pile] = x[0]+i*decision_vect[self.np+1]
250         # x coordinate of the considered pile
251         y[n_pile] = y[0]+j*decision_vect[self.np+2]
252         # y coordinate of the considered pile
253         """Set up a distance matrix of the piles"""
254         for i in range(self.np):
255             for j in range(self.np):
256                 if i==j:
257                     r[i,j]=decision_vect[self.np]
258                 else:
259                     r[i,j]=numpy.sqrt((x[i]-x[j])**2+(y[i]-y[j])**2)
260         """Set up the influence radius for each pile"""
261         # Initiates instances of the class RadiusOfInfluence [m]
262         # From Lutz (2003), Tabelle 7.1
263         for i in range(self.np):
264             rm[i] = InfluenceRadius.lutz_alpha(
265                 self, decision_vect[i], numpy.mean(self.nu), 2.5)
266
267     %% Calculate vertical and horizontal stresses in the middle of each soil layer
268     for i in range(self.np):
269         for k in range(self.n_layer):
270             sigma_zl_s[i,k] = sigma_zl_s_buffer[i]+(0.5*
271                 (z_pile[i,k+1]-z_pile[i,k]))*self.gamma[k]
272             sigma_zl_s_buffer[i] = sigma_zl_s_buffer[i]+(z_pile[i,k+1]-
273                 z_pile[i,k])*self.gamma[k]
274             # Stock the value at the extremity of each layer to calculate
275             # the next stress state in the next middle layer
276             sigma_xl_s[i,k] = sigma_zl_s[i,k]*self.K0[k]
277             sigma_z0_pile[i] = sigma_zl_s_buffer[i]
278             sigma_zl_s_buffer[i] = 0
279             fsigma_z0_pile[i] = sigma_z0_pile[i]+decision_vect[
280                 self.np]*self.gamma[self.n_bottom-1]
281             fsigma_x0_pile[i] = fsigma_z0_pile[i]*self.K0[self.n_bottom-1]
282
283     %% Calculate the stiffness modulus of soil Es
284     for i in range(self.np):
285         for k in range(self.n_layer):
286             Es[k] = self.ve*self.sigma_ref*(sigma_zl_s[i,k]/
287                 self.sigma_ref)**self.we
288
289     %% Calculate coefficient of influence from pile shaft j on pile shaft i (7.6)
290     # "Einflussbeiwert des Pfahlmantelwiderstandsanteiles"
291     # Here i and j indexes don't stick to x and y axes, each pile within
292     # the radius of influence is taken into account one after another
293     for k in range(self.n_layer): # For each layer
294         for i in range(self.np):
295             for j in range(self.np):
296                 fs[i,j,k] = (1+self.nu[k])/(Es[k]*numpy.pi*
297                     (z_pile[i,k+1]-z_pile[i,k]))*numpy.log(rm[i]/r[i,j])
298                 # NB: log corresponds to the neperian logarithmus
299                 if r[i,j] > rm[i]:
300                     fs[i,j,k] = 0
301                 # The coefficient is set to 0 if the radius of
302                 # influence is exceeded
303
304     %% Calculate the coefficient of influence from base j on base i (eq 7.7)
305     # 'Einflussbeiwert des Pfahlfußwiderstandsanteiles'
306     for i in range(self.np):
307         for j in range(self.np):
308             fb[i,j] = (1-self.nu[self.n_layer]**2)/(Es[self.n_layer-1]*
309                 numpy.pi*r[i,j])
310             if i == j:
311                 fb[i,j] = fb[i,j] * numpy.pi/2
312     %% Assemble matrix a (equation 7.15)
313     for k in range(self.n_layer):

```

```

314         for i in range (self.np):
315             for j in range (self.np):
316                 a[i+self.np*k,j+self.np*k] = fs[i,j,k]
317     for i in range (self.np):
318         for j in range (self.np):
319             a[i+self.np*self.n_layer,j+self.np*self.n_layer] = fb[i,j]
320     for i in range ((self.n_layer+1)*self.np):
321         a[(self.n_layer+1)*self.np,i] = 1
322         a[i,(self.n_layer+1)*self.np] = -1
323
324     %% Assemble vector c (equation 7.15)
325     c[(self.n_layer+1)*self.np] = 1 # equivalent to c[-1] = 1
326
327     %% Calculation procedure (see "7.3 Eigenes analytisches Berechnungsverfahren")
328     for iteration in range(self.n_iter_tot):
329         # Beginning of the loop
330         for i in range(self.np):
331             dFv[i] = self.Fv[i]/self.n_iter_tot
332         # Calculate the value of the additional force for each increment
333         laufwhile = 1
334         lauf1 = 0
335         while laufwhile != 0:
336             # The loop runs until two successive values of Rb, Rs or s don't
337             # differ of more than 1%
338             lauf1 += 1
339             if lauf1 > 100:
340                 print('Divergence')
341                 break
342
343     %% Resolution of the equation of equilibrium (1st time)
344     db = numpy.linalg.solve(a,c) #a*x=c solved by linalg.solve(a,c)
345     # db contains delta_Rs from line 1 to np*n_layer, delta_Rb from
346     # line np*n_layer to np*(n_layer+1), ds line 1+np*(n_layer+1),
347     # cf. equation (7.15)
348     for i in range(self.np):
349         delta_Rb[i] = db[self.n_layer*self.np+i]*dFv[i]
350         # eq (7.13b), calculation of the incremental stress state
351         # for the pile base
352         Rb1[i] = Rb[i]+delta_Rb[i]
353     for k in range (self.n_layer):
354         for i in range(self.np):
355             delta_Rs[i,k] = db[k*self.np+i]*dFv[i] # eq (7.13c),
356             # calculation of the stress state for the pile shaft
357             Rs1[i,k] = Rs[i,k]+delta_Rs[i,k]
358
359     %% Determination of the failure criterion for the base
360     for i in range(self.np):
361         fc[i] = decision_vect[i]
362         # Depth node j (unit load applied)
363         fz[i] = decision_vect[i]+decision_vect[self.np]
364         # Depth node i (where displacement evaluated)
365     for i in range(self.np):
366         n_failure_b[i] = 0
367         for f in range (self.f_iter):
368             fx[f] = f*2/9*2*decision_vect[self.np]
369             # Source unknown
370             fr[f] = (fx[f]**2+fy**2)**0.5
371             # fy was set to 0
372             fr1[i,f] = (fr[f]**2+(fz[i]-fc[i])**2)**0.5
373             # cf CHOW, eq (15), (1986)
374             fr2[i,f] = (fr[f]**2+(fz[i]+fc[i])**2)**0.5
375             fsigma_x[i,f] = fsigma_x0_pile[i]-
Rb1[i]/(8*numpy.pi*(1-self.nu[self.n_bottom-1]))*((1-2*self.nu[self.n_bottom-
1])* (fz[i]-fc[i])/(fr1[i,f]**3)-3*fx[f]**2*(fz[i]-fc[i])/(fr1[i,f]**5)+(1-
2*self.nu[self.n_bottom-1]))*(3*(fz[i]-fc[i])-4*self.nu[self.n_bottom-

```

```

1] * (fz[i] + fc[i])) / (fR2[i, f]**3) - (3 * (3 - 4 * self.nu[self.n_bottom - 1]) * fx[f]**2 * (fz[i] -
fc[i]) - 6 * fc[i] * (fz[i] + fc[i]) * ((1 - 2 * self.nu[self.n_bottom - 1]) * fz[i] -
2 * self.nu[self.n_bottom - 1] * fc[i])) / (fR2[i, f]**5) -
30 * fc[i] * fx[f]**2 * fz[i] * (fz[i] + fc[i]) / (fR2[i, f]**7) - 4 * (1 - self.nu[self.n_bottom -
1]) * (1 - 2 * self.nu[self.n_bottom - 1]) / fR2[i, f] / (fR2[i, f] + fz[i] + fc[i]) * (1 -
fx[f]**2 / (fR2[i, f] * (fR2[i, f] + fz[i] + fc[i])) - fx[f]**2 / fR2[i, f]**2))
376         fsigma_z[i, f] = fsigma_z0_pile[i] -
Rb1[i] / (8 * numpy.pi * (1 - self.nu[self.n_bottom - 1])) * (- (1 - 2 * self.nu[self.n_bottom -
1]) * (fz[i] - fc[i]) / (fR1[i, f]**3) + (1 - 2 * self.nu[self.n_bottom - 1]) * (fz[i] -
fc[i]) / (fR2[i, f]**3) - 3 * (fz[i] - fc[i])**3 / (fR1[i, f]**5) - (3 * (3 -
4 * self.nu[self.n_bottom - 1]) * fz[i] * (fz[i] * fc[i])**2 - 3 * fc[i] * (fz[i] + fc[i]) * (5 * fz[i] -
fc[i])) / (fR2[i, f]**5) - 30 * fc[i] * fz[i] * (fz[i] + fc[i])**3 / (fR2[i, f]**7))
377         ftau_xz[i, f] = -Rb1[i] * fx[f] / (8 * numpy.pi * (1 -
self.nu[self.n_bottom - 1])) * (- (1 - 2 * self.nu[self.n_bottom - 1]) / (fR1[i, f]**3) + (1 -
2 * self.nu[self.n_bottom - 1]) / (fR2[i, f]**3) - 3 * (fz[i] - fc[i])**2 / (fR1[i, f]**5) - (3 * (3 -
4 * self.nu[self.n_bottom - 1]) * fz[i] * (fz[i] + fc[i]) -
(3 * fc[i] * (fz[i] + fc[i])) / (fR2[i, f]**5) -
30 * fc[i] * fz[i] * (fz[i] + fc[i])**2 / (fR2[i, f]**7))
378         fsigma_1[i, f] =
0.5 * (fsigma_x[i, f] + fsigma_z[i, f]) + ((fsigma_x[i, f] -
fsigma_z[i, f])**2 / 4 + ftau_xz[i, f]**2)**0.5
379         fsigma_3[i, f] = 0.5 * (fsigma_x[i, f] + fsigma_z[i, f]) -
((fsigma_x[i, f] - fsigma_z[i, f])**2 / 4 + ftau_xz[i, f]**2)**0.5
380         # MC's fracture criterion for the pile base, eq (7.14)
381         MC_base[i, f] = 0.5 * fsigma_1[i, f] * (1 - numpy.sin(
382             self.phi[self.n_layer - 1] * numpy.pi / 180)) -
0.5 * fsigma_3[i, f] * (1 + numpy.sin(self.phi[self.n_layer - 1] * numpy.pi / 180)) -
self.cohes[self.n_layer - 1] * numpy.cos(self.phi[self.n_layer - 1] * numpy.pi / 180)
383         if MC_base[i, f] > 0:
384             n_failure_b[i] += 1 # increment of 1
385             # If the failure criterion of the base is not fulfilled
386             # adapt matrix a AND solve again the equation b = a \ c.
387             # If the failure criterion is fulfilled, don't adapt
388             # matrix a, verify directly the failure criterion for
389             # the shaft
390
391     %% Update of the coefficient of influence from pile base j on pile base i
392     for i in range(self.np):
393         for j in range(self.np):
394             fb[i, j] = (1 - self.nu[self.n_layer]**2) / (
395                 Es[self.n_layer - 1] * numpy.pi * r[i, j]
396                 ) * self.n_elem_b / (self.n_elem_b - n_failure_b[i]
397                     + 1e-10)
398             # equation (7.21)
399             if n_failure_b[i] == self.n_elem_b:
400                 fb[i, j] = 0
401                 # The failure occurred, coefficient set to 0
402             elif i is j:
403                 fb[i, j] = fb[i, j] * numpy.pi / 2
404     %% Adaptation of matrix a (first time) after the failure of the base, (7.16)
405     for i in range(self.np):
406         for j in range(self.np):
407             a[i + self.np * self.n_layer,
408                 j + self.np * self.n_layer] = fb[i, j]
409     for i in range(self.np):
410         a[(self.n_layer + 1) * self.np, i + self.np * self.n_layer] = 1
411         if n_failure_b[i] == self.n_elem_b:
412             a[self.n_layer * self.np + i,
413                 (self.n_layer + 1) * self.np] = 0
414         else:
415             a[self.n_layer * self.np + i,
416                 (self.n_layer + 1) * self.np] = -1
417
418     %% Resolution of the equation of equilibrium (2nd time)
419     db = numpy.linalg.solve(a, c)

```

```

420 # Solves a second time when failure criterion of the base
421 # not fulfilled (different solution due to the modification
422 # of matrix a)
423 for i in range(self.np):
424     s1[i] = db[(self.n_layer+1)*self.np]*dFv[i]
425 for i in range(self.np):
426     delta_Rb[i] = db[self.n_layer*self.np+i]*dFv[i]
427     Rb1[i] = Rb[i]+delta_Rb[i]
428 for k in range(self.n_layer):
429     for i in range(self.np):
430         delta_Rs[i,k] = db[k*self.np+i]*dFv[i]
431         Rs1[i,k] = Rs[i,k]+delta_Rs[i,k]
432
433 ### Determination of the failure criterion for the shaft
434 for k in range(self.n_layer):
435     for i in range(self.np):
436         if Failure_s[i,k] == 0:
437             tau_s[i,k] = Rs1[i,k]/((z_pile[i,k+1]-
z_pile[i,k])*2*decision_vect[self.np]*numpy.pi)
438             sigma_1_s1[i,k] =
(sigma_z1_s[i,k]+sigma_x1_s[i,k])/2+((sigma_z1_s[i,k]-
sigma_x1_s[i,k])**2/4+tau_s[i,k]**2)**0.5
439             sigma_3_s1[i,k] =
(sigma_z1_s[i,k]+sigma_x1_s[i,k])/2-((sigma_z1_s[i,k]-
sigma_x1_s[i,k])**2/4+tau_s[i,k]**2)**0.5
440             # MC's failure criterion for the shaft (7.14)
441             MC_shaft[i,k] = 0.5*sigma_1_s1[i,k]*(1-
numpy.sin((self.phi[k]+self.psi[k])*numpy.pi/180))-
0.5*sigma_3_s1[i,k]*(1+numpy.sin((self.phi[k]+self.psi[k])*numpy.pi/180))-
self.cohes[k]*numpy.cos((self.phi[k]+self.psi[k])*numpy.pi/180)
442             if MC_shaft[i,k] >= 0:
443                 Failure_s[i,k] = 1
444             #If the failure criterion of the shaft is not fulfilled,
445             # adapt another time the matrix a AND go back to the
446             # equation b = a\c "first time" If the failure criterion is
447             # fulfilled, go directly to the next iteration
448
449 ### Update of the coefficient of influence from pile base j on pile base i
450 for k in range(self.n_layer):
451     for i in range(self.np):
452         if Failure_s[i,k] == 1:
453             for j in range(self.np):
454                 if j is not i:
455                     fs[i,j,k] = 0
456                     # Coef set to 0 if failure appears
457 ### Adaptation of matrix a (second time) after the failure of the shaft, (7.16)
458 for k in range(self.n_layer):
459     for i in range(self.np):
460         for j in range(self.np):
461             a[i+self.np*k,j+self.np*k] = fs[i,j,k]
462 for k in range(self.n_layer):
463     for i in range(self.np):
464         a[(self.n_layer+1)*self.np,
i+self.np*self.n_layer] = 1
465         if Failure_s[i,k] == 1:
466             a[k*self.np+i,(self.n_layer+1)*self.np] = 0
467         else:
468             a[k*self.np+i,(self.n_layer+1)*self.np] = -1
469
470
471 ### Resolution of the equation of equilibrium (3rd resolution)
472 db = numpy.linalg.solve(a,c)
473 for i in range(self.np):
474     s2[i] = db[(self.n_layer+1)*self.np]*dFv[i]
475 # Second resolution
476 for i in range(self.np):

```

```

477         delta_Rb[i] = db[self.n_layer*self.np+i]*dFv[i]
478         Rb2[i] = Rb[i]+delta_Rb[i]
479         for k in range(self.n_layer):
480             for i in range(self.np):
481                 delta_Rs[i,k] = db[k*self.np+i]*dFv[i]
482                 Rs2[i,k] = Rs[i,k]+delta_Rs[i,k]
483
484     %% Verification of the iteration condition
485     # NB: the loop runs while boolean different from 0 (boolean is
486     # reset to 1 each time before entering the loop "while").
487     laufwhile = 0
488     # Set to 0, if difference < 1%, go out of the loop while
489     for i in range(self.np):
490         if abs((s2[i]-s1[i])/s2[i]) >= 0.01:
491             laufwhile = 1
492     for i in range(self.np):
493         if ((Rb2[i]-Rb[i])-(Rb1[i]-Rb[i]))/(Rb2[i]-Rb[i]) >= 0.01:
494             laufwhile += 1
495     for i in range(self.np):
496         for k in range(self.n_layer):
497             if ((Rs2[i,k]-Rs[i,k])-(Rs1[i,k]-
498                 Rs[i,k]))/(Rs2[i,k]-Rs[i,k]+1e-10) >= 0.01:
499                 laufwhile += 1
500     # End of the loop while
501
502     %% Calculate total settlement, load shaft and load base
503     """Total settlement"""
504     for i in range(self.np):
505         s_tot[i] = s_tot[i]+s2[i]
506     """Total load in the pile base"""
507     for i in range(self.np):
508         Rb[i] = Rb[i]+delta_Rb[i]
509     """Total load in each layer of the pile shaft"""
510     for k in range(self.n_layer):
511         for i in range(self.np):
512             Rs[i,k] = Rs[i,k]+delta_Rs[i,k]
513     """Sum of all the layer loads to obtain a single pile shaft load"""
514     for i in range(self.np):
515         Rs_tot[i] = 0
516         for k in range(self.n_layer):
517             Rs_tot[i] = Rs_tot[i]+Rs[i,k]
518     """Total load in a pile"""
519     R_tot = Rb+Rs_tot
520     %% Storage of the results after each iteration
521     Rb_plot[:,iteration] = Rb
522     Rs_tot_plot[:,iteration] = Rs_tot
523     #
524     #
525     #
526     R_tot_plot[:,iteration] = R_tot
527     s_tot_plot[:,iteration] = -s_tot*100
528     # End of the incremental loop, increase dFv for the next loop
529     %% Plot results
530     if self.plot_fig:
531         for i in range(2,5):
532             plt.figure()
533             plt.plot(Rs_tot_plot[i,:],s_tot_plot[i,:], color='#4682B4',
534                 linestyle=':', marker='.', label='Rs_ %s'%(i+1))
535             plt.plot(Rb_plot[i,:],s_tot_plot[i,:],color='orange',
536                 linestyle=':', marker='.', label='Rb_ %s'%(i+1))
537             plt.plot(R_tot_plot[i,:],s_tot_plot[i,:],color='#2F4F4F',
538                 linestyle='--', marker='o', label='Rtot_ %s'%(i+1))
539             plt.title('Pile %d, D = %s m'
540                 % (i+1, 2*decision_vect[self.np]))
541             plt.xlabel('Load (kN)')

```

```

542         plt.ylabel('Settlement (cm)')
543         plt.grid()
544         plt.box('on')
545         plt.legend()
546         graph_name = 'Load-settlement curve pile %s'%(i+1)
547         plt.savefig(graph_name+'.png')
548         plt.show()
549
550     fig = plt.figure()
551     plt.plot(x,y,'o', color='#2F4F4F', markersize=12)
552     plt.title('Position of the piles, a/D = %.1f'
553             % (decision_vect[self.np+1]/(2*decision_vect[self.np])))
554     plt.xlabel('x (m)')
555     plt.ylabel('y (m)')
556     plt.grid()
557     plt.box('on')
558     position = fig.add_subplot(111)
559     for i in range(self.np):
560         position.annotate('%s'%(i+1), xy=(x[i], y[i]),
561                               xytext=(x[i]+0.25, y[i]+0.06))
562         # Assignment of the numerotation to each point
563     graph_name = 'Position of the piles'
564     plt.savefig(graph_name+'.png')
565
566     fig = plt.figure()
567     plt.plot(x,y,'o', color='#2F4F4F', markersize=0)
568     plt.title('Distribution resistances (MN)\nand settlement (cm)')
569     plt.xlabel('x (m)')
570     plt.ylabel('y (m)')
571     plt.grid()
572
573     plt.box('on')
574     plt.ylim([-1, max(y)+1])
575     plt.xlim([-1.5, max(x)+1.5])
576     # plt.axis('equal')
577     subplot = fig.add_subplot(111)
578     for i in range(self.np):
579         subplot.annotate('%.1f'%(R_tot[i]/1000), xy=((x[i], y[i])),
580                               xytext=(x[i]-0.3, y[i]-0.1))
581         subplot.annotate('%.1f'%(s_tot[i]*100), xy=((x[i], y[i])),
582                               xytext=(x[i]-0.25, y[i]-0.9))
583         subplot.add_artist(matplotlib.patches.Circle((x[i], y[i]),
584               R_tot[i]/(2*numpy.mean(R_tot)), edgecolor =
585               '#2F4F4F', facecolor = 'none', linestyle='-'))
586     graph_name = 'Benchm KKP1, Resistance and settlement distribution'
587     plt.savefig(graph_name+'.png')
588
589     print("Settlement: %10.2f cm" %(numpy.mean(s_tot)*100))
590     # Round the float to 2 decimal places in a 10-place field
591     return(numpy.mean(s_tot))
592
593 class InfluenceRadius(object):
594     """ This class gathers functions calculating the radius of influence using
595     different empirical models:
596     - Cooke (1974)
597     - Wroth (1979)
598     - Lutz using the correction factor alpha (2003)
599     - Lutz using the thickness of the compressible layer (2003)
600     - Liu (1996)
601     For more information see M. Rudolf (2005) p. 75"""
602
603
604     def __init__(self, diameter = None , length = None, poisson = None,
605                 alpha = None, thickness = None):
606         self.diameter = diameter

```

```

607         self.length = length
608         self.poisson = poisson
609         self.alpha = alpha
610         self.thickness = thickness
611
612     def cooke(self, diameter):
613         """Radius of influence using Cook's formula with parameters:
614             - Diameter"""
615         radius = 10*diameter # [m]
616         return(radius)
617
618     def wroth(self, length, rg, poisson):
619         """Radius of influence using Wroth's formula (1979) with parameters:
620             - Length of the pile
621             - Radius rg of the circle having the same area as the pile group
622             rg = sqrt(a*b/pi) with a and b dimensions of the pile group
623             - Poisson's ratio"""
624         radius = 2.5*length*(1-poisson)+rg # [m]
625         return (radius)
626
627     def lutz_alpha(self, length, poisson, alpha):
628         """Calculation of the radius of influence using Lutz's formula relative
629         of the coefficient alpha (2003). Alpha is a factor correcting the
630         formula of Wroth (1979), comprised between 2.5 and 5.5. Parameters:
631             - Length of the pile
632             - Poisson's ratio
633             - Alpha coefficient
634         NB: For an infinitely extended half space, alpha = 5.5 and for
635         H/L = 2, alpha = 2.5"""
636         radius = alpha*length*(1-poisson) # [m]
637         return (radius)
638
639     def lutz_thickness(self, length, poisson, thickness):
640         """Calculation of the radius of influence using Lutz's formula relative
641         of the "thickness of the compressible layer"(2003). Parameters:
642             - Lengths of the pile
643             - Poisson's ratio
644             - Thickness of the compressible layer"""
645         radius = 1/(0.18182+0.43636*length/thickness)*(1-poisson)*length # [m]
646         return(radius)
647
648     def liu(self, diameter, poisson, length, thickness):
649         """Radius of influence using the formula of Liu (1996) with parameters:
650             - Diameter of the pile
651             - Poisson's ratio
652             - Length of the pile
653             - Thickness of the compressible layer"""
654         radius = diameter*1.1*(1-3.5*poisson**2.5)*(thickness/length)**0.68*(
655             length/diameter)**0.85 # [m]
656         return (radius)
657
658 if __name__ == '__main__':
659     instance_pile = PileGroup()

```

## A.2 Multi-optimisation of a pile group

```

# -*- coding: utf-8 -*-
1  """
2  Created on Tue Feb 20 16:04:37 2018
3
4  @author: Corentin
5  """
6
7  import time # Used to calculate the computation time
8
9  import pygmo as pg # Optimisation library, Pagmo 2.7
10
11 import matplotlib.pyplot as plt
12
13 from PileGroup_calculation_15param import PileGroup
14 # Imports the class "PileGroup"
15
16 tmps_total_1 = time.time() # Starts the measurement of the computation time
17
18 class PileOptimPareto(object):
19     """ Defines a User Defined Problem (UDP) with 2 objectives
20         (volume of the piles and settlement of the pile group), unconstrained """
21
22     def __init__(self, dim = 15):
23         self.dim = dim
24         # Set up the dimension of the problem (ie decision vector's dimension)
25         self.instance_pile = PileGroup()
26         # Creates one instance of the imported class PileGroup, defines
27         # it as a local variable
28
29     def get_nobj(self):
30         """ Sets up the number of objectives of the problem"""
31         return(2)
32
33     def get_bounds(self):
34         """ Sets up the lower and upper boundaries of the decision vector
35             (here pile length and pile radius, in meters)"""
36         return([10, 10, 10, 10, 10, 10, 10, 10, 10, 10, 10, 10, 0.6, 1.5, 1.5],
37               [25, 25, 25, 25, 25, 25, 25, 25, 25, 25, 25, 25, 1, 6, 6])
38         # of the form ([lower boudaries], [upper boudaries])
39         # ie lp = [10, 25], rp = [0.6, 1], dx = [1.5, 6], dy = [1.5, 6]
40
41     def get_name(self):
42         """ Sets up the name of the problem"""
43         return ("PileOptimPareto")
44
45     def fitness(self, decision_vect):
46         """ Defines the objectives of the problem.
47             "decision_vect" is of dimension "dim" """
48         objective1 = self.instance_pile.volume(decision_vect)
49         # Volume of the piles (m3)
50         objective2 = self.instance_pile.settlement(decision_vect)
51         # Settlement of the pile group (m)
52         return (objective1, objective2)
53
54 if __name__ == '__main__':
55     instance_pileoptim = PileOptimPareto()
56
57     ### Input
58     generations = 30
59     # Number of generations of the algorithm
60     popul = 72
61     # Number of individuals that will be evolved (NB: for the NSGA-2
62     # algorithm, a minimum of 5 and a multiple of 4 individuals is needed)

```



```

63 algo_name = "NSGA2"
64 #algo_name = "MOEAD"
65 # Only used to give information in the plot, not necessary to run the algorithm
66
67 %% Instantiates a problem and evolves it
68 probl = pg.problem(PileOptimPareto(15))
69 # Instantiates a pygmo problem constructing it from the UDP
70
71 nsga2 = pg.algorithm(pg.nsga2(gen = generations))
72 # Instantiates a pygmo algorithm (here the algorithm is defined in a class of
73 # the pygmo library, but it is possible to code our own algorithm (User Defined
74 # Algorithm, UDA))
75
76 tmps_init_1 = time.time()
77 # Starts the measurement of the initialisation of the population
78 pop = pg.population(probl, popul)
79 # Initialises the population made of individuals bound to the problem (number
80 # of fitness evaluations rises to the number of the population)
81 tmps_init_2 = time.time() - tmps_init_1
82
83 f = pop.get_f()
84 # Gets the initial fitness vector
85 plt.scatter(f[:,0], f[:,1]*100, color = 'black', label = 'Initial population',
86            marker = '.')
87 # Plots the initial fitness vector (one column contains one objective)
88
89 tmps_evolve_1 = time.time()
90 # Starts the measurement of the evolution of the algorithm
91 pop = nsga2.evolve(pop)
92 # Runs the evolution (optimisation) of the algorithm
93 tmps_evolve_2 = time.time() - tmps_evolve_1
94
95 nb_fitness_eval = pop.problem.get_fevals()
96 # Gets the number of times the objectives are calculated
97 x = pop.get_x()
98 # Gets the evolved decision vectors
99 f = pop.get_f()
100 # # Gets the evolved fitness vector
101
102 %% Visualisation
103 plt.scatter(f[:,0], f[:,1]*100, color = 'red', marker = 'v', label =
104            'Evolved population (Pareto front)\nFitness evaluations: %d'
105            %nb_fitness_eval)
106 plt.scatter(318.08, 3.0, color = 'blue', label = 'Reference solution')
107 plt.plot([318.08, 318.08], [0, 3.0], 'b--', lw = 1.5)
108 # vertical line between points [318.08,0] and [318.08,3.0]
109 plt.plot([0, 318.08], [3.0, 3.0], 'b--', lw = 1.5)
110 # Plots the evolved fitness vector (one column contains one objective)
111 plt.xlim([0, 800])
112 plt.ylim([0, 13])
113 plt.title('Benchmark CPR1 variant 2, 15 parameters \n algorithm %s, %s
114 generations, %s individuals' %(algo_name, generations, popul))
114 plt.xlabel('Volume of the piles ($m^3$)')
115 plt.ylabel('Settlement (cm)')
116 plt.grid()
117 plt.legend(loc = 1)
118 # Legend box fixed at the top right corner
119 plt.savefig('Benchmark KPP1 variant 2 15 parameters, algorithm %s, %s
120 generations, %s individuals.png' %(algo_name, generations, popul))
120 plt.show()
121
122 tmps_total_2 = time.time() - tmps_total_1
123 # Ends the measurement of the total computation time
124 print("Execution time, init population : %10.2f min" %(tmps_init_2/60))
125 print("Execution time, algorithm: %10.2f min" %(tmps_evolve_2/60))

```

```
126 print("Execution time, total: %10.2f min" %(tmps_total_2/60))
127
128 ### Saves data, just in case
129 with open('Data %s_%s_%s 15 param.txt'
130           %(algo_name, generations, popul),'w') as out_file:
131     # 'w' refers to 'write'
132     out_string = "Fitness \n"
133     out_string += str(f)
134     out_string += "\n"*2 + "Decision vector: \n"
135     out_string += str(x)
136     out_file.write(out_string)
```

## Appendix B Global and partial safety concept

With the introduction of Eurocode 7 in 2005 and its partial safety concept, a new approach concerning design in the geotechnics has been taking place. A single standard safety concept has been unified in Europe. The global safety factor made use of a single safety factor to ensure a sufficient safety level. The safety concept derived from Eurocode 7 (or its counterpart ÖNORM EN 1997-1 in Austria or DIN EN 1997-1 in Germany) is established by means of a reduction of the resistance values and an increased action calculated with different safety factors. It has to be said that other comparable codes (such as the DIN 1054:2005-01 in Germany [14]) have been maintained and applied as long as they do not contradict Eurocode 7 within a coexistence period. The old code DIN 1054:1976-11 [13] has no longer been applicable since 2008.

Two different limit states have to be analysed: the ultimate limit state aims at assuring a sufficient load-bearing capacity and at excluding any threat for humans, whereas the serviceability limit state guarantees the long-term usability of the construction.

### B.1 Global safety concept

A construction is said to be safe according to the global safety concept if the characteristic resistance (abbreviated  $R$ ) and the characteristic stress or action (commonly abbreviated  $S$ ) verify the following equation involving the global security factor  $\eta$

$$\eta S \leq R \quad (\text{B.1})$$

Note that the action effect is commonly called  $E$ . Only one parameter is used to take into account all the different types of inherent imponderability of the geotechnical construction. This parameter depends on the considered load case according to DIN 1054:1976 [13]. Some objections can thus be made to this concept, as exposed by *Adam* (2016) [1]:

- For a major part of the geotechnical designs (slippage, tipping, load-bearing capacity of piles...) differentiated safety factors exist, determined empirically or arbitrarily.
- Every design load cannot be evaluated separately, making the safety concept untraceable.
- This concept is not able to depict the safety reserves or the utilisation factor of the construction.

That is why a new concept was developed that aims to eliminate these drawbacks.

### B.2 Partial safety factor concept

For every calculation step, the dispersion of the influence parameters is directly included using the so-called partial safety factors  $\gamma$ . Resistances and stresses are described using characteristic values (index  $k$ ), representing the “safe” mean value of statistical analyses (that is to say somewhat more than the mean value of the action respectively somewhat less than the mean value of the resistance). The characteristic values are then increased or attenuated using partial safety factors, whether they operate favourably or unfavourably (see equation (B.2) and *Adam* (2016) [1]). The obtained values are called design values (index  $d$ ).

$$\begin{aligned}
 S_d &= S_k \gamma_E \\
 R_d &= \frac{R_k}{\gamma_R}
 \end{aligned}
 \tag{B.2}$$

The calculation of design values can be generalised. For actions, it is either directly determined or derived from a representative value  $F_{rep}$  that is multiplied by a partial factor  $\gamma_F$  (ÖNORM B 1997-1-1) as in Equation (B.3).

$$F_d = F_{rep} \gamma_F \tag{B.3}$$

For geotechnical parameters, they are calculated using the characteristic value divided by the partial safety factor of the material  $\gamma_M$ .

$$X_d = \frac{X_k}{\gamma_M} \tag{B.4}$$

Following ÖNORM B 1997-1-1 (the national guidance of Eurocode 7), all material safety factors  $\gamma_M$  used to design pile foundations or shallow foundations are equal to 1. That is to say, all design approaches in Austria are conducted using the characteristic soil parameters.

In Eurocode 7, three design approaches are presented. They depict the different calculation and design philosophies existing in Europe [1]. In Austria, only the Design Approaches (DA) 2 and 3 are employed. It is also stated that for pile and shallow foundations, the DA 2 has to be applied (ÖNORM B 1997-1-1). For the DA 2, it should be verified that “a limit state of rupture or excessive deformation will not occur using following combination of sets of partial factors” see [20]:

Combination: A1 “+” M1 “+” R2

The following terminology is adopted: A refers to the Actions, M to the Material properties and R to the Resistances. In this approach, partial factors are applied to actions or to the effects of actions A (equivalents of the German “Einwirkung” and “Beanspruchung”) and to ground resistances R. They do not apply to material properties (all material safety factors are set to  $\gamma_M = 1$  in the set M1). As an example, the table of sets A1 and A2 is presented in Table B.1 (see Annex A.3 of Eurocode 7-1). Using the design values outlined above, the two limit states can be verified.

### Ultimate limit state

The ultimate limit state is verified if the design value of the action  $S_d$  is not exceeding the design value of the resistance of a construction  $R_d$  or a construction part.

$$S_k \gamma_S = S_d \leq R_d = \frac{R_k}{\gamma_R} \tag{B.5}$$

**Table B.1:** Partial factors on actions following two different sets of partial factors [20].

Action		Symbol	Set	
			A1	A2
Permanent	Unfavourable	$\gamma_G$	1,35	1,0
	Favourable		1,0	1,0
Variable	Unfavourable	$\gamma_Q$	1,5	1,3
	Favourable		0	0

### Serviceability limit state

The design of the serviceability limit state is carried out by the equation

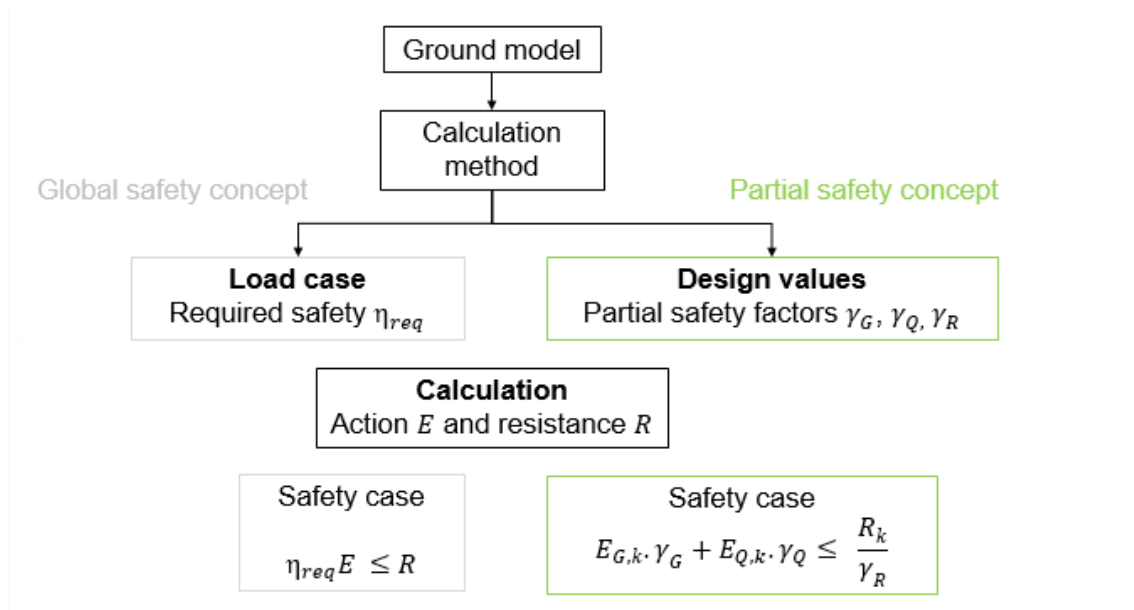
$$E_d \leq C_d \quad (\text{B.6})$$

in which  $C_d$  represents the design value of the decisive serviceability criterion. For example, a deformation serviceability criterion is the limit value of the deformation, after which the serviceability of a structure is not given (for example not admissible cracks). This limit value has to be set during the design of the structure.

## B.3 Comparison of the two concepts

Both concepts are summarised in Figure B.1. In particular, Eurocode 7 introduces new requirements regarding the calculation of piles. Some characteristics of a pile group have to be designed more precisely than it had been the case in DIN 1054:1976-11 [13], for example:

- the group effect of a pile group,
- the settlement differences between piles of a group and
- the non-linear load-bearing behaviour.

**Figure B.1:** Representation of the global and partial safety concepts.



# Appendix C Optimisation

## C.1 Academic benchmark

To study the influence of the input parameters on the efficiency of the algorithm, an academic benchmark is carried out. The problem considered in this study, i.e. the first problem of the ZDT family in two dimensions, was presented in Section 6.1.1 together with the associated metric used to quantify the quality of the solution.

### C.1.1 Influence of the number of generations

To optimise the ZDT1 problem, the number of individuals that are to be evolved for each simulation must be determined. One then varies the number of generations applied to this initial population and evaluates the precision of the obtained Pareto front. It is clear due to Figure C.1 that the higher the number of generations, the greater the precision of the convergence. If the initial population is not evaluated, selected, mutated and inserted in the new population a sufficient number of times, decision vectors are not able to converge to an optimal Pareto set. For only two generations, the distance to the Pareto front amounts to 2.45 but is reduced to 0.31 for 10 generations.

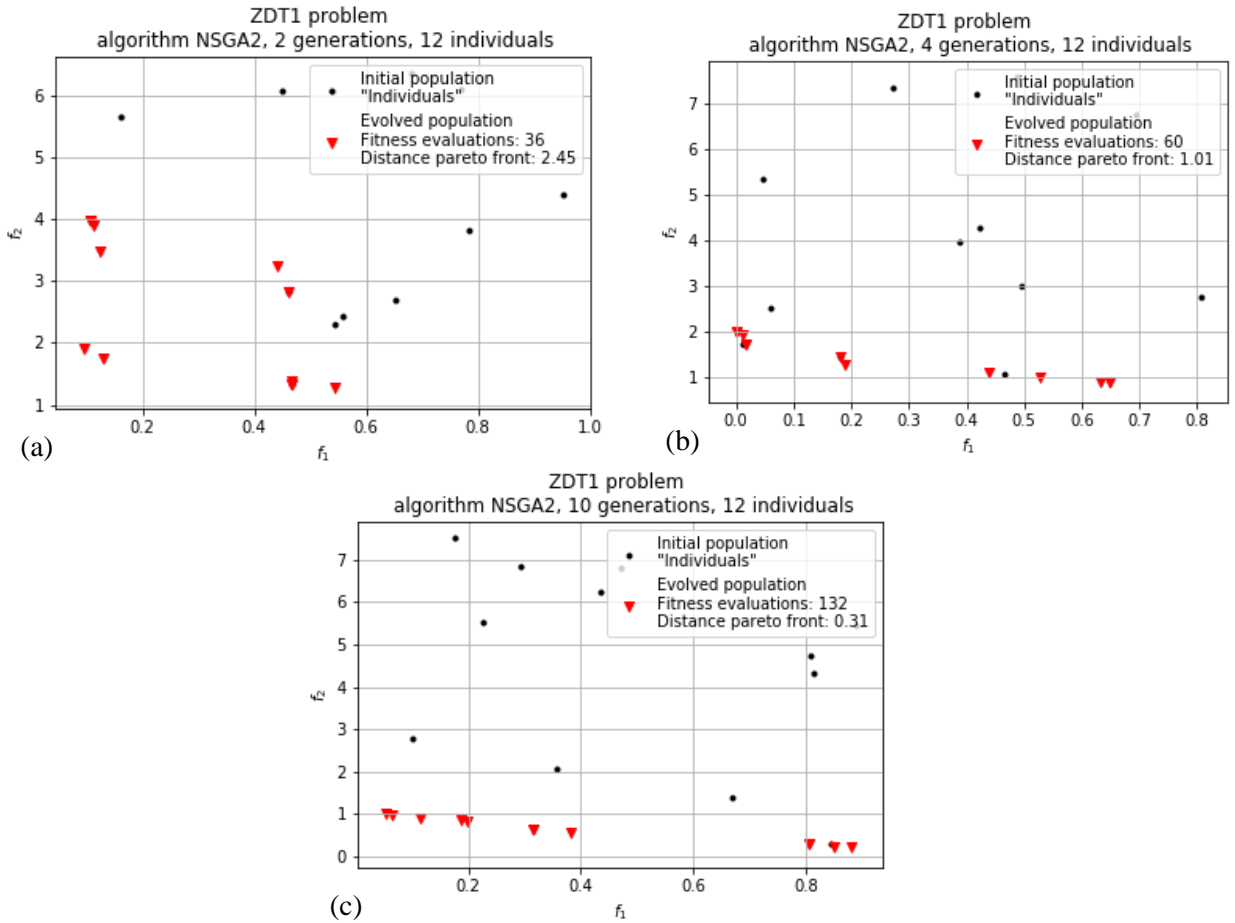


**Figure C.1:** Influence of the number of generations on the convergence of the genetic algorithm (a) 2 iterations (b) 4 iterations (c) 10 iterations.

### C.1.2 Influence of the population size

Here, the number of generations is fixed while the number of individuals is increased for each simulation. It is noteworthy in Figure C.2 that the larger the population, the better the convergence. This is due to mutations and crossovers, which occur for each iteration. Indeed, if the population is larger, more individuals are mutated, creating a more diverse offspring. This offspring possibly contains decision vectors closer to the analytical solution in comparison with a simulation featuring few individuals. Mutation and crossover increase the chance to evolve to the optimal Pareto front. For 10 generations and 12 individuals, the distance to the Pareto front is 1.56, whereas when using 60 individuals, the optimal Pareto front is almost reached (distance of 0.03).

With a sufficient number of iterations and an adequate population size, the convergence to the optimal Pareto front is reached (see Figure C.3).

It has to be added that some input parameters like the crossover rate can be optimal for one given problem and unsatisfactory for another one. Some parameters are specific to each problem, but an increasing number of generations or a larger initial population will unconditionally improve the quality of the result. However, it leads to a more significant computational complexity.

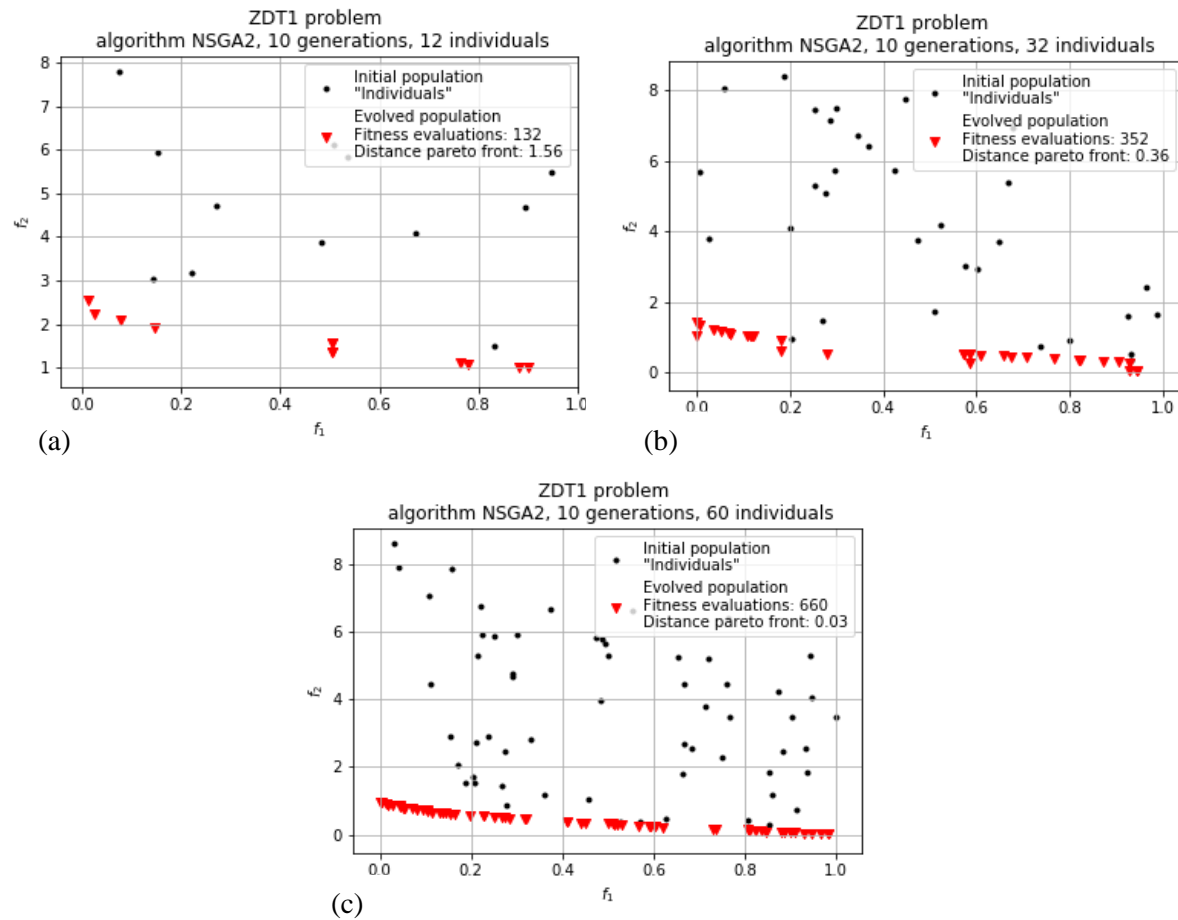


**Figure C.2:** Influence of the population size on the convergence of the genetic algorithm (a) 12 individuals (b) 32 individuals (c) 60 individuals.



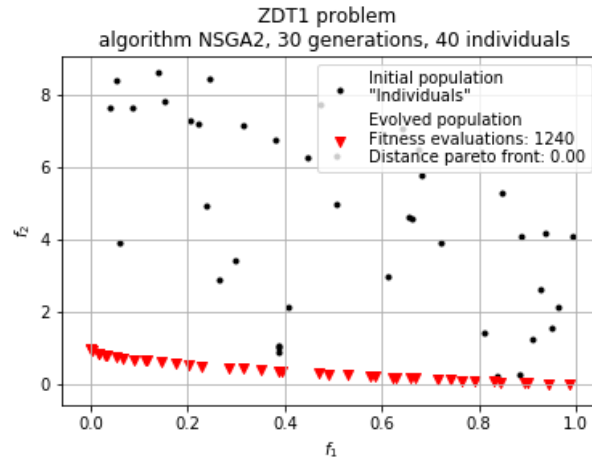


**Figure C.3:** Convergence to the optimal Pareto front for 30 generations and 40 individuals.

## C.2 Choice of the algorithm

As mentioned in Section 6.1.3, different algorithms are implemented in pygmo and selectable by the user. The algorithms MOEAD and NSGA-II were compared on the basis of the Benchmark “Guideline 1.2”.

The MOEAD algorithm turns out to be inapplicable for the present optimisation problem. In fact, the algorithm tends to favour one objective over the other; it exaggerates the impact of the volume reduction over the settlement objective, as pointed out in Figure C.4 (a) where only a part of the Pareto front is covered. Decision vectors mainly stay in the area of minimum volumes with high settlements and do not depict the whole range of optimal solutions.

Variations of the crossover and mutation rate as well as an increase of the number of generations and of the population size did not result in forming an evenly distributed set of solution over the possibility of the Pareto front in its entirety (see Figure C.4 (b)). Even if an improvement is to be attested, a lowest settlement solution cannot be reached. The NSGA-II algorithm permits to cover a more significant range of the optimal Pareto set as shown in Figure 6.4. This is why the NSGA-II is preferably chosen as a basis for the present study. Nevertheless, not all algorithms are suitable for all problems, i.e. the algorithm has to be chosen anew for each optimisation task.

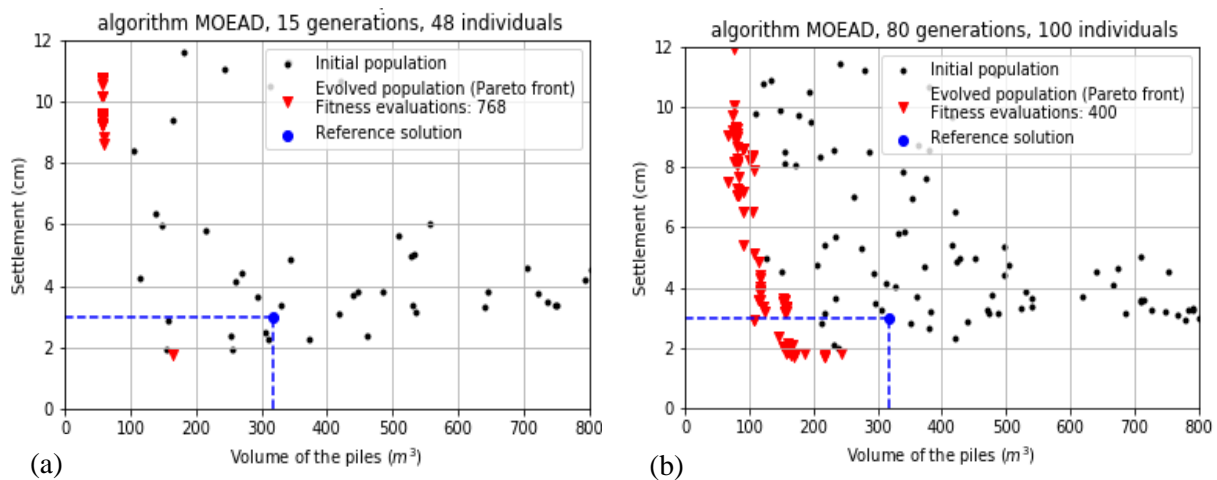


**Figure C.4:** Application of the MOEAD algorithm on the benchmark “Guideline 1.2” (a) 15 generations, 48 individuals (b) 80 generations, 100 individuals.